Department of Mechanical Engineering

Performance of End Milling Process on Advanced Ceramics

Moola Mohan Reddy

This thesis is presented for the degree of
Doctor of Philosophy
of
Curtin University

December 2012

DECLARATION

To the best of my knowledge and belief this thesis contains no material previously published by any other person except where due acknowledgement has been made. This thesis contains no material which has been accepted for the award of any other degree or diploma in any university.

Signature:

Date:

ABSTRACT

Advanced ceramics are important in modern manufacturing industries like automotive, electronics, aerospace, nuclear plants and cutting tool industries, because of their superior properties such as chemical inertness, resistance to corrosion, high strength, and high stiffness at elevated temperatures, high hardness, and oxidation resistance. Machining advanced ceramics economically and efficiently is the main barrier hindering further applications. Advanced Ceramics are challenging materials for machining by conventional methods such as turning, milling, and grinding due to the brittle nature and high hardness, and these in turn lead to poor machinability like cracks, and brittle fracture. Currently, the grinding process is a commonly used conventional method in the precision machining of advanced ceramics. However, the grinding process is a comparatively slow process and consumes extremely high energy, thus increasing the manufacturing cost and time for processing advanced ceramics. Non-conventional manufacturing methods such as electrical discharge machining, ultrasonic machining, laser beam machining, and chemical etching process are not economical in terms of productivity, and are suitable only for small production.

Recent developments of new tools, tool geometry and high speed CNC machines provide better options towards machining advanced ceramics using the conventional end milling process, and setting new prospects for essentially widening the scope of implementation. In this research study, an attempt has been made to use end milling on two types of advanced ceramics: Machinable Glass Ceramic (MGC) and Aluminum Nitride Ceramic (AlN) using three different types of tools, namely (1) two flute square end micro grain solid carbide end mill, (2) carbide tool insert coated with multiple layers of TiAlN and TiN deposited by the PVD process, and (3) CBN coated internal grinding tool grit to cover the wide range of shapes and applications. Experiments were conducted on low speed (V-30) and medium speed (V-55) vertical CNC milling machines. The effect of machining variables such as cutting speed, feed

rate and axial depth of cut have been studied on the output variables (surface roughness, tool wear, and cutting force).

The mathematical models for the surface roughness, tool wear and cutting force have been developed in terms of cutting speed, feed rate, and axial depth of cut using Response Surface Methodology (RSM). Central Composite Design (CCD) was used to design the number of experiments in developing the surface roughness, tool wear and cutting force models. The adequacy of the mathematical models was verified using the analysis of variance (ANOVA). Three dimensional and contour plots were developed for surface roughness, tool wear, and cutting force with respect to input parameters. In most cases the surface roughness decreased with an increase in the cutting speed, and increased with an increase of the feed rate and axial depth of cut. Tool wear increased with an increase in the cutting speed, feed rate, and the axial depth of cut. The cutting force value increased with the increase in the cutting speed and feed rate. The results have been analysed to establish the optimum end milling parameters for achieving good surface finish, high material removal rate and low cutting forces. The optimization results have been validated experimentally with a good surface roughness.

Analyses of experimental results show that the end milling process of advanced ceramics can be applied successfully with the proper selection of cutting parameters. Experimental study suggests that the surface finish on Machinable Glass Ceramic (MGC) and Aluminum Nitride Ceramic (AlN) generated using recently developed end milling tools are comparable to grinding process.

ACKNOWLEDGEMENTS

During the course of my PhD study, several individuals have provided guidance and positive suggestions which have enabled me to complete this work. Here I would like to thank and acknowledge these people.

First and foremost, I would like to express my sincere gratitude to my supervisors Prof. Alexander Gorin and Associate Prof. Khaled Abou Hossein for their continuous support, inspiration, motivation, and immense knowledge. Their supervision has helped throughout the duration of my research.

I would like to extend my gratitude to Associate Prof. Zhuquan Zang and Associate Prof. Chua Han Bing for serving on my Advisory Committee. Their time, patience, continuous guidance, and support along the way are certainly appreciated.

My earnest thanks also go to Dr. Sujan Debnath, Dr. Jayakumar Muthuramalingam, and Madam Sheila Gopinath for their continuous encouragement, insightful comments, proof reading and motivation to complete the thesis on schedule.

I would also like to use this opportunity to thank the School of Engineering and Science, Curtin University and Centre of Advanced Manufacturing and Material Processing (Special thanks to Mohd Sayuti Ab Karim for his time and support), University of Malaya, for providing the required facilities to carry out this research.

I would like to express my sincere gratitude to Curtin University Sarawak Malaysia, and Ministry of Science, Technology and Innovation (MOSTI) for financial support to buy the necessary equipment and to pursue my PhD.

I would like to also thank the lab technicians (Gideon Darias and Michael Ding) and final year project students (Wong Kiong, Ting Ming) for their support in conducting the experiments.

My sincere thanks also go to all my friends and colleagues, especially Lenin Gopal, Rajamohan Ganesan, Dr. Prasanna Mohan, Dr. Ashutosh Kumar, Zeya Oo, Veeramani Shanmugam, Dr. Ramasamy Nagarajan and Dr. Ujjal Kumar for their support to my work.

Most importantly, I would like to express my thanks and dedicate this thesis to my wife, Sumathi, my parents and my children, whose love and support kept me going throughout the period of my studies. Without them, this would not have been possible.

LIST OF PUBLICATIONS

JOURNAL PUBLICATIONS

1. Reddy, M.M., Alexander, G., and Abou El H.K.A., (2012). “Optimization of various cutting parameters on the surface roughness of the machinable glass ceramic with two flute square end mills of micro grain solid carbide”, International Journal of Precision Engineering and Manufacturing, 13(9), 1549-1554.
2. Reddy, M.M., Alexander, G., and Abou El H.K.A., Sujan, D., Ali, M.Y., and Malique, M.A., (2012). “Tool wear analysis in end milling of advanced ceramics with TiAlN and TiN coated carbide insert”, Advanced Materials Research, 576, 76-79.
3. Reddy, M.M., Alexander, G., and Abou El H.K.A., (2011). “Influence of cutting parameters on Machinable Glass ceramic processed by end milling”, Advanced Materials Research, 264-265, 825-830.
4. Reddy, M.M., Alexander. G., and Abou El H.K.A., (2011). “Development of cutting force model for aluminum nitride ceramic processed by micro end milling”, Applied Mechanics and Materials, 87, 223-229.
5. Reddy, M.M., Alexander, G., and Abou El H.K.A., (2011). “Surface roughness prediction in end milling of machinable glass ceramic and optimization by response surface methodology”, Advanced Materials Research, 189-193, 1376-1381.
6. Reddy, M.M., Alexander, G., and Abou El H.K.A., (2011). “Predictive surface roughness model for end milling of machinable glass ceramic”, IOP Science conference: Materials Science and Engineering, 17, 012002.
7. Reddy, M.M., Alexander, G., and Abou El H.K.A., (2011) “Surface roughness prediction in the end milling parameters of aluminum nitride ceramic by response surface methodology”, Advanced Materials Research, 154-155, 626-633.

CONFERENCE PUBLICATIONS

8. Reddy, M.M., Alexander, G., and Abou El H.K.A., and Sujan, D., (2012). "Performances of aluminum nitride ceramic in end milling using coated carbide tool", 15th International Conference on Advances in Materials & Processing Technologies, AMPT 2012, Sydney, Australia.
9. Reddy, M.M., Alexander, G., and Abou El H.K.A., (2009). "Development of cutting force model for machinable glass ceramic process by end milling", 2nd CUTSE, International conference, Curtin University, Sarawak, Malaysia.

TABLE OF CONTENTS

LIST OF FIGURES

LIST OF TABLES

NOMENCLATURE

Nomenclatures	*Description*	*Units*
N,A,	Spindle speed	*rpm*
f,B,	Cutting speed	*mm/min*
d,C,	Axial depth of cut	*mm*
MRR	Material removal rate	mm^3/min
Fr	Cutting force	*N*
R_a	Average surface roughness	μm
R_q	Root mean square roughness	μm
C	Central points	
α	Rotatability of Central Composite Design	
k	Total number of parameters	
2^k	factorial points	
$2k$	axial points	
y, R	Output response	
ε	Experimental error	
b_0 or β_0, b_1 or β_1, b_2 or β_{21}, b_3 or β_3	Estimated constants	
C, l, m, n	constants	

LIST OF ABBREVIATIONS

AlN	-	Aluminum Nitride Ceramic
ANN	-	Artificial Neural Network
ANOVA	-	Analysis of Variance
CBN	-	Cubic Boron Nitride
CCD	-	Central Composite Design
CNC	-	Computer Numerical Control
DOE	-	Design of Experiments
DOF	-	Degree of Freedom
EDM	-	Electrical Discharge Machining
GA	-	Genetic Algorithm
HSS	-	High Speed Steel
LAM	-	Laser Assisted Machining
MGC	-	Machinable Glass Ceramic
MMC	-	Metal Matrix composites
MRR	-	Material Removal Rate
PCD	-	Polycrystalline Diamond
PR	-	Photo-Resist
rpm	-	Revolutions per Minute
RSM	-	Response Surface Methodology
SEM	-	Scanning Electron Microscopy
TDM	-	Taguchi Design Method

CHAPTER 1: INTRODUCTION

1.1 Background

Machine components are needed to operate in special environments like vacuum, strong radiation, corrosion environment, non-magnetic, high temperature, high pressure, and high speed without lubrication etc. Metallic materials may not meet these requirements; however, newly developed engineering ceramics called as advanced ceramics possess the properties to meet the modern industry requirements. Advanced ceramics is a new family of industrial ceramics, designed as a combination of different kinds of oxides, non-oxides and composites (combination of oxides and non-oxides). These ceramics play an increasingly important role due to their superior properties such as chemical inertness, high strength, wear resistance with low density, ability to withstand high temperatures, high hardness, corrosion, and oxidation resistance. Therefore, advanced ceramics have a potential for increasing the lifetime of components, saving energy, and reducing pollution.

The usage of advanced ceramics is increasing rapidly in the fields of aerospace, automotive, military, medical, and nuclear, as well as cutting tools and other applications. Therefore a good surface finish and dimensional accuracy are significantly important factors for the advanced ceramic components.

Advanced ceramic materials are difficult to machine economically and efficiently by using conventional machining methods due to the brittle nature and high hardness. Among the conventional methods, currently the grinding process is used in machining advanced ceramics to produce high quality surface components. However, this process is comparatively slow, consumes extremely high energy, and subsequently increases the manufacturing cost and time.

The implementations of non-traditional machining processes also have several drawbacks. For instance, the surface quality of machined parts is relatively poor

when using laser beam machining method. Electrical discharge machining is only capable of machining electrically conductive materials. Other non-traditional methods like electron beam machining, ion beam machining, and ultrasonic machining are appropriate only for small batch production and are still subject to extensive research. Moreover, the complexity of the non-conventional manufacturing process very often increases processing time, manufacturing cost, reduces productivity, and suits only small production. Hence, the high machining cost is the primary impediment for the widespread application of advanced ceramics. Therefore, the machining process of advanced ceramics requires an effective solution to reduce cost, increase productivity and meet current market needs.

Recent developments of new tools, improved tool material properties (such as resistance to high temperature, coating tools, new tool design and geometry), and high speed Computer Numerical Control (CNC) machines, provide better options for machining advanced ceramics using the end milling process. Also, at high temperatures, brittle materials (like ceramics) may change to ductile nature, resulting in a smooth machining process. As a result, there is a significant reduction in grinding process and time. This will greatly reduce the cost of overall machining process without compromising the quality of the product. It is worth noting that besides the wide use of machining metal based alloys, many industries recommend CNC milling for advanced ceramics processes and use it in their manufacturing process. So for, limited laboratory studies that have been performed on advanced ceramics using conventional end milling, there is a need to conduct experimental studies in order to have the guidelines for operating cutting parameters, to minimize the cost, and to increase productivity.

1.2 Scope of the Project Work and Objectives

This research study examines the performance of the conventional CNC end milling machining technology for advanced ceramics. Selected samples of advanced ceramics, namely Machinable Glass Ceramic (MGC) under the category of glass

ceramics and Aluminum Nitride Ceramic (AlN) under the category of structural ceramics were investigated. MGC was selected based on its wide range of applications. AlN is relatively well suited for engineering applications (in comparison to other types of ceramics), and is very attractive as a model material because of the plastic deformation mechanism identified in this ceramic. Eexperiments were conducted based on the Response Surface Methodology (RSM), using the Central composite Design (CCD) approach. Further research was conducted to identify the optimum cutting parameters in order to achieve good machinability.

The objectives of the study are as follows:

- To investigate the influence of cutting parameters namely the cutting speed, feed rate, and axial depth of cut on the machinability of Machinable Glass Ceramic (MGC) and Aluminum Nitride Ceramic (AlN) in terms of the surface roughness, cutting force and tool wear, using various commercially available advanced tools

- To develop predictive mathematical models for surface roughness, cutting force and tool wear when cutting MGC and AlN

- To assess the effect of the cutting parameters (cutting speed, feed rate, and axial depth of cut) within the studied range, on MGC and AlN for improving surface quality

- To determine the optimal machining parameters for surface finish, tool wear and cutting force in order to achieve good surface finish, high material removal rate and low cutting forces

1.3 Methodology

The study involves three stages:

In stage one, preliminary experiments were carried out after receiving the various materials (advanced ceramics and tools) to ensure that the all the selected materials and tools were functioning satisfactorily, to study the individual effect of each cutting parameter on selected materials, and to identify the suitable range of cutting parameters for each combination of cutting tool and material.

In stage two, primary experiments were conducted to study the effect of simultaneous variation of three selected cutting parameters on the surface roughness, tool wear and cutting force. Response Surface Methodology (RSM) was chosen as the main tool to design an optimal number of experiments, which were selected based on the Central Composite Design (CCD)

Lastly, the predictive models were developed, and the model significance was verified with Analysis of Variance (ANOVA), and the most appropriate combination of cutting parameters was suggested for each combination of material and tool. The suggested combination of parameters was validated with experimental results.

1.4 Organization of the Thesis

The thesis comprises six chapters. The first chapter outlines the background information, problem statement, and the specific objectives of the study.

The second chapter is a general introduction and an extensive literature review on advanced ceramics, machining methods, end milling process, measurements for machinability, factors affecting the end milling, cutting tools, experimental design approaches and predictive models.

Chapter three emphasizes the selection of work piece materials, machining method, measurements for good machining, cutting parameters and cutting tools. It also covers apparatus used, methodology of experimentation, and experimental procedure.

Chapters four and five include experimental results on the low speed and high speed CNC end milling process on MGC and AlN using various cutting tools. The results were used to develop the mathematical models for surface roughness, cutting force and tool wear, and also to identify the optimum cutting parameters for the end milling of advanced ceramics.

The conclusions from the research and scope of the future work are presented in Chapter six.

CHAPTER 2 LITERATURE REVIEW

2.1 Introduction

This chapter presents a literature review of advanced ceramics and their machining methods. It covers an introduction to advanced ceramics describing their physical properties, material selection and machining methods, and measurements for efficient machining. In addition, it also highlights the influencing parameters for the end milling process as well as a literature review on the optimization of cutting parameters and development of predictive models. A summary of the proposed work is presented at the end of the chapter.

2.2 Advanced Ceramics

Materials are continuously tailored to meet specific applications to address demanding industrial and societal challenges in the highly competitive modern world. Similarly, the advanced ceramics industry is developing rapidly due to the increasing demand for new and innovative materials, with very specific properties for a variety of applications [Taylor 2001]. Advanced ceramics possess a number of unique properties that cannot be achieved by many other materials. For instance, a combination of properties, such as high strength and high stiffness at elevated temperatures, high wear resistance, high strength to weight ratio, corrosion and oxidation resistance, and chemical inertness are superior to metal-based systems as shown in Table 2.1 [Robert and Heimann 2010, Hockin and Jahanmir 1995, Klocke 1997 and Bianchi et al. 2003]. Therefore, advanced ceramics play a major role in the modern manufacturing industries, especially in aerospace (aircraft instrumentation and control systems, satellite positioning equipment, ignition systems, missile guidance systems, fire detection etc), automotive, electronic, military, medical and cutting tool industries [Malkin and Ritter 1989 and Jain et al. 2002].

Table 2.1: Comparison of properties of metals, plastics and advanced ceramics

Properties		Metals	Engineering Plastics	Advanced Ceramics
Maximum Temperature for continuous use (˚C)	Typical	1000	250	1200
	Maximum	1500	350	2500
Hardness		Medium-High	Low –Medium	High
Toughness	Flexibility	Medium-High	High	Low
	Impact Resistance	High	Medium-High	Low
Corrosion Resistance		Low -Medium	Medium	High
Coefficient of Thermal Expansion		High	Medium	Low
Electrical Properties		Conductive	Insulative to conductive (with fillers)	Insulative to conductive
Density		High	Low	Medium

The roadmap for advanced ceramics from 2010 to 2025 has been developed to provide guidelines for future investments [Jurgen et al. 2009]. It is presented for three applications and two knowledge fields. The selected application fields are (i) electronics, information and communication (ii) energy and environment (iii) mechanical engineering. The two knowledge fields are: (a) structural and functional properties (b) process technology. However, the cost of producing component shapes of advanced ceramics is often extremely high as it involves expensive equipment and

time consuming diamond grinding [Tuersley et al. 1994]. As advanced ceramics are manufactured and used for various industrial applications, the machining process of advanced ceramics require an effective solution to reduce cost, increase productivity, meet current market needs and increase further industrial applications.

2.3 Machining Methods of Advanced Ceramics using Conventional Machining Process

Advances in material science, as well as recent manufacturing techniques have led to the development of advanced ceramics. However, economical and efficient machining is the main barrier hindering further applications of advanced ceramics [Malkin and Ritter 1989]. Allor and Jahanmir [1996], Janssen et al. [2008] and Klocke [1997] reported that the cost of machining a ceramic component is much higher than the cost of the raw material itself. Advanced ceramic materials are difficult to do machining by conventional methods due to brittle nature and high hardness. The brittleness and high hardness often lead to poor machinability such as cracks, brittle fractures, and edge chipping [Inasaki 1987, Malkin and Ritter 1989, Li and Liao 1996, Jahanmir et al. 1999, Marinescu et al. 2000, and Raj 1993]. Moreover, the final machining (or grinding) is often responsible for damage to the surface integrity of the ceramic component. Therefore, it is very difficult to machine advanced ceramics especially at a very high material removal rate without compromising the surface integrity of advanced ceramic products [Allur and Jahanmir 1996].

Currently, among the conventional methods, the grinding process is used in the precision machining of ceramics. The grinding characteristics of advanced ceramics are different from metals [Mayer and Fang 1993]. Daniels [1989] studied the effect of surface grinding parameters such as diamond abrasive, wheel speed, and down feed on the rupture strength of silicon carbide. It was found that there was a insignificant reduction of the mean rupture strength of the material. Konig and

Sinhoff [1992] reported that flawless machining, free of brittle fracture was possible by having a critical depth of cut and flattened grains slightly protruding from the surface of the grinding wheel. Frei and Grathwohl [1992] conducted research on the microstructure and strength of advanced ceramics using ultrasonic machining, diamond grinding and diamond polishing process. They developed transmission electron microscopy preparation techniques to investigate surface samples and cross section specimens of Al_2O_3, Si_3N_4 and ZrO_2-Al_2O_3 ceramics after machining. The results suggested that optimization of machining methods was required in order to reduce defects such as enhanced roughness and cracks, as they cause material surface properties degradation.

Tuersley et al. [1994] discussed the performance of various machining methods of advanced ceramics including grinding process, ultrasonic machining, abrasive water jet machining, electrical discharge machining, and laser machining techniques. Since the grinding process develops strength-inhibiting defects in the ceramics, a few additional methods such as ductile-regime grinding, lapping, polishing, and ion beam implantation are required to prevent these defects. Consequently these methods will result in increasing the machining cost. The researchers also suggested that the cutting forces to be low during the material removal process in order to avoid work piece fracture. They also commented that the techniques involving contact between materials and tools are limited in the literature. They concluded that in the case of non-contact methods, the damaged surface regions should be subsequently removed in a more restrained manner.

Mayer and Fang [1995] studied the effect of grinding parameters on the surface finish of hot-pressed silicon nitride. The wheel grit sizes, wheel depth of cut and work speed in surface grinding have been investigated. The relationships between the grit depth of cut, grind direction with strength, and surface characteristics of the ground specimen were investigated experimentally, while grinding hot pressed silicon nitride with diamond grinding wheels at different work speeds.

Huang and Liu [2003], Klocke et al. [1999], Hwang et al. [1999] and Kovach et al. [1993] conducted experiments on high speed grinding of ceramics for achieving high removal rate. Huang and Liu [2003] focused on the material removal mechanism of advanced ceramics in high speed deep grinding. They observed that fractured and smeared areas were generated on the Al_2O_3-TiO_3 surface after the grinding process. These defects increased with smaller depths of cut. Chipping and cracking were clearly observed under a scanning electron microscope. Klocke et al. [1999] studied various process strategies for the high speed grinding of aluminum oxide and silicon-infiltrated silicon carbide at high removal rates. The results indicated that the high speed grinding at high removal rates did not reduce the fracture strength of the machined ceramic components.

A study by Zhong [2002] has revealed that the grinding of aluminum based MMC reinforced with Al_2O_3 or SiC particles using a 3000 grit diamond wheel at depths of grinding of 1 and 0.5 μm produced many ductile streaks on the Al_2O_3 and SiC particles, respectively. This resulted in a significantly shortened polishing time to secure an acceptable surface finish. Bianchi et al. [2003] presented results on the effect of grinding and cutting conditions on surfaces of advanced ceramics with diamond grinding wheels containing a binding resin bond. The results showed that the cutting conditions had a significant influence on the final quality of the ground surface as well as on its surface integrity. As the material removal rate increased the quality of the ground surface decreasesd with increasing number of cracks.

The major issues found in the case of turning operations of advanced ceramics are the tool wear and surface damage. The tool wear in the machining of advanced ceramics is mainly affected by tool materials and cooling conditions [Ma and Yu 2007]. High tool wear rate and surface damage of ceramics produced during machining are mainly due to the high cutting temperature and the high hardness of work materials. Wang et al. [1996] used liquid nitrogen cooling to control the

temperature in the cutting zone. Results showed that liquid nitrogen cooling was able to decrease the temperature and produce better surface roughness. The study by Yan et al. [1995] shows, that the temperature affects ceramic materials in the turning process. The study also showed that a poly crystalline diamond (PCD) tool is more superior than the carbide inserts and the ceramic tools for machining ceramics. Some research has been conducted on enhancing the turning performance in ceramic materials. Vermeulen et al. [2000] designed an optical diamond turning machine, to create the deterministic behavior required for sub-micrometer shape accuracy and mirror surface quality, thereby minimizing tolerances in manufacturing.

Cho et al. [2007] carried out experiments on the influence of various percentages of hexagonal crystalline Boron Nitride (h-BN) contents in Si_3N_4-hBN composite prepared using the hot-press method. Micro-end-milling and micro-drilling processes demonstrated the various weight percentages of h-BN content. The results indicated that good machinability is obtained for 20% h-BN composites. However, rough detachment of particles was observed at the cutting region of the tool due to brittle fracturing. Machinability and machined shapes were very poor for lower h-BN contents in the composites.

The conventional methods of machining SiC ceramic using diamond grinding or lapping are very slow and expensive due to the brittleness and high hardness. In addition, the brittleness and high hardness can also cause strength degradation due to the formation of surface and subsurface cracks and other defects [Yang et al. 2007, Shumyacher et al. 2009, Agarwal and Rao 2008].

Usually, good machinability is hard to achieve for advanced ceramic materials due to its inherent properties of high hardness, brittle, resistance to creep, and high strength. As a result, machining cost for ceramics is usually high and contributes to 80% of overall expenses [Davim, 2010]. Therefore, selection of proper machining parameters is crucial as it can improve machinability and reduce machining cost.

2.4 Machining Methods of Advanced Ceramics using Non- Conventional Methods

Apart from the conventional grinding process, non-conventional machining processes are extensively applied for processing advanced ceramics. Electrical Discharge Machining (EDM) is a good choice when it comes to the machining of very hard materials, provided they have enough electrical conductivity [Sanchez et al. 2001]. The main advantage of EDM in the machining of ceramics is its ability to produce complex shapes and residual stress-free components and to achieve high material removal rate. Lee and Lau [1991] have studied the EDM process of Al_2O_3 doped with up to 40% of TiC in order to improve its electrical conductivity. The results showed that a good surface finish is obtained with a removal rate of 0.6 $mm^{3/}$/min. However, low machining efficiency, poor surface finish and limited to machining only electrically conductive materials are the major disadvantages of EDM processes [Han et al. 2009, Liu et al. 2009, and Kunieda et al. 2003].

Abrasive Water Jet (AWJ) is a technique that involves forceful impingement of abrasive particles to remove surface material. AWJ depends on the water jet pressure, abrasive type, and flow rate. However, these choices are affected by external factors such as the work piece material structure and geometry of the jet nozzle [Tuersley et al. 1994]. Although AWJ has been recognized as the most efficient method to machine ceramics, results showed that the surface damage always occurred in the lower surface zone where a lot of pits were found, and this subsequently lowered the surface quality [Chen et al. 1996]

Ultrasonic Machining (USM) offers an effective alternative for precision machining of ceramics. Unlike EDM which suits only electrically conductive materials, USM can machine all hard and brittle materials [Eckert and Weatherall 1990]. Thoe et al. [1998] discussed the effects of process variables on material removal rate, tool wear, and work piece accuracy for USM. Rajurkar et al [1999] conducted experiments on the USM process in an attempt to analyze the material removal mechanism in

ceramic (Al_2O_3) machining. From the dynamic impact tests, material removal in the USM process appears to be a function of the impact velocity.

Rotary Ultrasonic Machining (RUM), also called ultrasonic assisted grinding is a relatively low cost environmentally benign process [Prabhakar et al. 1993, Treadwell and Pei 2003, and Spur et al. 1999]. RUM can achieve a relatively higher material removal rate, and a better surface finish compared to diamond grinding and USM. However, Ishikawa et al. [1998] and Hocheng et al. [2000] reported on edge chipping, which is unavoidable during machining advanced ceramics in RUM.

Laser Assisted Milling (LAM) is a relatively new machining process suitable for brittle materials like ceramics. This process uses an external heat source to heat and soften the work piece. As a result, the yield strength, hardness and strain hardening of the work piece reduce and the deformation behavior of the materials (especially ceramics) changes from brittle to ductile. This enables the difficult-to-machine materials to be machined more easily [Chryssolouries et al. 1997], and this leads to increased material removal rate and productivity. Lei et al. [2006] conducted some fundamental investigations on the LAM of silicon nitride ceramic. The authors examined the work piece temperature, surface integrity and the tool wear. The effects of laser parameters (laser power, preheat time and laser beam diameter) and milling parameters (feed rate and cutting speed) were investigated. Generally, in ceramics, plastic deformation does not occur during material removal. However, both the strength and brittleness reduced at high temperatures due to the softening of a glassy phase at the grain boundaries. When the cutting tool is engaged with the laser heated work piece, the material is removed mainly due to the combination of brittle fracture and plastic deformation [Chang and Kuo 2007, Lei et al. 2006].

Yang et al. [2009] focused on edge chipping during machining of advanced ceramics by LAM. When the cutting tool entered and exited the work piece during the milling of ceramics (Si_3N_4), it resulted in work piece edge chipping at both the entry and exit

location. The work piece edge chipping led to poor dimensional and geometric accuracy and it is the source of cracking. Increase in work piece temperature at the cutting zone during LAM of Si_3N_4 can eliminate both the macro-scale entry and interior edge chippings, but the macro-scale exit edge chipping cannot be avoided completely. However, LAM is a comparatively low cost process with improved efficiency and reduced surface/subsurface defects significantly.

Other methods like Electron Beam Machining, Ion Beam Machining, and Electro Chemical Machining still require a lot of research [Daudin and Martin 1989, Landolt et al. 2003, and Chang and Kuo 2007]. In addition, all the above non-conventional methods are not economical from the productivity point of view and can be applied only in limited conditions as discussed above.

The recent developments of advanced cutting tools such as resistance to high temperature, coated tools, new tool design and geometries, as well as usage of high speed CNC machines in the manufacturing industry have provided better options in using conventional methods. Generally, end milling is used in the manufacturing industry for the finishing of high strength metals. End milling is considered to be a versatile and rapid method for the removal of metallic materials among conventional methods like milling, drilling, and turning. Furthermore, the quality of the surfaces generated by milling is usually superior compared to the quality of the surfaces machined by shaping, turning, or drilling [Alauddin et al. 1996, Suresh et al. 2006]. The desired surface in the milling operations is usually obtainable in a single pass, and since a very good surface finish can be achieved, the milling operation is predominantly well suited for mass production.

End milling may avoid grinding process completely or may require minimum time for grinding since it is possible to get good surface finish. It has been extensively attempted previously on metallic materials like aluminum, copper, brass, steel and various other advanced metal alloys, to examine surface quality, cutting force, and

tool wear [Takacs et al. 2003, Rahman et al. 2001, Abou 2007, and Wang et al. 2005].

2.5 Literature Review on Selected Advanced Ceramics

Advanced ceramics otherwise known as engineering ceramics can be classified as oxides, non- oxides and composites (combination of oxides and non-oxides) [Taylor 2001, Kalpakjian and Schmid 2005]. Machinable Glass Ceramic (MGC) and Aluminum Nitride Ceramic (AlN) are under the category of composites. MGC and AlN are selected based on their wide range of applications and properties. MGC, a type of glass ceramics and AlN under the category of structural ceramics, are described in this section. AlN [Baik and Drew, 1996] is a relatively more used and attractive engineering ceramic because of its plastic deformation nature.

2.5.1 Machinable Glass Ceramic (MGC)

Machinable Glass Ceramic (MGC) is a fluorine rich glass with a composition approaching tetra-silicic fluorphlogopite mica [Baik et al. 1995]. MGC is an excellent non-flammable electrical and thermal insulator, dimensionally stable and can be used at high temperatures. The machinability or ability to be turned, milled, drilled and tapped with carbide tools without breaking, makes it the most popular choice for industrial applications. Glass and glass-ceramic substrates are commonly used in lasing systems, micro-optical components, mirrors and waveguides, opto-informatic devices [Balda et al. 2009].The use of MGC has become increasingly important in medical applications due to their aesthetics, biocompatibility, high abrasion resistance, high wear resistance, chemical inertness and both thermal and electrical insulation [Duangrudee al. 2011].

Takeuchi et al [1996] conducted an impressive study in which they machined a free-form surface on the glass work piece in the milling process. However, they removed glass in a small radial depth of cut only. Ng et al. [1996] and Cao [2001] described three kinds of edge chipping in milling glass ceramics namely entry edge chipping, interior edge chipping, and exit edge chipping. Entry edge chipping is

mainly caused by the impact of the cutting tool on the work piece when the tool initially contacts the work piece. Interior edge chipping is due to the brittle nature of ceramic material and occurs along the cutting path. Exit edge chipping is formed due to the sudden release of the stress energy built in the machining process and is related to the loss of material support when the tool is leaving the work piece.

Zhong [2002] revealed that grinding/lapping operations using inexpensive machine tools can produce ductile streaks on glass and silicon surfaces under good grinding/lapping conditions. This results in significantly shortened polishing time to secure an acceptable surface finish. Dabnun et al. [2005] studied the machinability of MGC in turning operations using uncoated carbide inserts under dry cutting conditions. The surface roughness equation showed that the feed rate was the main influencing factor on the roughness, followed by the cutting speed and the depth of cut. Matsumura et al. (2006) applied up-cut milling to develop a crack-free surface in a large radial depth of cut. The study performed peripheral milling with an end mill made of polycrystalline diamond to show a ductile–brittle complex mode. The outcome shows that glass can be removed in a ductile mode at the beginning of the cut in the milling process.

2.5.2 Aluminum Nitride Ceramic (AlN)

Aluminum Nitride Ceramic (AIN) has good chemical stability, excellent thermal conductivity, low permittivity, and good dielectric properties [Jin et al. 2006]. It is attractive as a model material because of its plastic deformation nature have been identified in this ceramic [Baik and Drew, 1996]. At high temperatures this material undergoes plastic deformation, which leads to the smooth machining process. Schixlir [1994] used conventional milling to machine ceramic green state bodies. The green bodies of 20% aluminum and 80% aluminum nitride were prepared, pre-sintered, and machined. The results showed that for the Al/AlN system, machining in the green state required pre-sintering. Attempting to machine pure powder compact form led to chipping and there-by resulted in an undesirable

product.The thermal expansion coefficient of AlN is close to that of silicon and it is one of the mechanically strong and thermally stable ceramics [Du et al. 2008].

AlN is widely used in the semiconductor industry and heat removal components. It is used as substrates and wafers for electronic packages, electronically insulating components for high power electronic industry, aerospace and telecommunication like research satellites and navy radio systems, and crucibles for molten metal [Katahira et al. 2005, Robert 2010]. AlN is Largely used in industries when its sintering aids are introduced which allows it to become fully densified and improve its properties after processing [Kumashiro, 2000]. During the processing of Aluminium Nitride Ceramic, a sintering aid like yttria is added for densification via either pressure sintering or hot pressing [Boch and Niepce, 2007].

So far, not many studies have reported on the machining of AlN by conventional methods; most studies focused on physical properties [Sheppard 1990, Guangli et al. 2011]

In the case of advanced ceramics, there are no clear and well defined experimental methodology, information on influence of main cutting parameters, and measurements for good machining by end milling. In the following sections, the literature on the machinability of metals is considered to incorporate the best practice for advanced ceramics.

2.6 Measurements for Efficient Machining of the End Milling Process

Kramer and Hartung [1981] pointed out that surface integrity, tool life, cutting force and chip shape are major parameters for the machinability assessment of a material. A good quality machined surface significantly improves fatigue strength, wear resistance, corrosion resistance and creep life. Thus, the quality of the surface is significantly important to evaluate the productivity of machine tools and machine parts. Tool wear has a pronounced effect on the quality of the machined surface, and

productivity of the end milling process. It can directly affect the surface finish and lead to excessive cutting force. There are three possible modes of tool failure, namely, fracture failure, temperature failure and gradual failure. Fracture failure is caused by excessive cutting force that leads to brittle fracture. Temperature failure occurs when the tool point softens and causes plastic deformation on it. Gradual failure is due to the fact that the tool had lost its shape with time, thus reducing its efficiency.

The cutting force also plays an important role in analyzing the performance of the cutting process. Cutting force analysis is important when considering tool type and material, machine power selection and work piece deformation calculation. Reen [1997], and Shaw [1986] also pointed out that three factors, namely tool life, surface finish, and power consumption during cutting need to be considered for accurate rating of machinability. According to Sandvik [1994] long tool life, good surface finish, and low cutting force are generally the main measurements for good machinability. Efficient machining indicates good surface roughness with low cutting forces, longer tool life, high material removal rate, and acceptable economy [Suresh et al. 2006, Ozcelik and Bayramoglu 2006]. Usually, these cutting forces depend not only on the tool material and geometry, but also the physical properties of work piece [Mason et al. 2007].

The above parameters are also applicable to brittle materials like ceramics in order to achieve good machinability. These parameters depend on the microstructure and properties of the advanced ceramics. In particular, fracture strength, hardness, and fracture toughness have been considered for the prediction of the machinability of glass-ceramics [Xu and Jahanmir 1994, Taira and Yamaki 1994]. Baik et al. [1995] also confirmed tool wear, surface roughness, cutting force, and cutting energy as the ‘measurement’ of the machinability for brittle materials like ceramics, depending on the testing conditions employed.

2.7 Important Parameters that Influence the End Milling Process

Among conventional machining methods like milling, drilling, and turning, end milling is one of the most widely used machining processes for manufacturing complex shapes of products. The selection of appropriate cutting conditions is very important in the conventional end milling process because of difficulty in the machining of hard and brittle materials.

Surface roughness, tool wear, and cutting forces are related to each other. In other words any changes in one specific factor may lead to changes in another factor. Therefore, it is necessary to develop a predictive mathematical model in order to know surface roughness, tool wear and cutting force in advance [Benardos and Vosniakos 2003, Alauddin et al. 1995]. Generally, a number of factors influence surface roughness, tool wear, and cutting forces. The most influential factors are machining parameters like spindle speed, feed rate, axial and radial depth of cut. The other factors are properties of work piece, type of tool, tool material, tool geometry, cutting time, work piece-setup, chatter, and type of cutting fluids.

Development of the output response models is quite hard if too many factors are considered. In addition, large numbers of experimental tests and time will be required when more factors are to be considered; this in turn, may lead to high machining cost. The influence of machining parameters on the surface roughness, by end milling process has been studied by several researchers [Alauddin et al. 1995, Suresh et al. 2006, Mansour and Addalla 2002, and Ozcelik and Bayramoglu 2006]. Alauddin et al. [1995] developed a surface roughness prediction model for the end milling of 190 BHN steel. The study was conducted on the influence of 3 cutting parameters including feed rate, depth of cut and cutting speed. It was observed that the surface roughness increased with an increase of the feed rate and the depth of cut, whilst the surface roughness decreased with an increase of the cutting speed. Mansour and Addalla [2002] investigated the surface roughness for the end milling of carbon case hardening steel (EN320). It was observed from the surface output contours that a

combination of the cutting speed and feed rate parameters could be selected to increase the metal removal rate without sacrificing the quality of the surface roughness. Their study suggested that an increment of either the feed or axial depth of cut increased the surface roughness, whilst an increment in the cutting speed decreased the surface roughness.

Benardos and Vosniakos [2003] reviewed the models of the surface roughness in machining with different systematic statistical approaches. Most of the work published is based on machining and takes into account such controllable parameters as the cutting speed, depth of cut and feed rate. The authors stated that the Design of Experiment (DOE) and the Artificial Intelligence (AI) approach were able to develop adequately predictive models for machinability with proper co-factors limitations (which are not controllable directly such as tool geometry, chattering, and tool deflection). However, in case of high precision machining which emphasizes the surface roughness quality, the reliability of the model is questionable. It was suggested that co-factors such as the cutting tool deflection and the heat generation during the cutting process must be considered in future modeling. In order to produce a more realistic depiction of the surface roughness model, the cutting tool wear in machining must be considered as well.

Ozcelik and Bayramoglu [2006] developed the statistical modeling of the surface roughness in the high speed end milling of AISI 1040 high speed steel under wet cutting conditions. In their study, factors such as the cutting speed, feed rate, depth of cut and step-over have been considered. They developed first and second order models based on the experimental results. In order to improve the reliability of the models, the tool wear was included as a linear term in the model. The total machining time of the tool was selected as the most suitable variable for the improved model. The significance of the machining variables for surface roughness model was rated in the following order: total machining time > depth of cut > step over > feed rate. This means that the total machining time which reflects the tool

wear will affect the surface roughness most dominantly.

Suresh et al. [2006] investigated the effect of solid lubricants on cutting forces and surface quality in the end milling process. According to their study, dry machining leads to high frictional contact between a tool and a work piece. In their research, graphite and molybdenum disulfide were used as powdered lubricants in the cutting of AISI1045 steel with a coated carbide end mill cutter. The authors demonstrated that the use of solid lubricants reduces cutting forces, specific energy, and chip size with significant improvements of surface roughness. Alauddin et al [1995, 1996, and 1998] studied the influence of cutting speed, feed rate, and axial depth of cut on the cutting forces, surface roughness, and tool wear in the end milling process. The surface roughness increased with the increase of the feed rate and the depth of cut, and it decreased with increase in the cutting speed. An increase in the cutting speed, the feed rate, and the axial depth of cut decreased the tool wear.

A lot of research work has been done on the behaviour of the cutting force in end milling operations [Alauddin et al. 1996; Alauddin et al. 1998; Abou et al. 2007]. According to Alauddin et al. [1996, 1998] the cutting force decreased with increasing the cutting speed, whereas the cutting force increased with the feed rate and axial depth of cut. Li and Liang [1999] estimated the forces involved when cutter engaged and disengaged from a work-piece. Fussell and Srinivasan [1989] experimented with the cutting forces by changing the feed rate, the axial and radial depths of cut values. Some authors attempted micro milling to study the effect of machining parameters on the cutting force for various metallic materials [Bao and Tansel 2000, Cheeet al. 2006, Newby et al. 2007, and Kang et al. 2007]. Most of their research results show that the cutting force increased with an increase of the feed rate, axial depth of cut, and radial depth of cut, and the cutting force decreased with an increase in the cutting speed.

Alam et al. [2009] studied the factors affecting the surface roughness in the high speed end milling of the titanium alloy, Ti-6Al-4V, and its optimization via the desirability function. The high speed milling is ideal for producing parts that require less post-processing on surface treatment such as grinding or polishing. However, proper combination of cutting tools and machining variables are required for optimizing the process. Three cutting parameters such as the cutting speed, depth of cut and feed rate were considered. It was shown that the depth of cut was the most influential factor that contributed to the surface roughness changes, followed by the cutting speed and feed rate. Sahin and Riza [2005] also studied the surface roughness model for machining mild steel with coated carbide tools.The machining tests were carried out with TiN-coated carbide cutting tools under various cutting conditions. The results show that the feed rate is the most influencing factor in the surface roughness model. The results also indicated that the surface roughness decreased with an increase of the cutting speed and depth of cut, but it increased with the increase of the feed rate. Suhaily et al. [2011] showed the effect of the cutting parameters on the surface roughness of Inconel 718 in high speed end milling. A 4mm solid carbide fluted flat end mill tool was used to machine the Inconel 718. This research showed that the surface roughness was mostly affected by the feed rate, followed by the cutting speed and axial depth of cut.

An adaptive-network fuzzy inference system for the prediction of the work piece surface roughness in the end milling of 6061 aluminum alloy was studied by Lo [2003]. It was noted that the feed rate had the most impact on the work piece surface roughness, followed by the cutting speed and depth of cut. Recently, the role of the step over ratio in the prediction of the surface roughness in the end milling of AISI 1040 steel was analyzed by Topal [2009]. In his study, the role of the step over was incorporated along with the cutting speed, depth of cut and feed rate in a predictive model. The study showed that the surface roughness was significantly influenced by the step over ratio, and its omission might cause inaccuracy of model prediction.

Many researchers have contributed to studies in the analysis of the surface roughness, tool wear, and cutting force in end milling. However, these studies were conducted with metallic materials and the results might not be applicable for the advanced ceramics.

2.8 Cutting Tools

In machining, the proper selection of an appropriate type of cutting tool material is very important as it can improve productivity, increase the tool life and reduce the cost of machining. Since the tools for semi-finishing and finishing operations must generate complex forms, they have curved edges, like the toroidal and ball nose end mills. These tools may be either solid-shaped with sharp curved edges or with replaceable inserts in a tool holder [Sandvik 2007]. The most commonly used tool materials for milling operation are High Speed Steel (HSS), Carbides, Ceramics, Cermets, Cubic Boron Nitride (CBN), and Polycrystalline-Diamond (PCD). However, molybdenum-based HSS is usually cheaper and has a higher wear resistance compared to tungsten based HSS [Kalpakjian and Schmid 2005]. Carbides were first developed in the 1930s due to the demand of higher rate of production. The carbides were also able to withstand high temperature applications which were a limitation in the cases of earlier cutting tools. Tungsten carbide known as cemented carbide uses cobalt as a binder and generally has a higher hardness and better chemical stability than HSS [Black et al. 2007].

The design of tool edge geometry influences distribution of temparature, stresses on the tool face and cutting forces. Kishawy and Elbestawi [1998] revealed that for a sharp cutting tool edges the magnitude of the residual stresses on the machined surface reduced with increasing cutting speed. Matsumoto et al. [1999] studied four types of edge tools (sharp, chamfered, double chamfered, honed) on the residual stesses in turning process. Honed and double chamfered edge tools produce higher stresses on the machined surface. Abou and Yahya (2005) examined the high-speed

end-milling of AISI 304 stainless steels using new geometrically developed carbide inserts. This research was conducted to study the performance of multilayered (TiN/TiCN/TiN) carbide inserts for the end milling of AISI 304 stainless steels. It showed that an increase in the cutting speed increased the tool wear, whereas an increase of the feed rate decreased the tool wear. Ghani et al. [2004] analysed the wear mechanism of TiN-coated carbide and uncoated cermets tools at various combinations of the cutting speed, feed rate, and depth of cut for the end milling of hardened AISI H13 tool steel. The wear mechanism of the the tool was examined using Scanning Electron Microscope (SEM). It was observed that the time needed for the cutting edge of TiN-coated carbide tools to initiate crack and fracture was longer compared to that of uncoated cermets tools, especially in a combination of high cutting speed, high feed rate, and high depth of cut.

Li et al. [2006] studied the tool wear and the cutting force variation in the end milling of Inconel 718 with coated carbide inserts. The experimental results showed that significant flank wear was the predominant failure mode affecting the tool life. The cutting force variation along with the tool wear propagation was also analysed. While the thermal effects could be a significant cause for the peak force variation within a single cutting pass, the tool wear propagation was believed to be responsible for the gradual increase of the mean peak force in successive cutting passes. Cubic Boron Nitride (CBN) is the second hardest substance after diamond, and is commonly used in machining hardened metal alloys due to its properties of excellent wear as well as oxidation resistance. CBN is normally used in dry conditions, where there is no application of coolant to prevent thermal shock caused by rapid temperature change, especially in milling operations [Kalapakjian and Schmid 2005].

Tool wear that takes place in machining of advanced ceramics are mainly affected by the tool materials and cooling conditions [Ma and Yu 2007]. The extremely high tool wear rate and surface damage of ceramics produced during machining are mainly due to the high cutting temperature and the extreme hardness of work materials.

Gradual flank wear is the dominant tool failure mode at high cutting temperature in the case laser assisted milling of advanced ceramics. The flank wear is significantly reduced with increasing work piece temperature up to an optimum point. Further temperature increase less or negative influence on the reduction in tool wear [Yang and Lei 2008, Tian et al. 2008].

2.9 Dry Machining

In the manufacturing industry, the roles of the cutting fluid is to remove heat generated due to friction during cutting, to prevent the formation of built-up edges, and to facilitate the transportation of chips. At the same time, the elimination or minimization of cutting fluids in the machining process is a necessity in modern manufacturing industries, due to strong environmental and economic requirements [Sreejith 2008]. From an environmental perspective, dry cutting can be characterized as green machining. Dry machining has numerous advantages including non-pollutant to the atmosphere, cost saving in terms of usage, maintenance and disposal of coolant, and environmental friendly.

According to Klocke [1997], and Byrne and Scholta [1993] the costs associated with the use of cutting fluids are estimated to be more than the cutting tools. Hence the implementation of dry machining will reduce manufacturing costs, and protect the environment and health (especially, in preventing skin and respiratory damage).

Advanced ceramics are generally brittle in nature and these may change from brittle to ductile at higher temperatures, and lead to a smooth surface of the work piece. The development of new coated tool materials has provided some options for the removal or minimizing the cutting fluids in machining processes. Tools with high hardness, low coefficients of friction, and low-adhesion coatings can greatly help in dry machining. Schulz et al. [2001] showed the performance of oxide Al_2O_3 and ZrO_2 PVD-coatings in the dry cutting operations of high strength graphic cast iron. New tool design and geometry have allowed machining speeds to become faster. The

increased rigidity enables high speed cutting operations to be used [Derflinger et al. 1999]. At high cutting speeds, the lubrication in the cutting zone is not really effective [Dudzinski et al. 2004]. This suggested that high speed machining would be used some times without coolant.

2.10 Design of Experiments (DOE) and Response Surface Methodology (RSM)

Finding the right combination of the cutting tool and optimal cutting parameters can be expensive and time consuming. A large number of tests are needed for all the variables using the historical one-variable-at-a-time experiment approach. This increases the total number of tests and as a result, the experimental cost increases dramatically. The use of Design of Experiments (DOE) allows creating an efficient procedure for conducting experiments with a plausible number of trials. The DOE approach consists of a systematic method in relation to the planning of experiments, collection of data and development of empirical models based on the data analysis, with near-optimum use of available resources [Benardos and Vosniakos 2002].

Response Surface Methodology (RSM) is a vital tool for designing experiments and analyzing data in the model prediction and selection of the best mathematical model that represents the experimental results [Alauddin et al. 1995, Sahin and Riza 2005]. It is practical, economical and relatively easy to use. The experimental data was utilized to build a mathematical model by the regression method [Myers et al. 2009]. This method has been extensively used by researchers for the surface roughness, cutting force, and tool life. The most popular RSM design is the Central Composite Design (CCD), which uses 2 to 4 operating parameters [Sahin and Riza 2005]. Figure 2.1 shows an example of CCD to select the number of experiments for a mathematical model [Sahoo et al. 2011].

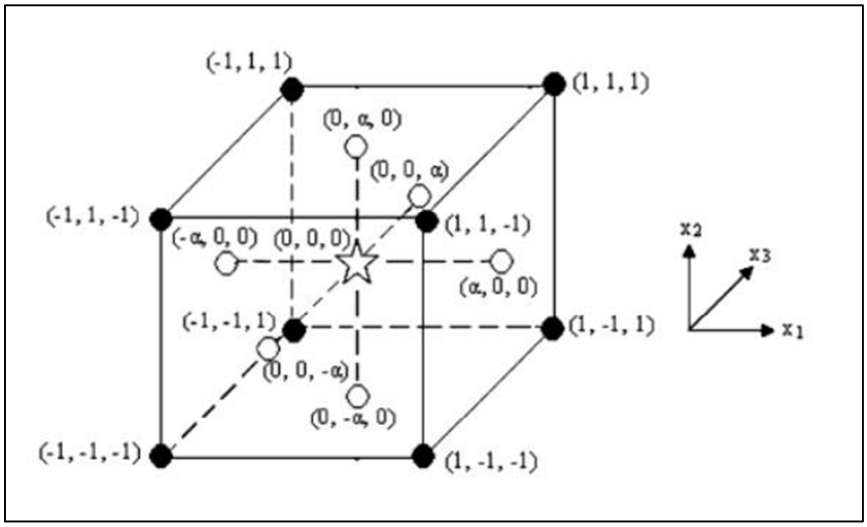

Fig. 2.1: Generation of a Central Composite Design for Three Factors, face centred type [Sahoo et al. 2011]

CCD, first established and employed by Box and Wilson in 1951, has now become a very popular design for 2nd-order model in RSM [Myers et al. 2009]. In CCD, experimental points are classified as factorial points, central points, and axial points as shown in Fig 2.1. Factorial points are specifically located at each of the corners and generally identified as the domain of the experiments. Central points are the points of replications which are situated at the core of the cube. The maximum central points can go up to 6 runs for the experiments. Axial points are positioned at the middle on the faces of a cube [Sahoo et al. 2011].

For CCD, the number of experimens required can be determined by Eqn. 2.1.

$$n = 2^k + 2k + C \qquad (2.1)$$

where n represents the number of experimentations, k is the total number of parameters considered, 2^k is the factorial points, $2k$ is the axial points and C is the central points at the core.

Various industries have applied the DOE method over the years to improve products

or the manufacturing processes [Montgomery, 2004]. Alauddin et al. [1995], Mansour and Addalla [2002], Ozcelik and Bayramoglu [2006] Alam et al. [2009], and Suhaily et al. [2011] successfully used the DOE to optimize cutting parameters by the RSM and CCD approach. The Analysis of Variance (ANOVA) checks the adequacy of the developed mathematical model. ANOVA was used by the researchers for the interpretation and obtaining detailed effects of the cutting parameters of the process [Padmanabhan 1991, Ozcelik and Bayramoglu 2006]. Puertas and Luis [2004] used the DOE method to optimize the machining parameters for the electrical discharge machining of Boron Carbide. Yang [2006] used the DOE approach to determine the optimal parameters of Photo-Resist (PR) coating process for photolithography in wafer manufacturing. A study by Benardos and Vosniakos [2003] revealed that DOE and the Artificial Intelligence (AI) approaches are most suitable to predict the surface roughness models. The authors stated that these approaches could promise accurate models with proper co-factors limitations.

2.11 The Predictive Models of Advanced Ceramics

It is necessary to develop predictive mathematical models in order to determine the surface roughness, tool wear and cutting force in advance. Ceramics components can be easily machined to near-net-shape using present technology. However, there is still room to improve the surface quality of a product. Frei and Grathwohl [1993] investigated the microstructure and strength of advanced ceramics after machining. The experiment was carried out for three types of advanced ceramics: Al_2O_3, Si_3N_4 and ZrO_2-Al_2O_3, each machined with various machining methods. The authors found that very high residual stress was induced during the machining of advanced ceramics. They suggested that optimization of machining methods was required in order to reduce defects such as enhanced roughness or cracks.

Zhang et al. [2007] studied the surface roughness of aluminum in an end-milling operation using the Taguchi Design Method (TDM). The three main control factors of the model were the cutting speed, depth of cut and feed rate. One of the main

advantages in TDM is to allow noise factors such as temperature and tool wear to be considered in the design with minimal runs (36 in their experiment). The results showed that the effects of the cutting speed and feed rate were more significant than the depth of cut on the surface roughness. It was also found that the tool wear (noise factor) influenced the surface roughness significantly.

Oktem et al. [2006] predicted the minimum surface roughness in end milling mold parts using the Artificial Neural Network (ANN) and Genetic Algorithm (GA) approach. Two hundred forty-three runs were conducted on the mold cavity on a block of Aluminum 7075-T6. The authors also introduced machining tolerance as one of the cutting parameters, other than the cutting speed, depth of cut and feed rate. They concluded that the surface roughness was higher for the higher machine tolerance.

Zeng, et al. [2005] studied the tool wear in Rotary Ultarsonic Machining (RUM) of SiC, an advanced ceramics. The tool wear ocuured in the RUM of SiC in two stages: in the first stage, an attritious wear dominated and in the second stage, a bond fracture dominates. The maximum cutting force in RUM of SiC was related to a tool wear stage. The maximum cutting force increased with the number of holes drilled during the first tool wear stage, and starts decreasing during the second tool wear stage.

Dabnun et al. [2005] modeled the surface roughness based on the DOE for the turning of MGC with the aid of CCD. The experiments were conducted using uncoated carbide inserts under dry cutting conditions. The factors considered were the cutting speed, depth of cut and feed rate. The first order predictive model was constructed with 95% confidence interval in the speed range of 15-60 m/min. Results showed that the dual-response contours could provide useful information about the maximum achievable surface roughness, based on a given material removal rate as a function of 3 independent machining variables. In addition, the model also predicted

that the feed rate had the dominant influence on the surface roughness followed by the cutting speed and depth of cut.

2.12 Summary

There are a limited number of published studies that considers both productivity and the quality surface finish produced in the machining of advanced ceramic materials. From the literature, many researchers have attempted to predict surface roughness and its optimization for end milling operations of metals. However, very little literature is available on advanced ceramic materials using the end milling process. Moreover, no systematic study has been conducted on surface roughness prediction and its optimization for the end milling process of advanced ceramics.

Due to the brittle nature of advanced ceramics, most of the researchers have worked on non-conventional machining methods in order to achieve good surface quality. However, these methods have exhibited several drawbacks: they are not economically viable and are mostly appropriate for small production. As such, the high cost of machining is the primary obstacle in the wide spread application of advanced ceramics. Moreover, these methods can be applied only under specific conditions and are still subject to extensive research.

In the case of conventional methods, most studies have focused on the grinding process. However, this process is relatively slow and consumes extremely high energy, subsequently increasing the manufacturing cost and processing time.

Therefore, it is necessary to adopt the conventional end milling method as the most practical and rapid machining process for removing excess material, and producing a well-defined and high quality surface in order to achieve quality and economical productivity. The CNC conventional end milling process with recently developed cutting tools and cutting parameter optimization techniques will greatly improve the surface quality, with a significant reduction in grinding process and time. This will

significantly reduce the cost of the overall machining process without compromising the quality of the product. While some industries recommend the milling process for advanced ceramics, the literature shows that there is a lack of substantial research on the performance of end milling on advanced ceramics. There is a need, therefore, to conduct research and to develop guidelines on the machining of advanced ceramics, by using end milling process.

The surface finish, tool life and cutting force are the commonly accepted measuring parameters for machinability assessment of materials. The cutting conditions like cutting speed, feed rate, axial depth of cut, radial depth of cut, type of coolant, type of tool and tool shape may influence the surface roughness, tool wear and cutting force. Some of these cutting conditions may also interact with combined effects. Thus, it is not easy to identify how certain combinations will influence the output, and in this case even general guidelines will be very valuable. As it follows from the analysis of published studies, the feed rate, cutting speed, and axial depth of cut are the most dominant factors to influence good machinability (low surface roughness, long tool life, and low cutting forces) by the end milling process.

The scope of this study is to examine the machining of advanced ceramics by using end milling on two types of advanced ceramics, Machinable Glass Ceramic (a type of glass based ceramic) and Aluminum Nitride Ceramic (a type of structural ceramic), selected based on their wide range of applications and properties. Low speed and high speed CNC machines with various cutting tools, which suit most of the applications of end milling process, have been used for the experimental tests conducted under dry cutting process.

The study considers the effect of simultaneous variations of three cutting parameters, i.e. the cutting speed, feed rate, and axial depth of cut on the selected ceramics, and focuses on the development of predictive models to accomplish good machinability in terms of minimum surface roughness, tool wear, and cutting force. Eexperiments

were conducted based on the RSM using CCD approach. Lastly the optimal cutting parameters were recommended for low surface finish, tool wear and cutting force.

CHAPTER 3: MATERIALS AND METHODS

3.1 Introduction

This chapter describes two advanced ceramics, machining methods, and type of tools used. It also covers measurements for good machinability, selection of cutting parameters, apparatus used, methodology of experimentation, and experimental procedure etc.

The performance of the end milling process has been studied on two advanced ceramics with a promising future:

a) Machinable Glass Ceramic (MGC) under the category of glass based ceramics
b) Aluminum Nitride Ceramic (AlN) under the category of structural ceramics

3.2 Machinable Glass Ceramic (MGC)

MGC has a number of prominent physical properties which makes it a popular choice for industrial applications. It can sustain continuously at temperatures as high as 1000°C [Corning Lighting and Materials]. This ceramic is non-wetting with zero porosity and brittle in nature. The ability to insulate high voltage and high temperature applications makes MGC a unique material. The ability or the characteristic of machinability such as turning, milling, drilling and tapping with carbide tools, without breaking makes it, the most popular choice for industrial applications.

In this study, a commercial grade of MGC, a product from Goodfellow, UK, was used. Table 3.1 shows the properties of the MGC used for this experimental study.

Table 3.1: Properties of MGC

Property	Value SI/Metric
Density	2.52g/cm^3
Porosity	0%
Young's Modulus, 25^{o}C	66.9GPa
Poisson's Ratio	0.29
Shear Modulus, 25^{o}C	25.5GPa
Compressive Strength	345MPa
Fracture Toughness	1.53MPa m$^{0.5}$
Coefficient of thermal expansion, 25^{o}C	74x10^{-7}/ ^{o}C
Specific Heat, 25^{o}C	0.79kJ/Kg ^{o}C
Thermal Conductivity, 25^{o}C	1.46W/m °C
Thermal Diffusivity, 25^{o}C	7.3x10^{-7}m^2/s
Continuous operating temperature	800^{o}C
Maximum operating temperature	1000^{o}C

3.2.1 Material Composition

MGC is composed of approximately 55% of fluorphlogopite mica and 45% of borosilicate glass. Like common porcelain, it bears a white and milky appearance and its inertness characteristics are non-toxic to the human body. The work piece of MGC supplied by Goodfellow is shown in Fig 3.1. The composition of the MGC used for this study is given in Fig 3.2.

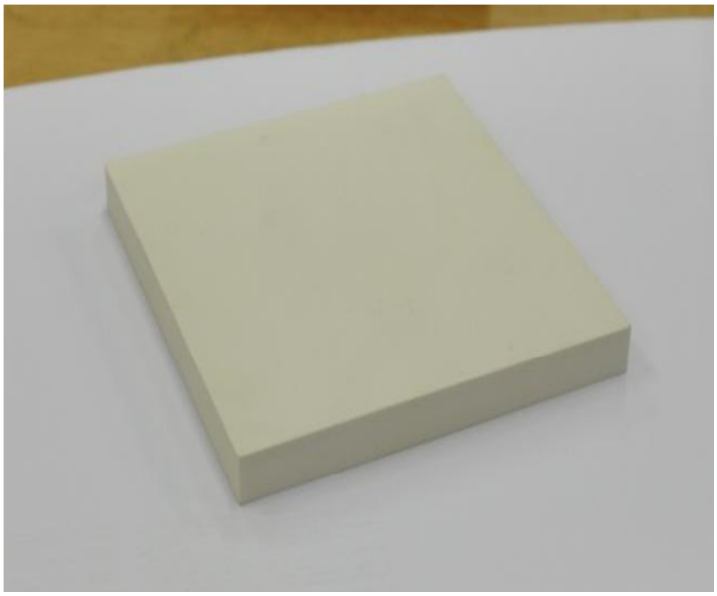

Fig 3.1: MGC (supplied by Goodfellow Cambridge limited)

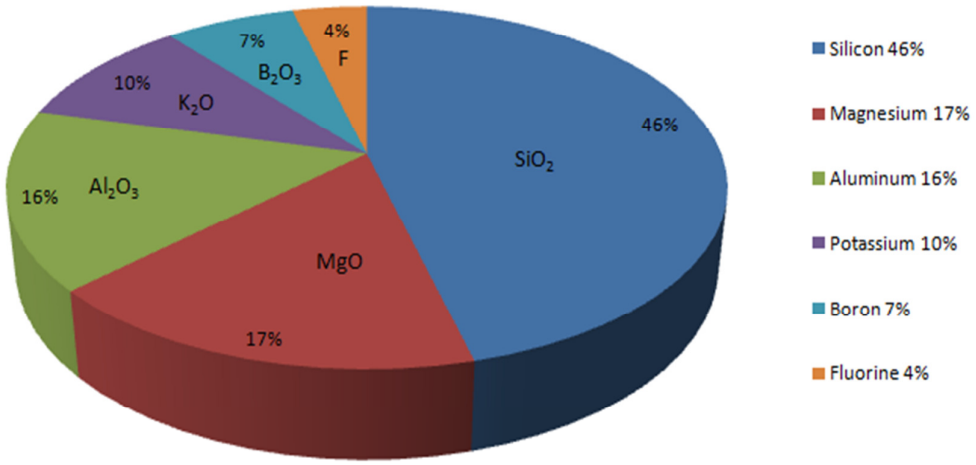

Fig 3.2: MGC composition by approximate weight

3.2.2 Fields of Applications

The MGC has been manufactured with properties that can be used in various types of applications. The typical use of the MGC in important applications is as follows:

- MGC is the main material of NASA's space shuttle obiter's hinge points, windows and doors. It is also used in the NASA space borne gamma radiation detector. NASA chooses MGC for its reliability in terms of low thermal expansion and zero permeability, as these are important design considerations for space applications. [Corning Lighting and Materials].
- MGC is widely used as an insulator or coil support for vacuum feed through. The conductive material is sustained with the help of MGC parts to produce a vacuum tight hermetic seal.
- MGC has low thermal conductivity and good electrical properties making it adequate for applications such as electrical cutting operations, and a burner block in several high industrial heat and electrode supports.
- Usually glass ceramics are used as reference pieces to measure the dimensional change in nuclear plants, since they are not dimensionally affected by irradiation. Moreover, these ceramics can be machined to a tolerance of one micron.
- For welding equipment, manufacturers use MGC as nozzle on the tips of oxyacetylene torches. The non-wetting characteristic of the MGC does not allow the molten metal to adhere easily, thus increasing the effectiveness of the nozzle (Machinable Glass Ceramic, 2008).
- The ability to machine ceramics with precise dimension stability makes it attractive in medical appliances. Glass ceramic materials are developed for repair and replacement of human hips, knees, and other body parts. In Bypass Surgery, doctors use stents which are made of ceramics for replacement of heart valves. The most common application of glass ceramics is in dentistry especially in replacement of implants and braces. (Machinable Glass Ceramic, 2008).

- The development of communication technology nowadays solely depends on glass optic fibers. Previously, information was transferred through thousands of copper connected telecommunication cables. Glass optic fibers are capable of transferring the same amount of information or even more, at a faster speed (Machinable Glass Ceramic, 2008).

3.3 Aluminum Nitride Ceramic (AlN)

Aluminum Nitride (AlN) is a relatively new material in the technical ceramics family. While its discovery occurred over 100 years ago, it has been developed into a commercially viable product with controlled and reproducible properties within the last 15 years.

Fig 3.3: AlN (supplied by Goodfellow Cambridge limited)

AlN has a hexagonal crystal structure and is a covalent bonded material with high bending strength (300–400 MPa) and Vickers hardness (560 kgf). It has good chemical stability, excellent thermal conductivity, low permittivity, and good dielectric properties [Jin et al.]. Its thermal expansion coefficient is close to that of silicon and it is one of the most mechanically strong and thermally stable ceramics [Du, et al. 2008; Kumashiro 2000]. The most common applications of AlN are in the electronic industries where heat removal is important. These excellent attributes make AlN a useful material for widespread applications. One of the most useful

applications of AlN is in replacing beryllium oxide (BeO) in the semiconductor industry. This substitution is due to BeO's toxicity. The thermal expansion coefficient of AlN is lower than BeO or alumina, and closely matches that of the silicon wafers used in electronics. However, due to the brittle fracture behavior of AlN, it is difficult to machine complex and precision components out of it (Beck, et al. 2008). The mechanical, thermal and electrical properties of the Aluminum nitride ceramic used for this study are given in Table 3.2.

Table 3.2: Properties of AlN

Properties	**SI/Metric**
Density	2.95 g/cm^3
Porosity	0 %
Flexural Strength	320 Mpa
Young's Modulus	160 Gpa
Poisson's Ratio	0.24
Compressive Strength	1000 Mpa
Hardness (Vickers)	560 kgf/mm
Fracture Toughness	2.6 MPa•m$^{1/2}$
Modulus of Rupture - Hot Pressed at 25°C - 1000 °C - 1400 °C	 0.2655 GPa 0.1862 GPa 2624.5 GPa
Thermal Conductivity (20 °C)	100 W/m•K
Coefficient of Thermal Expansion (20-1000°C)	5.2 10^{-6}/K
Upper continuous use temperature	1000-1900 °C
Dielectric Strength (25°C)	40 kV/mm
Dielectric Constant	7.3 @ 1 MHz
Electrical Resistivity (25°C)	1.8×10^{13} ohm.cm

3.3.1 Fields of Applications of AlN

The excellent properties of AlN are used in various types of applications. Selected important applications of AIN are as follows:

- AlN is widely used in semiconductor industries and heat removal components due to their excellent electrical insulation, dielectric properties, and high thermal conductivity that is approximately 10 times that of alumina [Katahira et al. 2005].
- AlN can be found in various types of heat sink materials such as highly integrated thick-film and thin-film components and water-cooled power converters in rail transport systems, due to its high thermal conductivity and electrical insulation.
- AlN is usually used to produce substrates and wafers due to high thermal conductivity. Substrates and wafers are the base and the hearts or brains of IC chips, which have high power microelectronic circuits and need to withstand high temperature.

3.4 Measurements for Efficient Machining

Machining advanced ceramics economically and efficiently is the main barrier hindering further applications. Advanced ceramics are difficult to machine using conventional machining methods, due to the inherent hardness and brittle nature. Advances in cutting tool materials, coating techniques, machine tools, CAD/CAM systems, and high speed CNC machines have provided better options for machining advanced ceramics with conventional methods. End milling has been extensively employed for metallic materials in the areas of aerospace as well as automotive divisions, as it can create parts with desired dimensional accuracy and tolerances. A good quality surface significantly improves fatigue strength, corrosion resistance, and creep life. However, there is very limited research work available on advanced ceramics by using conventional end milling. In this study, end milling was utilized as a machining process for advanced ceramics. Three criteria for good machinability, namely, surface roughness, tool wear and cutting force were considered to measure the performance of end milling on selected advanced ceramics.

Surface roughness is one of the important criteria to measure the quality of machine components. The cutting tool should be in good condition, as it produces parts with good finish and accurate dimensional tolerance. By knowing the tool wear rate in advance, the milling process can be conducted more efficiently and can avoid surface damage by replacing the tool. Cutting force plays an important role in analyzing tool wear, surface roughness of work piece in end milling. The literature study has shown that surface finish, tool life and cutting force are the important measuring parameters for machinability assessment of materials.

In order to acquire better surface finish, tool wear and cutting force, the factors that contribute within the core machining scope must be determined. Proper selection of cutting parameters would lead to improvement in surface finish, tool life and reduction of cutting force while reducing the overall machining costs.

The literature shows that machining parameters like feed rate, cutting speed, axial depth of cut, radial depth of cut, cutting tool material, shape and size of tool are the influential factors for quality machining. In this study, easy to control and most influential factors namely feed rate, cutting speed and axial depth of cut were considered as the variable cutting parameters with end milling process. The simultaneous variations of these three dominant cutting parameters were used to study the surface roughness, tool wear and cutting force on selected advanced ceramics. For this purpose, the Response Surface Methodology (RSM) was utilized to predict the mathematical models in order to evaluate surface roughness, tool wear and cutting force in advance.

3.5 Cutting Tools

In machining, choosing the appropriate type of cutting tool material is very important as it affects the surface quality, productivity, tool life and cost of machining. These tools may be either solid type (mainly for small diameters) or tool-inserts [Sandvik 2007]. In this study, three cutting tools namely (1) two flute square end micro grain

solid carbide end mill, (2) carbide tool insert coated with multiple layers of TiAlN and TiN deposited by the PVD process, and (3) CBN coated internal grinding tool grit were used. The first two tools cover a wide range of shapes and applications in end milling. The third tool is considered as a specimen for the grinding process and used to compare with the end milling process. Generally, the grinding process is very slow and consumes large power, thus increasing the machining cost. If the end milling is comparable to grinding process in surface finish, it may be avoided completely or can reduce grinding processing time. This could significantly improve the productivity and reduce the manufacturing cost of advanced ceramic components. In this study, end milling tests were conducted on CNC machines while different cutting parameters were employed based on preliminary tests for each tool material. The details of each cutting tool are given in subsections 3.4.1 to 3.4.3.

3.5.1 Solid Carbide End Mill

The end mill used in this experiment was two-flute square end micro grain solid carbide with 30° right hand spiral shown in Fig. (3.4-3.6). It is recommended that for slotting and end milling, the 2-flutted end miller is the ideal choice for roughing mill or maximum chip removal purpose. This end mill also suitable for medium range cutting speeds. Table 3.3 shows the tool dimensions referring to Fig. 3.5

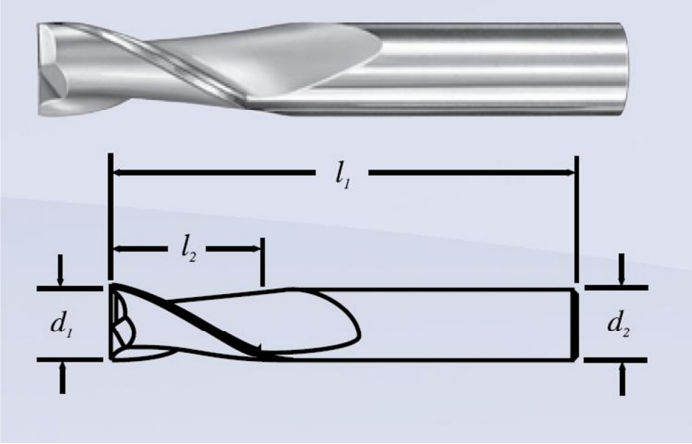

Fig 3.4: Dimension of solid carbide

Table 3.3: Specification of two flute carbide end mill

Symbol	Definition	Length (mm)
l_1	Overall length	63
l_2	Length of cut	20
d_1	Cutting diameter	6
d_2	Shank diameter	6

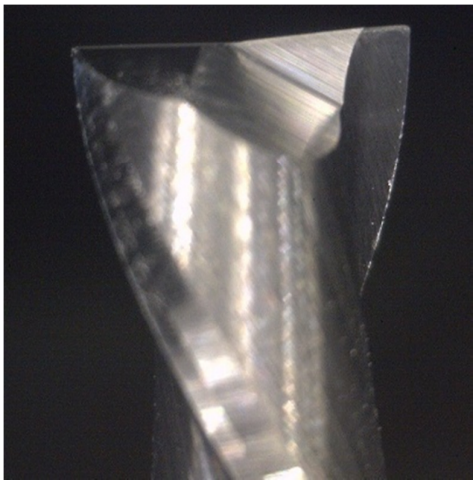

Fig 3.5: Side view of the solid carbide end mill

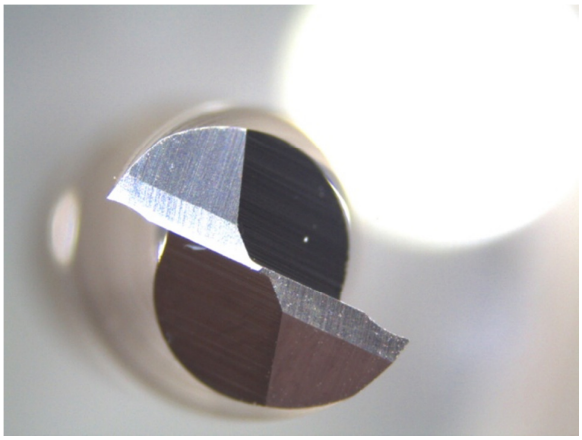

Fig 3.6: Top view of solid carbide end mill

3.5.2 Carbide Tool insert Coated with Multiple Layers of TiAlN and TiN A combination of TiAlN and TiN coated carbide tool insert manufactured by Kyocera was used. The end mill spindle can be equipped with four inserts, where only one edge is used for cutting. In this study, only one insert per experiment was mounted on the end mill cutter. The shape, size and detailed tool dimensions are shown in figures (3.7- 3.8), and Table 3.4. This type of tool is applicable from low to high cutting speed, and able to perform finishing, heavy interruption and roughing. It is suitable for milling, cut off, threading, grooving, and various types of cutting.

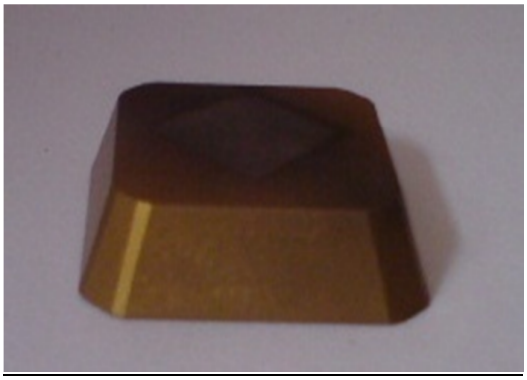

Fig 3.7: TiAlN and TiN coated carbide tool insert

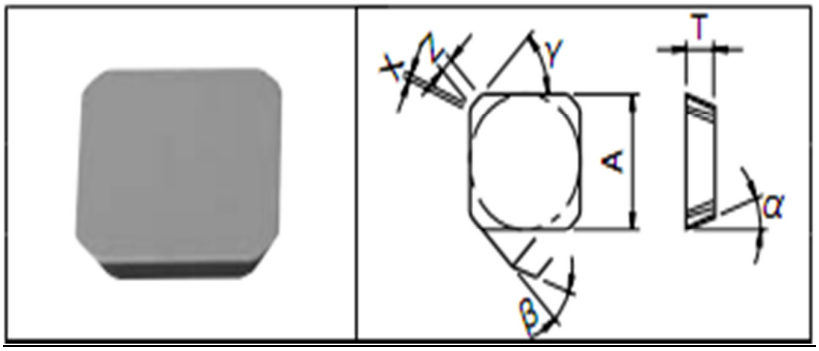

Fig 3.8: Dimensions of coated carbide tool insert

Table 3.4: Coated tool inserts dimensions

Symbols	Dimension (mm)	Angle (°)
A	12.70	-
T	3.18	-
X	0.5	-
Z	1.4	-
α	-	20°
β	-	25°
γ	-	45°

3.5.3 CBN coated Internal Grinding Tool Grit

CBN coated internal grinding tool grit is considered as a specimen tool for the grinding process and its dimensions like diameters and grit size shown in Fig 3.9 and 3.10.

Fig 3.9: Geometry of internal grinding tool grit

Where D =4 mm, L=80 mm, T =10 mm, and L1 = 25 mm.

Fig 3.10: CBN coated internal grinding tool grit

3.6 Apparatus Selection and Set up, Experimental Facility, Devices and procedure

After identifying the most influential cutting parameters, selection of advanced ceramics and type of cutting tools for the end milling process, the next step is the experiment set up.

The cutting experiments were carried out on V-55 CNC (10000 rpm to 20000 rpm) vertical milling machine shown in Fig 3.11, and V-30 CNC (1000 rpm to 5000 rpm) vertical milling machine shown in Fig 3.12.

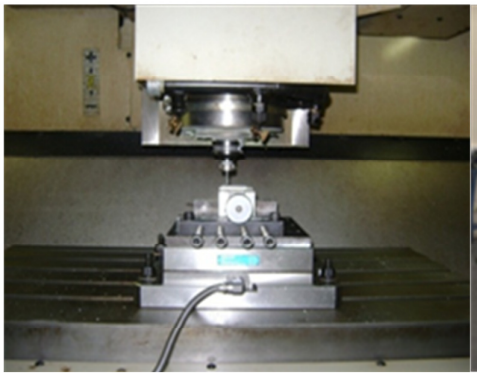

Fig 3.11: V-55 CNC milling machine

Fig 3.12: V-30 CNC milling machine

3.6.1 Surface Roughness Measurement

The Mitutoyo SJ 301 surface tester shown in Fig 3.13 was used to measure the surface roughness of milled surface. During all the milling experiments the surface roughness was recorded at three locations [Appendix B, Figure 1] and the average of three Ra values noted, to establish surface roughness model using Response Surface Methodology (RSM). In order to cover the overall surface roughness the three places considered were: one at the middle of the slot and the other two were quarter from the edge of the slot.

Fig 3.13: Mitutoyo SJ-301 roughness Tester

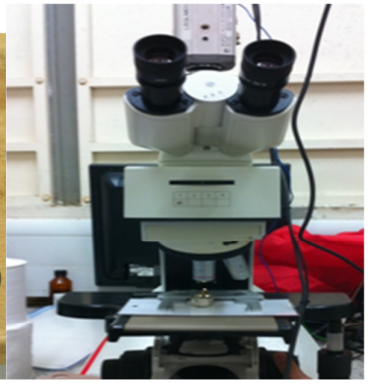

Fig 3.14: Leica microscope

3.6.2 Tool Wear Measurement:

After each cutting process, the cutting tool insert was checked for tool wear. Leica EZ4D Stereomicroscope (shown in Fig 3.14) was used to measure the wear of cutting tools. The measurement of the tool wear was taken at the location [Appendix B, Figure 8] where highest wear on tool had occurred.

3.6.3 Cutting Force Measurement

The work piece was mounted on the rigid vice, which was placed on a Kistler dynamometer set 9275 A, connected to the charge amplifier and oscilloscope shown in the schematic diagram, Fig 3.15. The connection was set to measure the cutting forces in X, Y and Z directions during the machining process. Cutting forces F_X, F_Y and F_z values were noted at three intervals during machining (starting, middle and end of machining slot), and the average of the three interval values was considered. The resultant cutting force (resultant of F_X, F_Y and F_z) acting on the work piece was calculated and used to analyze the cutting force.

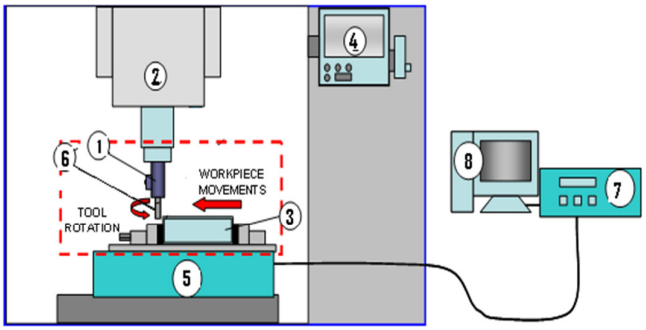

Fig 3.15: Schematic diagram of CNC machine

1. High speed spindle, 2. CNC milling center, 3. Work piece, 4. CNC milling center controller, 5. Dynamometer 6. Cutting tool, 7. Charge amplifier 8. Oscilloscope

3.7 Experimental Procedure

The experimental study involved the preliminary and primary stages. In the preliminary stage experiments (Appendix A) were conducted to identify a suitable range of cutting parameters (cutting speed, feed rate and axial depth of cut) within the capacity of CNC machines and cutting tools. The selected ranges of cutting parameters were based on the capacity of CNC milling machine, cutting tool and recommendations by the manufacturers' data book. The primary stage was simultaneous variation of all three cutting parameters examined for a selected range of cutting parameters.

3.7.1 Design of Experiment (DOE)

In order to produce parts with desired surface quality by end milling, the cutting parameters should be selected properly. The cutting speed, the feed rate, and the axial depth of cut are the selected machining parameters, which influence the machining process to a great extent. In order to know the surface roughness, tool wear and cutting force in advance, it is necessary to develop predictive mathematical models. In the case of surface roughness prediction, cutting force and tool wear prediction, the most used DOE is the RSM and the Taguchi design. From various research, it has been noted that the most widely used DOE is the RSM.

3.7.2 Response Surface Methodology (RSM)

RSM is used for predicting surface roughness, tool life and cutting force in terms of cutting speed, feed rate, and axial depth of cut .This design approach was selected based on the amount of resources available and the degree of controls, over the process variables of the experiment. In this experiment three cutting parameters were selected, hence the choices were reduced to Central Composite Design (CCD) and Box-Behnken Design (BBD) [Myers at al. 2009] shown in Table 3.5. The most preferred class of response surface designs, the CCD was used for this study.

Table 3.5: Experimental design selection guidelines

Number of Factors	Comparative Objective	Screening Objective	Respond Surface Objective
1	1-factor completely randomized design	-	-
2-4	Randomized block design	Full or fractional factorial	Central composite or Box-Behnken
5	Randomized block design	Fractional factorial or Plackett-Burman	Screen first to reduce number of factors

3.7.3 Central Composite Design (CCD)

Experiments were carried out according to the experimental plan based on central composite second-order design (CCD).

For CCD, the number of experimentations required was determined by,

$$n = 2^k + 2k + C \quad (3.1)$$

Where n represents the number of experimentations, k is called as the total number of parameters considered, 2^k is the factorial points, $2k$ is the axial points and C is the central points at the core.

CCD is more preferable and it is capable of constructing a uniform precision design which will increase the accuracy of the empirical model generated, using response surface methodology [Sahoo, Davim, and Barman 2011]. However, CCD depends on the value of α which is obtained from the Eqn (3.2). The list of α values and number of experimentations are tabulated in Table 3.6.

$$\alpha = (2^k)^{1/4} \tag{3.2}$$

where k denotes the number of parameters

Table 3.6: List of $\boldsymbol{\alpha}$ values and number of trials for different number of parameters

Number of Parameters	Factorial Points	Value of α	Number of Trials
2	2^2	1.414	13
3	2^3	1.682	20
4	2^4	2.000	31
5	2^5	2.378	32
6	2^6	2.828	53

3.7.4 Response Model

The proposed relationship between the output response and input variables can be represented by the following equation.

$$R = C\, A^l B^m C^n \tag{3.3}$$

where R is response and A, B, and C are the different machining factors, and C, l, m and n are constants.

The general second order polynomial response surface mathematical model, which is given below is considered to determine the parametric influences on the various response criteria.

In RSM, the experiments are performed using CCD to develop a second order model as shown in Eqn (3.4)

$$R = b_0 + b_1 \times A + b_2 \times B + b_3 \times C + b_{11} \times A^2 + b_{22} \times B^2 + b_{33} \times C^2 + b_{12} \times AB + b_{23} \times BC + b_{13} \times AC \quad (3.4)$$

where R is the response and A, B, and C are the different machining factors. The regression coefficients $b_{i=1, 2, 3}$ can be computed by the regression method using experimental results. Significance of factors and their interactions can be computed using statistical analysis. The magnitude of the regression co-efficient is a good indication of the significance of the parameters. The adequacy of the quadratic model was verified using the analysis of variance (ANOVA) technique [Padmanabhan 1991]. Optimum response model and setting of parameters can be produced by using the above response model.

The experimental design, CCD needs minimum and maximum values of input independent variables (Spindle speed, feed rate, and axial depth of cut). In the present work, the minimum and maximum values have been selected after performing preliminary experiments.

Template Table 3.7: Actual coded factors for experiment

Factors	Minimum	Maximum
Coded factor	-1	1
Spindle Speed (rpm)		
Feed Rate (mm/min)		
Depth of Cut (mm)		

In this research, three cutting factors viz., cutting speed, feed rate and the axial depth of cut were considered. When considering these three factors, a total number of 20 sets

runs were needed (Centre points are repeated 6 times to get a good estimate of experimental error) according to CCD. For three cutting parameters, according to Table 3.6, the value of α was 1.682. The selected range for three factors is shown in Table 3.7, and the details of total number of 20 experimental sets shown in Table 3.8. Here -1 indicates minimum value, 0 indicates middle of minimum and maximum, and +1 indicates higher value.

Template Table 3.8: Actual coded factors for the CCD experiment

Standard Order	Spindle Speed (rpm)	Feed Rate (mm/min)	Depth of Cut (mm)	Response
1	0	1.68	0	
2	0	0	0	
3	1	1	-1	
4	0	0	-1.68	
5	-1	1	-1	
6	0	0	0	
7	1	1	1	
8	0	0	0	
9	0	0	0	
10	-1	-1	1	
11	0	0	0	
12	-1	-1	-1	
13	-1	1	1	
14	1	-1	1	
15	1.68	0	0	
16	0	0	0	
17	1	-1	-1	
18	0	1.68	1.68	
19	-1.68	0	0	
20	0	0	0	

3.7.5 Experimental Tests

Machining was carried out by a low speed CNC milling machine and medium speed CNC machine to meet the large range of applications. In this case a low speed range was (1000 rpm to 5000 rpm) chosen for the V-30 vertical milling machine and a medium speed range (10000 rpm to 20000 rpm) was chosen for the V-55 vertical milling machine.

In this study, three controlled inputs: cutting speed, feed rate and depth of cut were selected. These inputs also known as continuous input factors, and can be manipulated as independent variables in the experiment. They give the desired continuous outputs in the form of surface roughness, resultant cutting force and tool wear. The cutting tests were performed on the CNC vertical milling machine without using any cutting fluid i.e. dry cutting. Details of the range of selected cutting parameters for specific tools and work piece (Cutting speed, feed rate and axial depth of cut) based on performance of preliminary experiments are shown in Table 3.9 and 3.10. In the case of low speed CNC machines (V-30), surface roughness of the work piece was measured for all type of tools. Similarly, tool wear was measured only for the case of TiAlN+TiN coated carbide tool insert. The cutting force was not measured due to the unavailability of dynamometer on low speed CNC machine. In the case of high speed CNC machine (V-55), only two tools were used, namely, two flute square end micro grain solid carbide end mill and CBN coated internal grinding tool grit. Surface roughness of the work piece and cutting force were measured for high speed machine.

Table 3.9: Details of range of selected cutting parameters

Work piece: Machinable Glass Ceramic (MGC)					
1. Low spindle speed V-30 CNC vertical milling Machine(up to 8000 rpm) Output: Surface roughness and tool wear 2. High spindle speed V-55 CNC vertical milling Machine (up to 20000 rpm) Output : Surface roughness and resultant cutting force					
Type of tool	Cutting parameters	Low spindle speed CNC (v-30)		High spindle speed CNC(V-55)	
		min	max	min	max
1.Two flute square end micro grain solid carbide end mill	Spindle speed (rpm)	3000	5000	10000	20000
	Feed rate (mm / Min)	10	30	30	90
	Axial depth (mm)	0.1	0.3	0.03	0.05
2. TiAlN+TiN coated carbide tool insert	Spindle speed (rpm)	3000	5000	-	-
	Feed rate (mm / Min)	10	30	-	-
	Axial depth (mm)	0.3	0.5	-	-
3. CBN coated internal grinding tool grit	Spindle speed (rpm)	3000	5000	10000	20000
	Feed rate (mm / Min)	1	3	1	3
	Axial depth (mm)	0.1	0.3	-	-

Table 3.10: Details of range of selected cutting parameters

Work piece: Aluminum nitride ceramic (AlN)					
1. Low spindle speed V-30 series CNC vertical milling Machine(up to 8000 rpm) Output : Surface roughness and tool wear 2. High spindle speed V-55 CNC vertical milling Machine (up to 20000rpm) Output : Surface roughness and resultant cutting force cutting force					
Type of tool	Cutting parameters	Low spindle speed CNC (v-30)		High spindle speed CNC(V-40)	
		min	max	min	max
1.Two flute square end micro grain solid carbide end mill	Spindle speed (rpm)	3000	5000	10000	20000
	Feed rate (mm / Min)	10	30	30	90
	Axial depth (mm)	0.1	0.3	0.03	0.05
2. TiAlN+TiN coated carbide tool insert	Spindle speed (rpm)	3000	5000	-	-
	Feed rate (mm / Min)	10	30	-	-
	Axial depth (mm)	0.1	0.3	-	-
3. CBN coated internal grinding tool grit	Spindle speed (rpm)	3000	5000	10000	20000
	Feed rate (mm / Min)	1	3	1	3
	Axial depth (mm)	0.1	0.3	-	-

3.8 Summary

Work piece Materials: Machinable Glass Ceramic (MGC) and Aluminum Nitride Ceramic (AlN)

Cutting Tools: Two flute square end micro grain solid carbide end mill, carbide tool insert coated with multiple layers of TiAlN and TiNdeposited by the PVD process, and CBN coated internal grinding tool grit

CNC Milling Machine: V-30 CNC vertical milling machine (1000 rpm to 5000 rpm) and V-55 CNC vertical milling machine (10000 rpm to 20000 rpm)

Measuring Parameters for machinability process: Surface roughness, Tool wear and Cutting force

Measuring Equipment: Mitutoyo SJ 301 surface tester, Leica EZ4D stereo microscope and Kistler Dynamometer

Machine Cutting Parameters: Cutting speed, Feed rate and Axial depth of cut

Methodology of Experimentation: The Design of Experiment (DOE) used in this study is Response Surface Methodology (RSM) based on Central Composite Design (CCD)

CHAPTER 4: EXPERIMENTAL RESULTS AND ANALYSIS FOR MACHINABLE GLASS CERAMIC (MGC)

4.1 Introduction

The aim of the present chapter is to examine the performance of the end milling of MGC by using three types of tools, 1) two flute square end micro grain solid carbide end mill 2) TiAlN+TiN coated carbide tool insert and 3) CBN coated internal grinding tool grit . The first and the second tools cover a wide range of cutting shapes in end milling. The third tool is considered as a specimen for the grinding process, this is useful when comparing the end milling and the grinding process. Generally, the grinding process is the main reason for increasing the machining cost. If better surface quality could be achieved by the end milling process alone, the machining cost will be minimized by partially or completely avoiding the grinding process for the finished product.

The surface roughness (Ra) is examined using all three tools, while tool wear is studied only with coated carbide tool insert when machining on low speed machines. The surface roughness and the cutting force are studied with solid carbide end mill and CBN coated grinding tool grit when machining on high speed machines.

In preliminary tests [Appendices A], all three cutting parameters showed significant influence independently or in combination with another parameter. It was therefore decided that examining the simultaneous variations of the three cutting parameters would help to produce better results.

By using the Response Surface Method (RSM), surface roughness, cutting force and tool wear models were developed in terms of cutting speed, feed rate and axial depth of cut. Experiments were conducted separately on low spindle speed and high spindle speed machines. For each case the total numbers of experiments were planned based on the Central Composite Design (CCD).

The Mitutoyo SJ 301 Surface tester was used to measure the Ra of a milled surface. During all milling experiments the surface roughness was recorded at three locations (starting point, middle and end) and the average of the three Ra values was tabulated. The Leica Microscope was used to measure the wear of cutting tools. Measurements were taken at the location where the highest tool wear occurred. A Kistler Dynamometer set 9275 A was used to measure the cutting forces in x, y and z directions, and the resultant cutting force of Fx, Fy and Fz values were recorded. The influencing tendency of each cutting parameter and also the cross effect of three factors were considered for the analysis. The quadratic equation was then proposed for the surface roughness, the tool wear and the cutting force using the RSM. Analysis of Variance (ANOVA) was used to verify the adequacy of the model.

4.2 Results of Experiments Conducted on a Low Spindle Speed (CNC V-30) Vertical Milling Machine

The following sections describe the effect of cutting parameters, cutting speed, feed rate and axial depth of cut on surface roughness and tool wear, using three types of tools. The Leadwell V-30 series CNC vertical milling machine (Maximum capacity of spindle speed: 8000 rpm) was used for these experiments.

4.2.1 Surface Roughness Analysis by using a Two Flute Square End Micro Grain Solid Carbide End Mill

The influence of the cutting speed (A), feed rate (B) and axial depth of cut (C) on the surface roughness (Ra) was studied by using a two flute square end micro grain solid carbide end mill. The ranges of cutting parameters were selected on the basis of preliminary tests [Appendix A], capacity and limiting cutting conditions of the tool and a low spindle speed machine. The three machining parameters and their selected ranges are shown in Table 4.1.

Table 4.1: Range of cutting parameters for experiment

Factors	Minimum value	Maximum value
Coded factor	-1	1
Spindle Speed (rpm)	3000	5000
Feed Rate (mm/min)	10	30
Depth of Cut (mm)	0.1	0.3

The cutting conditions of a total of 20 runs (14+6 repeated at the center) according to Table 3.11, were generated relying on the RSM, using the CCD as shown in Fig 4.1. The details of 20 cutting tests and the measured surface roughness values are indicated in Table 4.2.

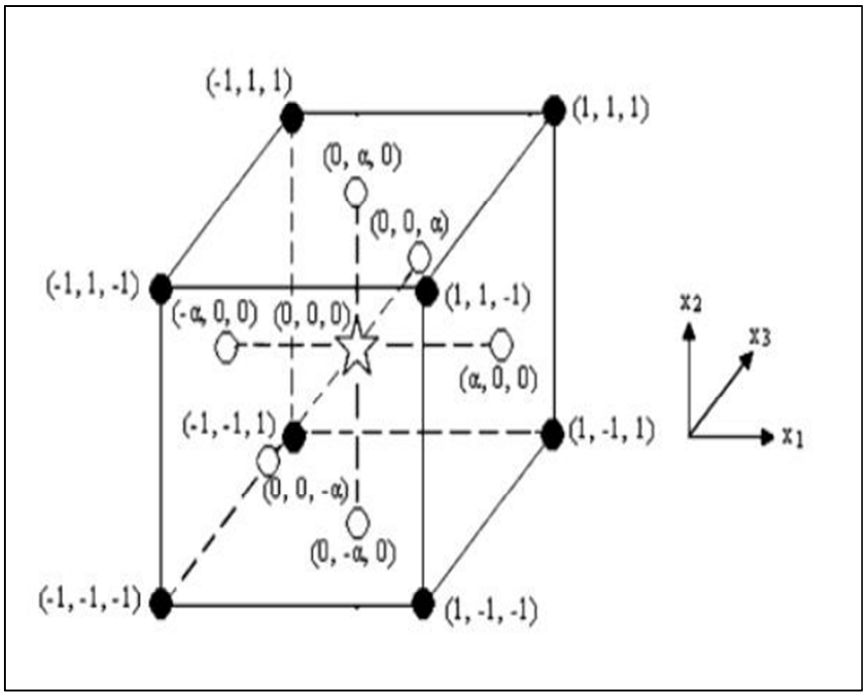

Fig 4.1: Generation of a CCD for three factors [Sahoo et al. 2011]

Table 4.2 Surface roughness values for total number of experiments

Standard Order	Cutting Speed (rpm)	Feed Rate (mm/min)	Depth of Cut (mm)	Surface Roughness (μm)
1	4000	36.81	0.2	0.73
2	4000	20	0.368	0.76
3	4000	20	0.2	0.55
4	3000	30	0.3	0.65
5	2318	20	0.2	0.49
6	5000	30	0.1	0.61
7	4000	20	0.2	0.51
8	3000	10	0.1	0.52
9	4000	20	0.031	0.49
10	5000	10	0.1	0.5
11	4000	20	0.2	0.55
12	3000	30	0.1	0.56
13	4000	20	0.2	0.54
14	4000	20	0.2	0.52
15	4000	3.18	0.2	0.5
16	5000	10	0.3	0.61
17	3000	10	0.3	0.54
18	5681	20	0.2	0.57
19	4000	20	0.2	0.55
20	5000	30	0.3	0.81

After conducting 20 runs of experiments, surface roughness (Ra) readings were used to find the parameters appearing in the second order model in Eqn (4.1). The method of least square was used to calculate these parameters by using the design expert software. In this study A (spindle speed), B (feed rate) and C (axial depth of cut)

were the main factors considered for the experiment of Ra; the combined effect of the three factors was also considered. The relation between cutting parameters and surface roughness was generated by the quadratic equation. Ra was measured at three locations (starting, middle and end) and the average Ra was considered for analysis of the results. Based on the results the second order quadratic equation for predicting the Ra is expressed in Eqn (4.2):

$$R_a = b_0 + b_1 \times A + b_2 \times B + b_3 \times C + b_{11} \times A^2 + b_{22} \times B^2 + b_{33} \times C^2 + b_{12} \times AB + b_{23} \times BC + b_{13} \times AC + b_{32} \times BC + b_{31} \times AC \quad (4.1)$$

where R_a is the output response and A, B, and C are the different cutting parameters. The b values i.e. b_0, b_1, b_2, b_{12} are to be estimated using experimental data by the regression method. The magnitude of the regression co-efficient is a good indication of the significance of the parameters.

The surface roughness (R_a) equation can be written in terms of actual factors as shown below:

$$R_a = 0.84112 - 5.36743 \times 10^{-5} \times A - 0.017448 \times B - 2.06629 \times C + 2.0 \times 10^{-6} \times A \times B + 2.5 \times 10^{-4} \times A \times C + 0.020 \times B \times C - 9.295 \times 10^{-1} \times A^2 + 2.91225 \times 10^{-4} \times B^2 + 3.2658 \times C^2 \quad (4.2)$$

The adequacy of the quadratic model was verified using the analysis of variance (ANOVA) technique shown in Table 4.3. As per this technique, the calculated value, "F", of the model developed does not exceed the standard tabulated value of "F" for a desired level of confidence of 95%.The results show that the second order model is adequate with 95% confidence intervals (the Model P-value < 0.05). In this case B, and C are significant model terms.

Table 4.3: ANOVA table for the response surface quadratic model

Source	Sum of Squares	DOF	Mean Square	F-value	P-value	
Model	*0.16*	*9*	*0.017*	*35.39*	*<0.0001*	*significant*
A-Cutting Speed	0.011	1	0.011	23.12	0.0007	
B-Feed Rate	0.053	1	0.053	106.53	*<0.0001*	
C-Depth of Cut	0.056	1	0.056	113.50	*<0.0001*	
AB	3.2×10^{-3}	1	3.2×10^{-3}	6.49	0.0290	
AC	5.0×10^{-3}	1	5.0×10^{-3}	10.14	0.0097	
BC	3.2×10^{-3}	1	3.2×10^{-3}	6.49	*0.0290*	
A^2	1.245×10^{-5}	1	1.245×10^{-5}	0.025	0.08769	
B^2	0.012	1	0.012	24.80	0.0006	
C^2	0.015	1	0.015	31.18	*0.0002*	
Residual	4.929×10^{-3}	10	4.929×10^{-4}			
Lack of Fit	3.396×10^{-3}	*5*	6.792×10^{-4}	*2.21*	*0.2017*	*not significant*
Pure Error	1.533×10^{-3}	5	3.067×10^{-4}			
Cor Total	0.16	19				

Fig 4.2(a) gives the influencing effects of each cutting parameter on the surface roughness. The surface roughness, Ra, increases with increasing the cutting speed, feed rate and axial depth of a cut. The rate of surface roughness increases in linear formation in the case of cutting speed (A), and it is quadratic in the case of feed rate (B) and axial depth of the cut (C).

Figure 4.2(b-d) presents the interaction effect of cutting parameters on the surface roughness. These figures show a general trend where an increase of any one cutting parameter leads to an increase in the surface roughness. The most interesting point is observed in Fig 4.2 (b-c); the Ra is almost the same at low feed rate and low axial depth of cut, regardless of the variation of the cutting speed value.

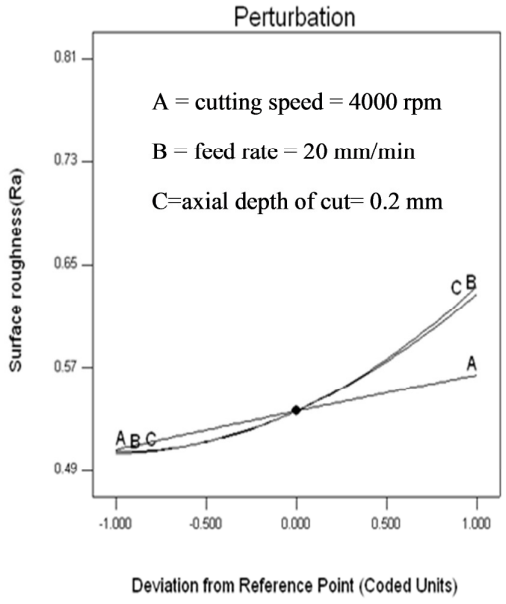

Fig 4.2(a): Perturbation plot for Ra

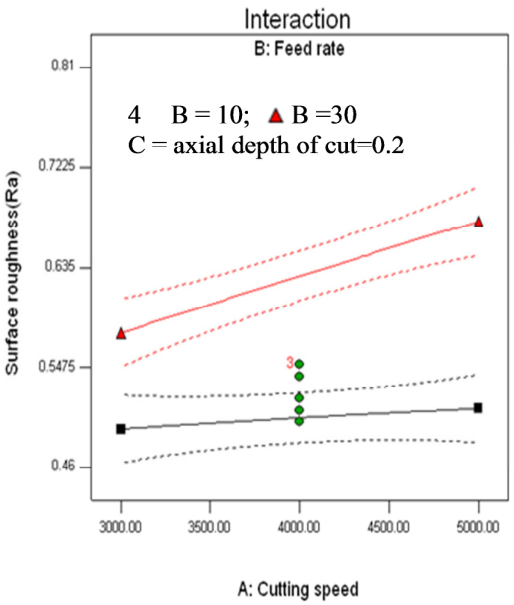

Fig 4.2(b): Interaction plot for A and B

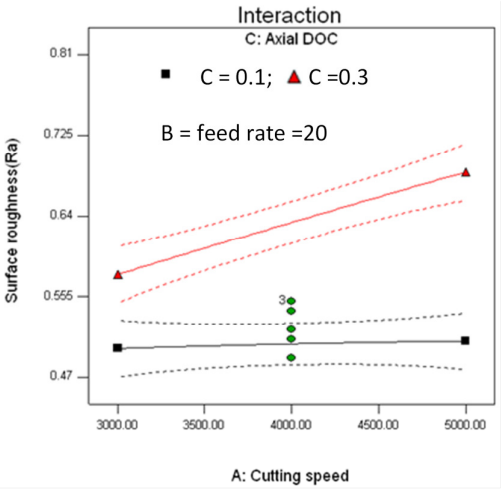

Fig 4.2(c): Interaction plot for A and C

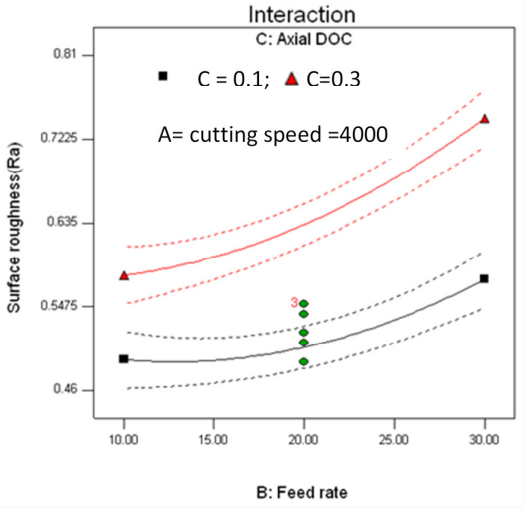

Fig 4.2(d): Interaction plot for B and C

The effect of the cutting parameters on the surface roughness in 3-D and contour plots is shown in Fig 4.3(a-d).

Figure 4.3(a) is constructed by plotting the cutting speed (A) and feed rate (B) against the surface roughness at the particular axial depth of cut (C) 0.2mm. It shows that the surface roughness increases with increases in cutting speed, feed rate, and the axial depth of cut. In this case one can observe that the surface roughness increases by increasing the cutting speed, but it differs from the experimental results applicable to metals [Alauddin et al. 1995, Suresh et al. 2006, Mansour et al. 2002, Ozcelik and Bayramoglu 2006]. During the cutting process ceramic material chips are produced in powder form, whereas metallic materials are produced in the form of long chips. At high speed, powder form material may be stuck on the surface of the tool or on the surface of the work piece material due to high heat generation; this may be result in large surface roughness.

Figure 4.3(b) is depicts the cutting speed (A) and the axial depth of cut (C) plotted against the surface roughness at a given feed rate (B) 20 mm/min. Here, surface roughness increases with increase in the axial depth of cut and, this increase is rapid at high cutting speeds.

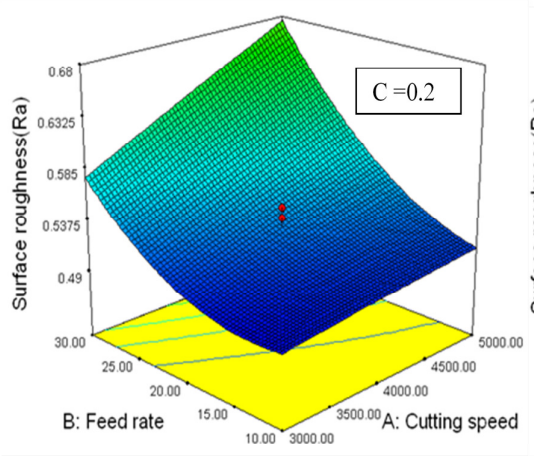

Fig 4.3(a): 3-D plot for A and B

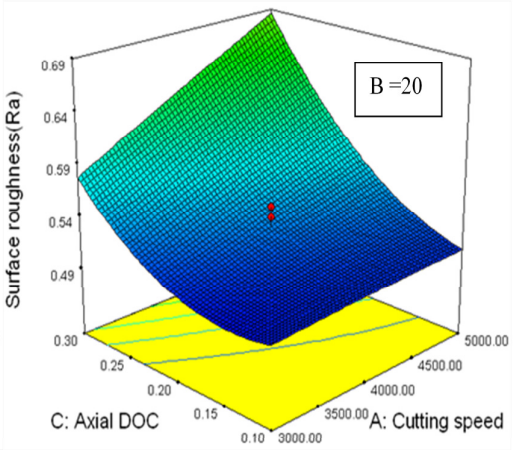

Fig 4.3(b): 3-D plot for A and C

Figures 4.3(c-d) shown, the feed rate (B) and the axial depth of cut (C) against the surface roughness at a cutting speed (A) of 4000 rpm. Maximum surface roughness value appeared at the maximum values of the cutting parameters and, the rate of

increase is the same for both the feed rate and the axial depth of cut. Based on the experimental results the axial depth of cut and the feed rate are the most influenced factors for the identified range of the cutting parameters.

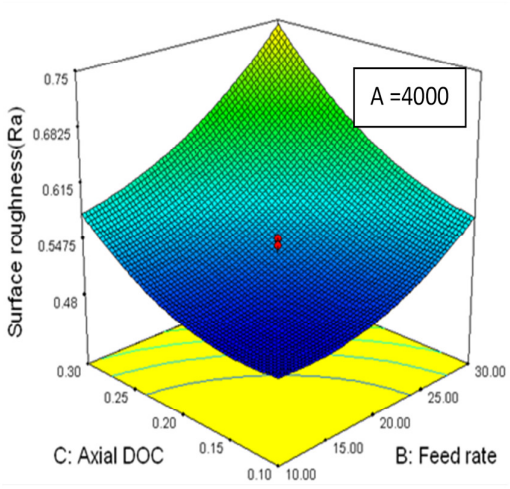

Fig 4.3(c): 3-D surface plot for B and C

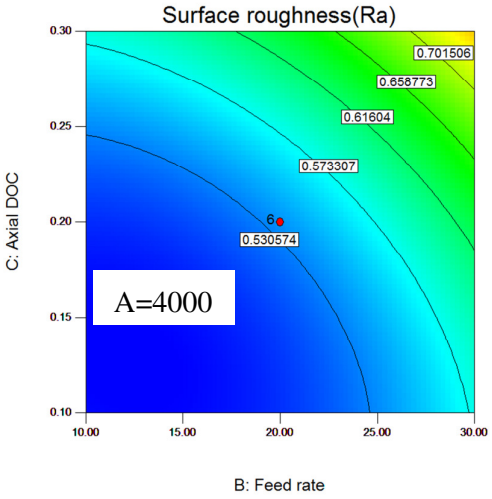

Fig 4.3(d): Contour plot for B and C

The developed quadratic model Eqn (4.2) was used for further optimization of the operating cutting parameters for the minimum surface roughness. Experimental test was conducted for the selected combination (39 solutions were obtained). Experimental test results show that the surface roughness value of 0.4520 µm was close to the predicted surface roughness value of 0.4790 µm for the selected combination of 4933 rpm (cutting speed), 11.5mm/min (feed rate), and 0.12 mm (axial depth of cut).

From the results above, one can conclude that the feed rate, axial depth of cut, and the combined effect are the most influential factors for the selected range of the cutting parameters. The effect of the cutting speed is not so significant and it is advisable to check its effect beyond the selected range. These results confirm that it is essential to select the low cutting parameters within the selected range, in order to produce smooth surface finish.

4.2.2 Surface Roughness Analysis using a Coated Carbide Tool insert:

The influence of the cutting speed, feed rate, and axial depth of cut on the surface roughness was studied by using a TiAlN and TiN coated carbide tool insert.

The independent variables are coded in Table 4.4, taking into consideration the preliminary tests, tool limitation and capacity of the milling machine

Table 4.4: Range of cutting parameters for the experiment

Factors	Minimum	Central	Maximum
Coded factor	-1	0	1
Cutting speed (rpm)	3000	4000	5000
Feed Rate (mm/min)	10	20	30
Depth of Cut (mm)	0.3	0.4	0.5

Table 4.5 shows the results of the 20 experiments in this study. During all the 20 experiments the surface roughness was recorded at three locations (starting point of slot, middle, and end) on the work piece. The average values of the Ra are displayed in the Table 4.5. The tool wear was measured at the location where the highest tool wear had occurred.

The surface roughness and the tool wear readings were used to develop the quadratic Eqn (4.1). To develop this equation, the regression analysis method was used with the help of the design expert software. For predicting the surface roughness (Ra), the quadratic Eqn 4.3 is presented.

$$R_a = 0.65045 - 7.41323 \times 10^{-5} \times A + 0.011447 \times B + 1.73302 \times C + 1.375 \times 10^{-6} \times A \times B - 3.25 \times 10^{-4} \times A \times C - 0.01825 \times B \times C + 1.9048 \times 10^{-8} \times A^2 - 2.341 \times 10^{-5} \times B^2 + 5.069 \times C^2 \quad (4.3)$$

Table 4.5: Surface roughness values for total number of experiments

Standard Order	Cutting Speed (rpm)	Feed Rate (mm/min)	Depth of Cut (mm)	Surface Roughness (µm)	Tool wear (µm)
1	5000	30	0.3	0.543	51.23
2	4000	20	0.4	0.481	38.4
3	3000	10	0.3	0.324	28.57
4	4000	20	0.4	0.453	44.12
5	5000	30	0.5	0.651	68.32
6	5000	10	0.3	0.424	58.56
7	4000	20	0.4	0.491	42.83
8	5681	20	0.4	0.412	63.12
9	4000	20	0.231	0.427	23.3
10	2318	20	0.4	0.528	25.22
11	4000	36.8	0.4	0.583	59.9
12	4000	20	0.4	0.416	49.9
13	4000	3.18	0.4	0.236	46.33
14	5000	10	0.5	0.412	63.5
15	3000	30	0.5	0.626	46.42
16	4000	20	0.5681	0.692	64.13
17	3000	30	0.3	0.581	31.97
18	3000	10	0.5	0.635	51.55
19	4000	20	0.4	0.382	46.23
20	4000	20	0.4	0.426	44.12

Table 4.6: ANOVA table for response surface quadratic model

Source	Sum of Squares	DOF	Mean Square	F-value	P-value	
Model	*0.22*	*9*	*0.025*	*6.54*	*0.0035*	*significant*
A-Cutting Speed	8.027×10^{-3}	1	8.027×10^{-3}	2.11	0.1774	
B-Feed Rate	0.1	1	0.1	27.18	*0.0004*	
C-Depth of Cut	0.059	1	0.059	15.48	*0.0028*	
AB	1.513×10^{-3}	1	1.513×10^{-3}	0.40	0.5429	
AC	8.450×10^{-3}	1	8.450×10^{-3}	2.22	0.1674	
BC	2.664×10^{-3}	1	2.664×10^{-3}	0.70	*0.4227*	
A^2	5.229×10^{-3}	1	5.229×10^{-3}	1.37	0.2687	
B^2	7.9×10^{-5}	1	7.9×10^{-5}	0.021	0.8884	
C^2	0.037	1	0.037	9.71	*0.0109*	
Residual	0.038	10	3.812×10^{-3}			
Lack of Fit	0.030	*5*	5.909×10^{-3}	*3.45*	*0.1003*	*not significant*
Pure Error	8.574×10^{-3}	5	1.715×10^{-3}			
Cor Total	0.26	19				

The ANOVA Table 4.6 shows that the feed rate and the axial depth of cut (Large F-value) have the most significant effect on the surface roughness.

The perturbation plot results presented in Fig 4.4(a) show that the surface roughness decreases with an increase in the cutting speed, and increases as the feed rate and axial depth of cut increases. These tendencies in behavior of the cutting parameters are very similar to end milling of metallic materials [Benardos and Vosniakos 2003, Bao et al. 2000, Chee et al. 2006, Newby et al. 2007, and Kang et al. 2007].

The analysis continues with the interaction and 3-D figures that show the effect of each cutting parameter and the interaction effect of cutting parameters on the response surface roughness. The interaction effect of the cutting parameters is shown in Fig 4.4(b-d); the surface roughness is high at a high feed rate of 30 mm/min and a high axial depth of cut at 0.5 mm.

Fig 4.4(b) shows that the surface roughness decreases with an increase of the cutting speed, and this trend is similar to both minimum (10 mm/min) and maximum values (30 mm/min) of the feed rate. From this figure, one can observe that the surface roughness is high at a high feed rate (feed rate 30 mm/min) and a low cutting speed (3000 rpm) at a given axial depth of cut 0.4 mm. Better surface roughness i.e. low value was obtained at low feed rate (10 mm/min) and high cutting speed (5000 rpm).

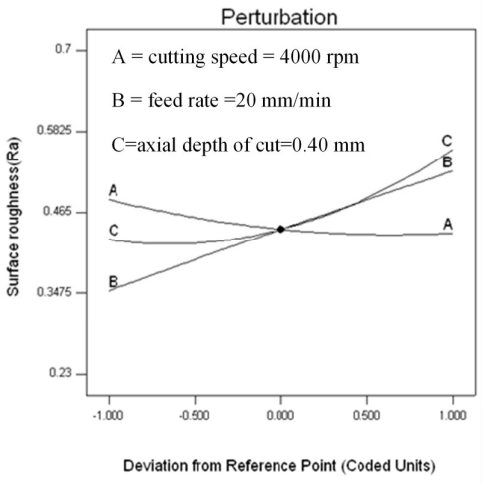

Fig. 4.4(a): Perturbation plot for Ra

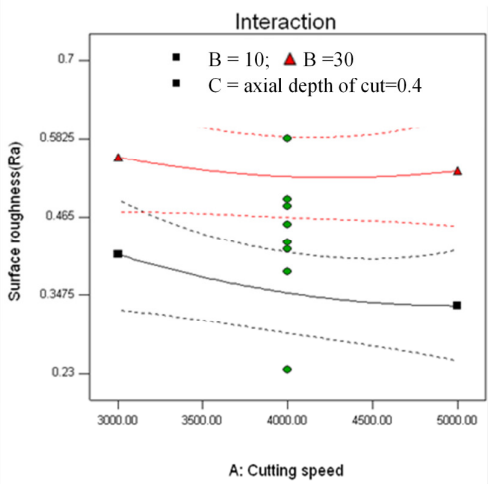

Fig 4.4(b): Interaction plot for A and B

At a low axial depth of cut (up to 0.4 mm), an increase in the cutting speed causes a reduction of the surface roughness. On the contrary, an increase in the axial depth of cut results in an increase in surface roughness. Hence, a better surface roughness is obtained at a combination of a low axial depth of cut and a high cutting speed. However in order to reduce machining time (to achieve a high production rate) the axial depth of cut should be as high as possible

Fig 4.4 (d) shows the feed rate B and the axial depth of cut C against the surface roughness at a particular cutting speed of 4000 rpm. The figure shows that the low surface roughness is observed at a low feed rate (10 mm/min) and a low axial depth of cut (0.3 mm), for a selected cutting speed 4000 rpm.

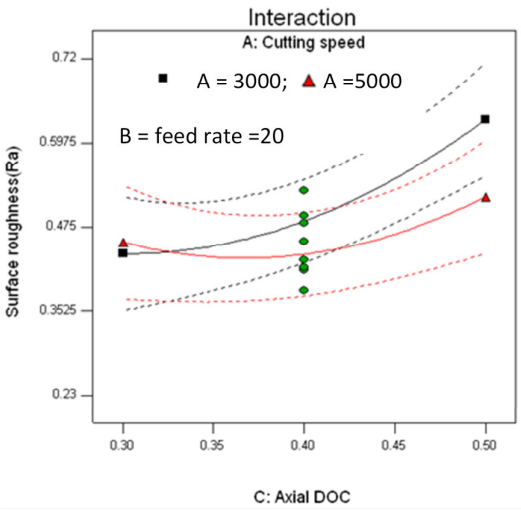

Fig 4.4(c): Interaction plot for C and A

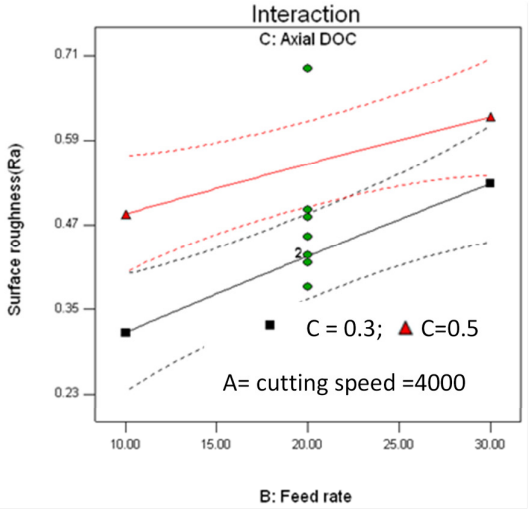

Fig 4.4(d): Interaction plot for B and C

The combined effects of the cutting parameters on the surface roughness in 3-D and contour plots are shown in Fig 4.5(a-d). Figure 4.5(a) demonstrates a rapid increase on the surface roughness with an increase in feed rate at a given axial depth of cut of 0.4mm. A similar phenomenon was observed in Fig 4.5(b) between the axial depth of cut and the cutting speed at the common feed rate of 20 mm/ min.

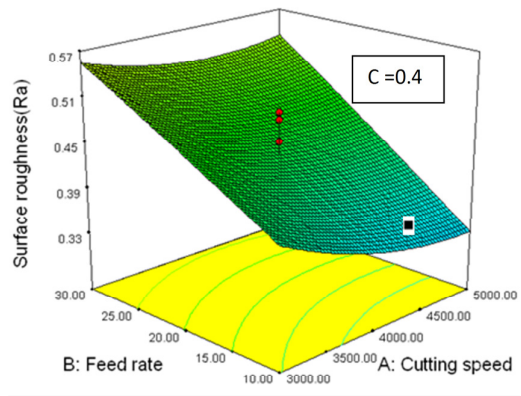

Fig 4.5(a): 3D plot for A and B

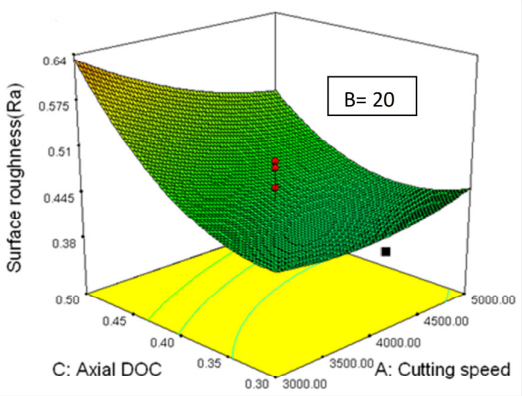

Fig 4.5(b): 3D plot for A and C

3-D and contour plots in Fig 4.5(c-d) demonstrate an increase in the surface roughness with an increase of the feed rate and axial depth of cut at a given value of cutting speed 4000 rpm. This shows that the feed rate and axial depth of cut are the

most significant parameters in surface roughness for this case. The minimal surface roughness is achievable with the cutting speed as high as 5000 rpm, along with the least feed rate of 10 mm/min and a moderate depth of cut of 0.4 mm.

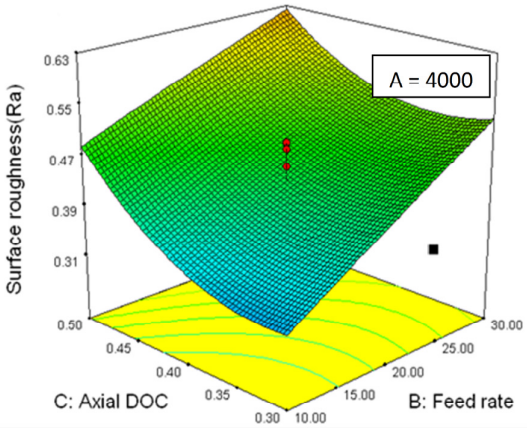

Fig 4.5(c): 3D plot for B and C

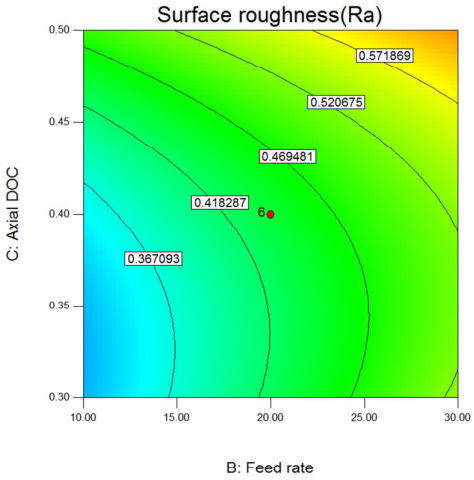

Fig 4.5(d): Contour plot for B and C

The quadratic model, Eqn (4.3), was used for optimization of the cutting parameters. Twenty three solutions were obtained and the minimum surface roughness (0.3136 µm) was predicted for the selected combination of 4398 rpm (cutting speed), 10 mm/min (feed rate), and 0.33 mm (axial depth of cut). An experimental test was conducted on the selected combination of parameters. The experimental value of 0.358 µm was very close to the predicted surface roughness value, 0.3136 µm.

From the experimental studies above, one can conclude that the feed rate and axial depth of cut are the most significant factors, in the surface roughness model for the case of coated carbide tool insert. A minimal surface roughness value is obtained with the highest cutting speed along with least feed rate and a moderate depth of cut for the studied range of cutting parameters. These results are very similar to those in end milling of metallic materials. However, in order to reduce machining time and to increase the material removal rate, both the feed rate and axial depth of cut should be as high as possible.

4.2.3 Tool Wear Analysis by using Carbide Tool inserts Coated with Combined Layers of TiAlN and TiN

The Leica EZ4D Stereomicroscope (shown in Fig 3.15) was used to measure the wear of a coated carbide tool insert. After each cutting process, the cutting tool insert was examined for tool wear, with measurements taken at the location where the highest wear had occurred. Tool wear results are represented for 20 cutting conditions in Table 4.6, along with the surface roughness values. Based on the results the second order tool wear model was developed to adequately express the relationship between the tool wear and the cutting parameters. The model parameters Eqn (4.1) have been estimated based on experimental results, with the help of the Design Expert software. The fit and summary tests suggest that the following second order Eqn (4.4) is significant.

$$Tool\ wear = -36.55 + 0.0141 \times A - 1.497 \times B + 129.27 \times C - 9.75 \times 10^{-6} \times A \times B - 0.0192 \times A \times C + 0.452 \times B \times C + 5.670 \times 10^{-7} \times A^2 + 0.0372 \times B^2 + 40.620 \times C^2 \quad (4.4)$$

ANOVA was used to check the adequacy of the developed model shown in Table 4.9. The ANOVA Table 4.7 shows that the model is significant with 95% confidence level ($P < 0.05$). In this case A, C, B^2 are significant model terms. The following results and analysis has been all ready published in the Journal [Reddy et al. 2012]

Table 4.7: ANOVA table for tool wear response quadratic model

Source	Sum of Squares	DOF	Mean Square	F-value	P-value	
Model	*3038.59*	*9*	*337.62*	*11.39*	*0.0004*	*significant*
A-Cutting Speed	1578.84	1	1578.84	53.25	<0.0001	
B-Feed Rate	25.28	1	25.28	0.85	*0.3775*	
C-Depth of Cut	1202.08	1	1202.08	40.54	<0.0001	
AB	0.076	1	0.076	2.5×10^{-3}	0.9606	
AC	29.64	1	29.64	1.0	0.3409	
BC	1.64	1	1.64	0.055	*0.8189*	
A^2	4.63	1	4.63	0.16	0.7009	
B^2	200.46	1	200.46	6.76	0.0265	
C^2	2.38	1	2.38	0.080	*0.7828*	
Residual	296.50	10	29.65			
Lack of Fit	224.39	*5*	44.88	*3.11*	*0.1192*	*not significant*
Pure Error	72.11	5	14.42			
Cor Total	3335.09	19				

Confirmation of all significant and valid data brings the analysis to the next level which is graph based. Figures 4.6(a-c), displays the effect of each cutting parameter against the tool wear. It can be deduced from the Fig 4.6(a-c) that the cutting speed (A) and the axial depth of cut (C) are the most sensitive factors which influence tool wear. This wear increases with an increase in the cutting speed and axial depth of cut.

Interaction plots Fig 4.6(d-f), show the effect of the cutting speed, feed rate and axial depth of cut on the tool wear. Figure 4.6(d) presents the effect of the cutting speed with two different feed rates on the tool wear. There is a general trend of the tool wear increase with cutting speed increase; the effect of the feed rate is, however, negligibly small. Figure 4.6(e) shows the results of the tool wear plotted against axial depth of cut at two different cutting speeds (3000 rpm and 5000 rpm) at a given feed rate of 20 mm/min. Figure 4.6(f) indicates that the feed rate does not have much influence on the tool wear at a given cutting speed. However, the tool wear is large at the axial depth of cut as high as 0.5 mm, irrespective of the other two parameters.

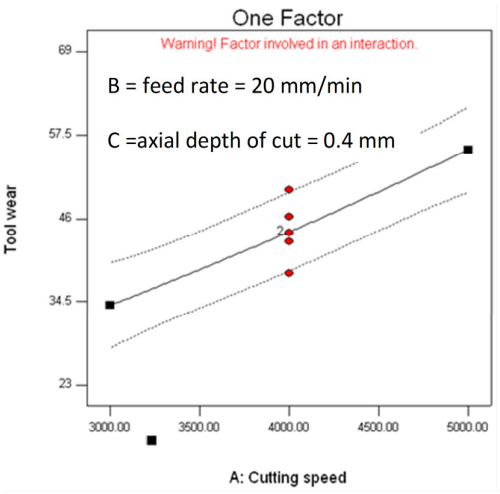

Fig 4.6(a): Surface roughness against A

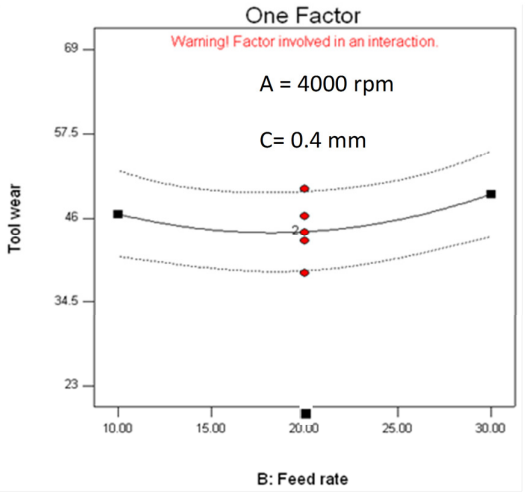

Fig 4.6(b): Surface roughness against B

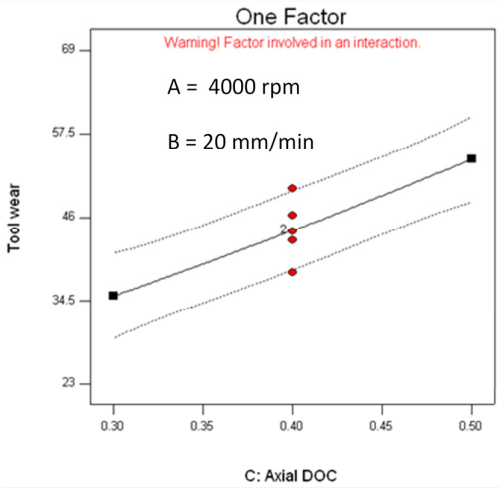

Fig 4.6(c): Surface roughness against C

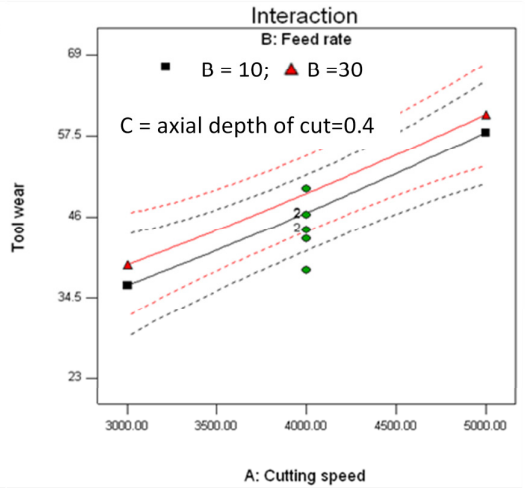

Fig. 4.6(d): Interaction plot for A and B

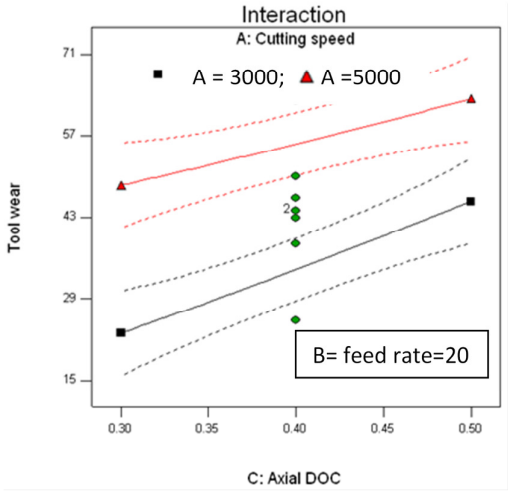

Fig 4.6(e): Interaction plot for A and C

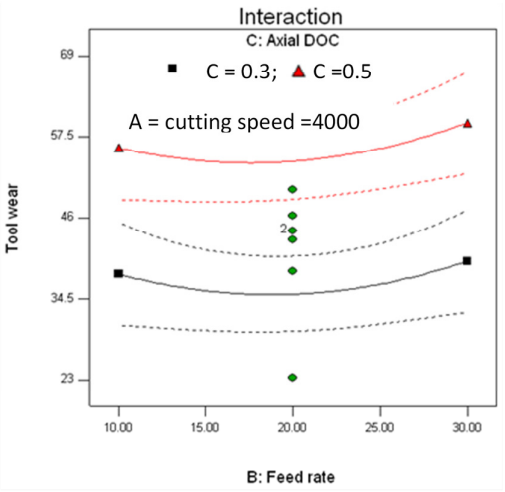

Fig 4.6(f): Interaction plot for B and C

The contour and 3-D graphs developed on the basis of model Eqn (4.4), explain the combined effects of the cutting speed, feed rate and axial depth of cut on the tool wear.

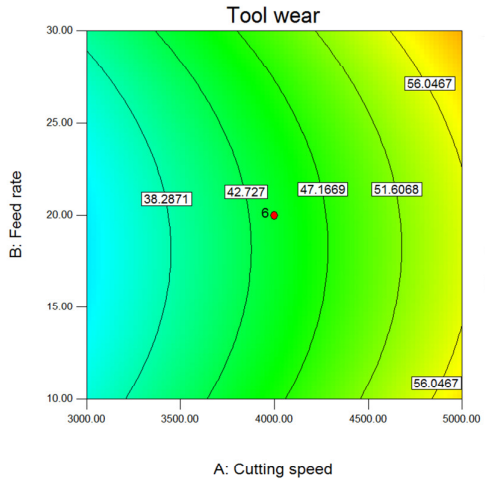

Fig 4.7(a): Contour plot for A and B

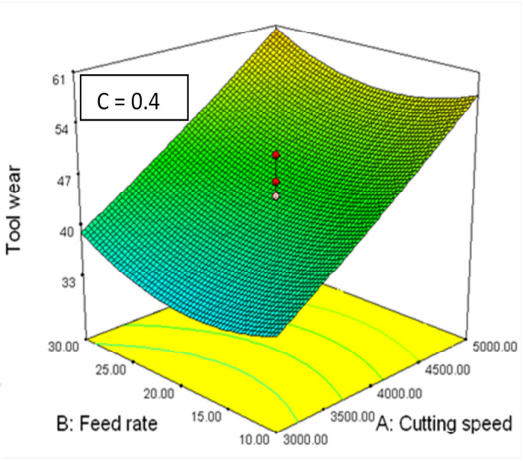

Fig 4.7(b): 3-D tool wear for A and B

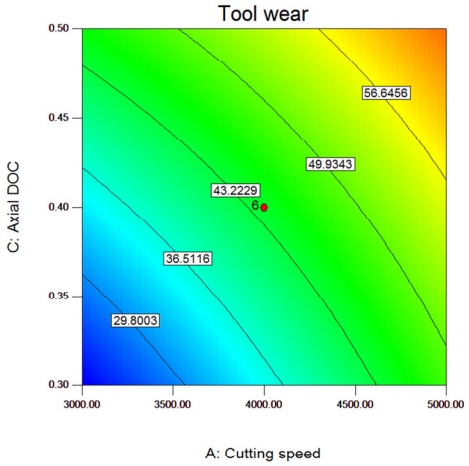

Fig 4.7(c): Contour plot for A and C

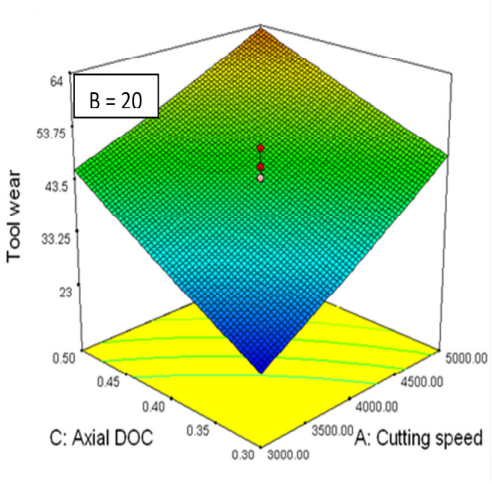

Fig 4.7(d): 3-D tool wear for A and C

From the contour and 3-D plots, Fig 4.7(a-f), it is clear that the cutting speed and axial depth of cut are influential machining parameters on the tool wear. The tool wear increases with an increase in the cutting speed and the axial depth of cut. When the cutting speed and axial depth of cut are higher, the tool is prone to more wear due to high friction temperature. An increase in the feed rate will increase the loading on a cutting tool edge but shorten the machining period, resulting in higher machining

efficiency. A rapid increase in tool wear with increase in the cutting speed and axial depth of cut is observed. Low tool wear value is obtained with a combination of a low cutting speed, low axial depth of cut, and a moderate feed rate.

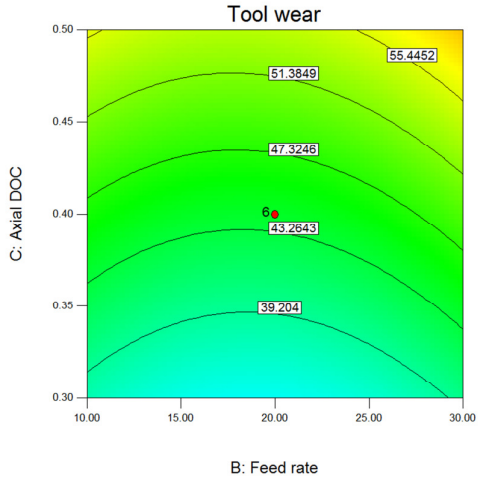

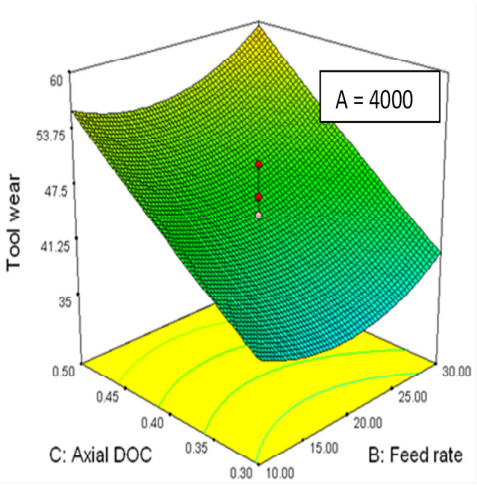

Fig 4.7(e): Contour plot for B and C

Fig 4.7(f): 3-D tool wear for B and C

The developed quadratic model Eqn (4.4) was used for further optimization of the operating cutting parameters for the low tool wear. Experimental tests were conducted for the selected combination (34 solutions were obtained). These tests show that the tool wear value 26.88 µm was close to the predicted tool wear value 23.12 µm for the selected combination of 3007 rpm (cutting speed), 19 mm/min (feed rate), and 0.3 mm (axial depth of cut).

The optimized cutting parameters (10 solutions obtained) based on the minimum surface roughness and minimum tool wear was 3000 rpm (cutting speed), 10 mm/min (feed rate), and 0.3 mm (axial depth of cut) in the studied range of cutting parameters. These cutting parameters combination were tested experimentally (surface roughness value 0.4016 µm and tool wear value 26.10 µm was observed) and were close to the predicted values of surface roughness (0.3419 µm) and tool wear (25.81 µm).

The experimental results reveal that the cutting speed and the axial depth of cut are the most significant terms in the tool wear model for the studied range of conditions. At low values of the cutting speed and the axial depth of cut, one can choose high feed rate B without sacrificing the tool life, thus reducing machining time due to high material removal rate.

4.2.4 Surface Roughness Model using CBN Coated Internal Grinding Tool grit

The end milling operation was carried out under dry conditions using CBN coated internal grinding tool grit on V-30 vertical CNC milling machine. Twenty experiments are conducted by varying all the three identified cutting parameters, based on RSM, to study the influence of these parameters on the surface roughness. The values of the variables are chosen in Table 4.8, taking into consideration, the results of preliminary tests, and the limitation of end milling machine and tool capacity.

Table 4.8: Range of cutting parameters for experiment

Factors	Minimum	Central	Maximum
Coded factor	-1	0	1
Spindle Speed (RPM)	3000	4000	5000
Feed Rate (mm/min)	1	2	3
Depth of Cut (mm)	0.1	0.2	0.3

The surface roughness was measured at three locations (starting point, middle and end) and the average of three surface roughness values was considered for analysis. The details of the cutting conditions and measured surface roughness values are shown in Table 4.9.

Table 4.9: Parameter conditions and surface roughness values

Standard Order	Spindle Speed (rpm)	Feed Rate (mm/min)	Depth of Cut (mm)	Surface Roughness (µm)
1	3000	1	0.1	0.526
2	5000	3	0.3	0.626
3	4000	2	0.031	0.314
4	4000	0.318	0.2	0.314
5	4000	3.68	0.2	0.524
6	5681	2	0.2	0.514
7	4000	2	0.368	0.474
8	4000	2	0.2	0.26
9	5000	1	0.1	0.48
10	3000	3	0.1	0.546
11	3000	1	0.3	0.573
12	4000	2	0.2	0.354
13	5000	3	0.1	0.54
14	4000	2	0.2	0.294
15	4000	2	0.2	0.324
16	5000	1	0.3	0.56
17	3000	3	0.3	0.632
18	2318	2	0.2	0.374
19	4000	2	0.2	0.28
20	4000	2	0.2	0.26

The results were used to develop the second order model using the RSM. For predicting the final surface roughness, Eqn (4.5) is proposed.

$$R_a = 2.0138 - 6.544 \times 10^{-4} \times A - 0.2817 \times B - 2.386 \times C + 5.875 \times 10^{-6} \times A \times B + 4.125 \times 10^{-5} \times A \times C + 0.0562 \times B \times C + 8.081 \times 10^{-8} \times A^2 + 0.0719 \times B^2 + 6.313 \times C^2 \quad (4.5)$$

To verify the adequacy of the second order CCD model, ANOVA was used and the results are shown in the Table 4.10.

Table 4.10: ANOVA table for response surface quadratic model

Source	**Sum of Squares**	**DOF**	**Mean Square**	**F-value**	**P-value**	
Model	*0.24*	*9*	*0.026*	*3.41*	*0.0346*	*significant*
A-Cutting Speed	1.980×10^{-3}	1	1.980×10^{-3}	0.26	0.6245	
B-Feed Rate	0.023	1	0.023	2.94	*0.1173*	
C-Depth of Cut	0.024	1	0.024	3.04	*0.1117*	
AB	2.761×10^{-4}	1	2.761×10^{-4}	0.036	0.8542	
AC	$1.361.0\times10^{-4}$	1	$1.361.0\times10^{-4}$	0.018	0.8973	
BC	2.531×10^{-4}	1	2.531×10^{-4}	0.033	*0.8603*	
A^2	0.094	1	0.094	12.12	0.0059	
B^2	0.075	1	0.075	9.61	0.0112	
C^2	0.057	1	0.057	7.40	*0.0216*	
Residual	0.078	10	7.766×10^{-3}			
Lack of Fit	0.071	*5*	0.014	*10.10*	*0.0120*	*significant*
Pure Error	6.997×10^{-3}	5	1.399×10^{-3}			
Cor Total	0.32	19				

From the ANOVA table the F-value of 3.41 implies that the model is significant ($P< 0.05$). A significant lack of fit indicates that other factors like radial depth of cut, tool geometry, and coolant, which are not considered as variables, may affect the model.

From the perturbation and interaction plots in Fig 4.8(a-d), it can be observed that for all the three cutting parameters (A, B, and C), a move to the right from the middle point results in an increase of the surface roughness (Ra). The opposite phenomenon is observed when moving to the left from the middle point for all cutting parameters. This clearly indicates that the effect of interaction factors is more dominant.

Figure 4.8(b) represents the effect of cutting speed on the surface roughness at two different feed rates, while Fig 4.8(c) represents the effect of the cutting speed on the surface roughness at two different axial depth of cut. Figure 4.8(d) represents the effect of feed rate on the surface roughness at two different axial depth of cut.

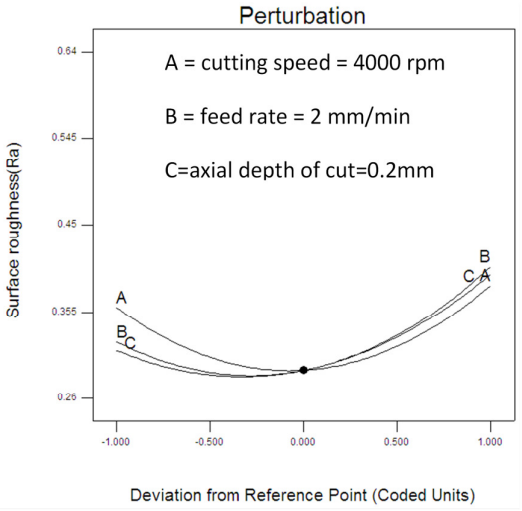

Fig 4.8(a): Perturbation plot for Ra

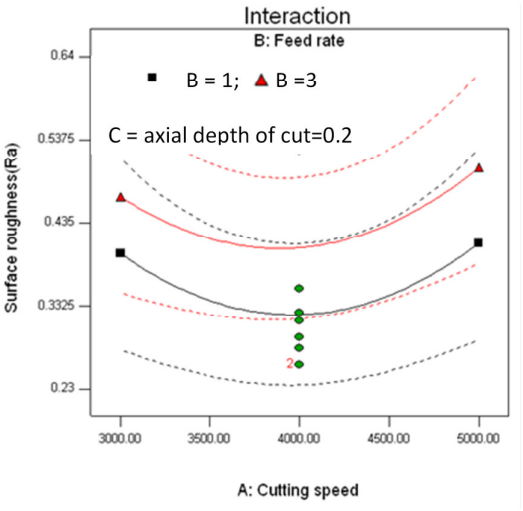

Fig 4.8(b): Interaction plot for A and B

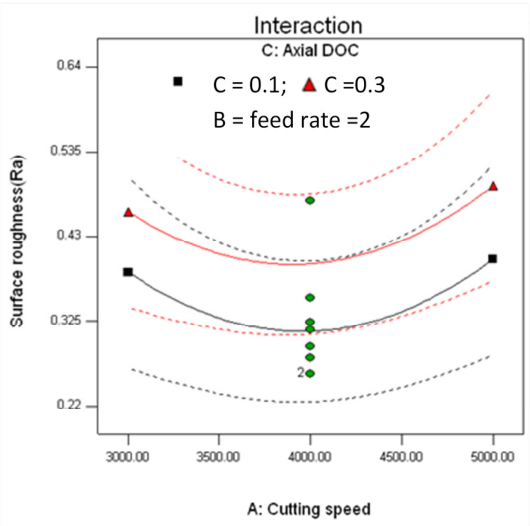

Fig 4.8(c): Interaction plot for A and C

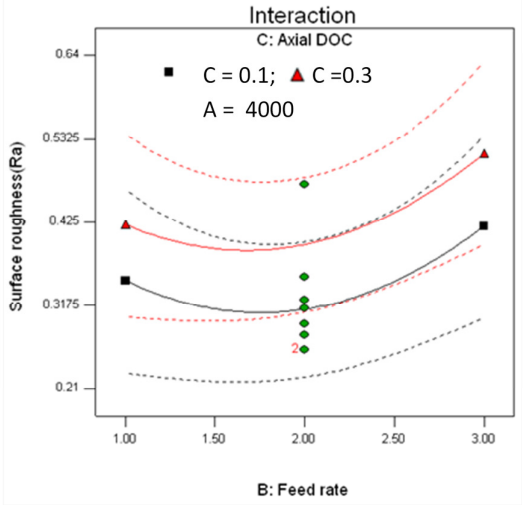

Fig 4.8(d): Interaction plot for B and C

The combined effect of the cutting parameters on the surface roughness can be seen in the 3-D and contour plots in Fig 4.9(a-d). The figures show the effect of the cutting speed, feed rate and axial depth of cut against the surface roughness. The

cutting speed gradient is less compared to the gradient of the feed rate and the axial depth of cut. This shows that the feed rate and the axial depth of cut are the more influential parameters in the surface roughness model. In this case the minimal surface roughness value is obtained at the middle of the selected range of the cutting parameters.

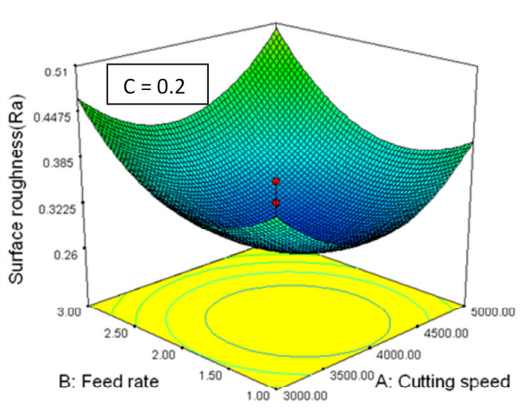

Fig 4.9(a): 3-D Ra plot for A and B

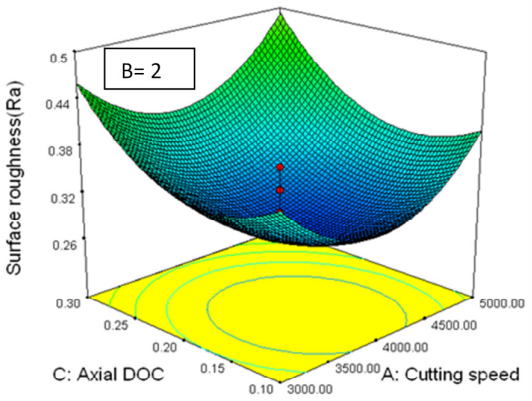

Fig 4.9(b): 3-D Ra plot for A and C

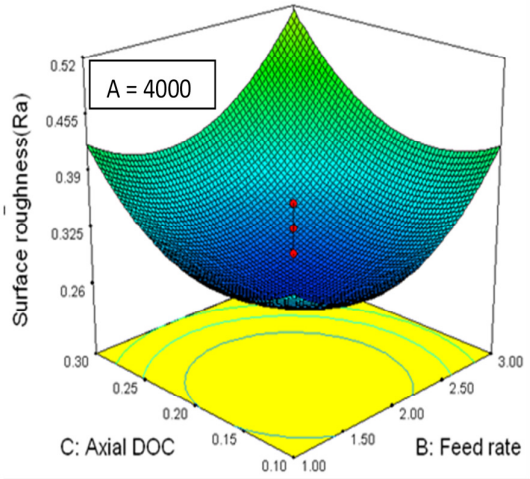

Fig 4.9(c): 3-D Ra plot for B and C

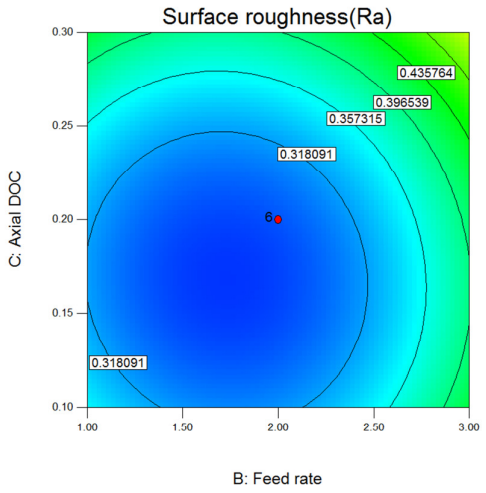

Fig 4.9(d): Contour plot for B and C

The developed quadratic model, Eqn (4.5), was used for further optimization of the operating cutting parameters for the minimum surface roughness. Low surface roughness was predicted (0.2786 µm) at a combination of 3943 rpm (cutting speed), 1.7 mm/min (feed rate), and 0.17 mm (axial depth of cut) in the studied range of

cutting parameters. The experimental value of 0.2733 was very close to the predicted surface roughness value of 0.2786 for the combination of optimized cutting parameters.

From the analysis above, one can conclude that the medium range of the cutting parameters provides an improved surface roughness. ANOVA Table 4.10 shows that the noise factor is significant; in this case, it indicates other factors like radial depth of cut, tool type, and tool geometry (which are not considered as variables) may be significantly influence.

4.3 Experimental Results using a High Spindle Speed Vertical Milling Machine

The cutting experiments were carried out on a V-55 vertical CNC milling machine (spindle speed capacity: 20000 rpm) using the two flute square end micro grain solid carbide end mill and the CBN coated internal grinding tool grit. The effect of the cutting speed, feed rate, and axial depth of cut on the surface roughness and the cutting force were then analyzed. By using RSM, surface roughness and cutting force models were developed, in terms of the cutting speed, feed rate and axial depth of cut. For each case the total numbers of experiments were planned based on Central Composite Design (CCD). According to CCD, twenty tests are required for the three cutting parameters. The Mitutoyo SJ 301 was used to measure the surface roughness (Ra) of a milled surface. During all the milling experiments the surface roughness was recorded at three locations and an average of the three Ra values was calculated. Measurements of the cutting forces in the X, Y and Z directions during the machining process was carried out using Piezoelectric Kistler Dynamometer. The resultant cutting force was used to analyze the effect of the cutting parameters under study.

4.3.1 Surface Roughness Analysis by using Two Flute Square End Micro Grain Solid Carbide End Mill

The cutting experiments were conducted on a V-55 vertical milling machine, using a two flute square end micro grain solid carbide end mill. The independent variables are coded in Table 4.11, taking into consideration the preliminary tests, limitation of cutting tool and capacity of the CNC machine.

Table 4.11: Range of cutting parameters for experiment

Factors	Minimum	Central	Maximum
Coded factor	-1	0	1
Spindle Speed (RPM)	10000	15000	20000
Feed Rate (mm/min)	30	60	90
Depth of Cut (mm)	0.03	0.04	0.05

A total of twenty tests were conducted based on CCD using RSM. The Mitutoyo SJ 301 was used to measure the surface roughness of the milled surface. During all the milling experiments the surface roughness was recorded at three locations and an average of the three Ra values represented in Table 4.12 to establish a surface roughness model. The resultant cutting forces in the X, Y and Z directions during the machining process were measured using a Kistler Dynamometer. The resultant cutting force is represented in Table 4.12 and these were used to establish cutting force model.

Table 4.12: Cutting conditions and output responses

Standard Order	Spindle Speed (rpm)	Feed Rate (mm/min)	Depth of Cut (mm)	Surface Roughness (μm)	Resultant cutting force (N)
1	15000	60	0.0568	0.536	49.20
2	15000	110.4	0.04	0.716	64.98
3	20000	90	0.03	0.633	78.41
4	15000	60	0.04	0.593	45.711
5	10000	30	0.03	0.473	49.66
6	15000	60	0.04	0.58	24.81
7	15000	60	0.023	0.463	54.59
8	15000	9.54	0.04	0.426	30.23
9	20000	90	0.05	0.693	76.81
10	15000	60	0.04	0.526	50.82
11	6591	60	0.04	0.52	20.28
12	20000	60	0.04	0.53	78.60
13	10000	90	0.05	0.693	51.07
14	15000	60	0.04	0.53	54.32
15	20000	30	0.03	0.353	70.34
16	10000	90	0.03	0.653	65.43
17	15000	60	0.04	0.47	53.76
18	10000	30	0.05	0.58	32.97
19	15000	60	0.04	0.581	36.79
20	20000	30	0.05	0.41	80.06

Based on the results, the fit and summary test suggests the following quadratic equation, Eqn (4.6), for predicting the surface roughness.

$$R_a = 0.25110 - 6.075 \times 10^{-6} \times A - 1.151 \times 10^{-3} \times B + 13.044 \times C + 2.25 \times 10^{-7} \times A \times B - 7.5 \times 10^{5} \times A \times C - 0.0267 \times B \times C - 3.231 \times 10^{-1} \times A^2 + 1.768 \times 10^{-5} \times B^2 - 93.588 \times C^2 \quad (4.6)$$

where A is the cutting speed, B is the feed rate and C is the axial depth of cut

Table 4.13: ANOVA table for response surface quadratic model

Source	Sum of Squares	DOF	Mean Square	F-value	P-value	
Model	*0.17*	*9*	*0.018*	*8.74*	*0.0011*	*significant*
A-Cutting Speed	7.396×10^{-3}	1	7.396×10^{-3}	3.52	0.0903	
B-Feed Rate	0.13	1	0.13	62.85	*<0.0001*	
C-Depth of Cut	0.011	1	0.011	5.21	*0.0456*	
AB	9.113×10^{-3}	1	9.113×10^{-3}	4.33	0.0641	
AC	1.125×10^{-4}	1	1.125×10^{-4}	0.053	0.8218	
BC	5.120×10^{-4}	1	5.120×10^{-4}	0.24	*0.6324*	
A^2	5.907×10^{-4}	1	5.907×10^{-4}	0.28	0.6077	
B^2	3.683×10^{-3}	1	3.683×10^{-3}	1.75	0.2152	
C^2	1.273×10^{-3}	1	1.273×10^{-3}	0.61	*0.4547*	
Residual	0.021	10	2.104×10^{-3}			
Lack of Fit	0.010	*5*	2.008×10^{-3}	*0.91*	*0.5384*	*Not significant*
Pure Error	0.011	5	2.199×10^{-3}			
Cor Total	0.19	19				

Table 4.13 shows that the second order model is adequate with 95% confidence intervals (Model *P*-Value 0.0011 < 0.05, implies that the selected model is significant). In this case B, and C are significant model terms. The F value of 62.85 means that feed rate B has the strongest effect on the surface roughness.

The perturbation plot in Fig 4.10 (a) shows the effect of the cutting parameters on the surface roughness. One can observe that the feed rate is the most influential factor for the surface roughness.

The variations of the surface roughness in relation to two different feed rates are shown in Fig 4.10(b). This figure shows that for a given axial depth of cut, an increase in the cutting speed results in an increase in the value of the surface roughness at a feed rate as high as 90 mm/min. An opposite trend is observed when the feed rate is as low as 30 mm/min. The surface roughness decreases rapidly by increasing the cutting speed. In contrast, at a high feed rate, the surface roughness increases slightly with the increasing cutting speed. One can then conclude that a good surface roughness is obtained at a low feed rate.

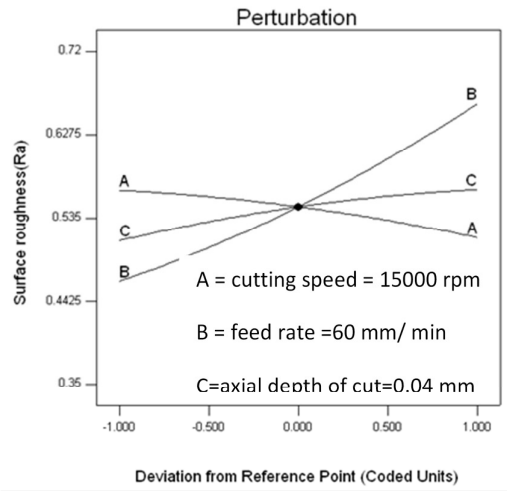

Fig 4.10(a): Perturbation plot for Ra

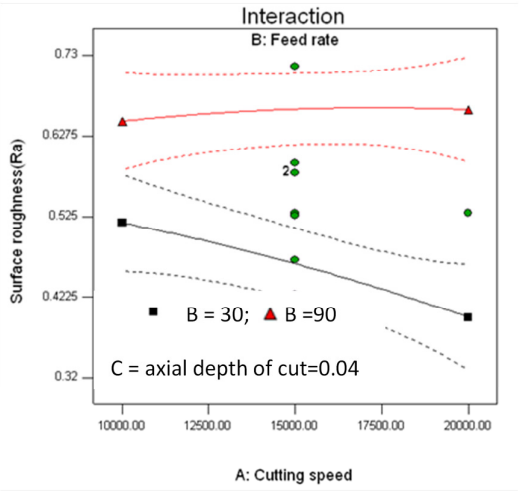

Fig 4.10(b): Interaction plot for A and B

From the interaction plot in Fig 4.10(c), one can see that the tendencies of the surface roughness are very similar at both the low and high axial depth of cut values against the cutting speed. The surface roughness value decreases with increases in the cutting speed. The value of surface roughness is high at the axial depth of cut as high as 0.05 mm for a constant feed rate 60 mm/min.

Figure 4.10(d) shows the effects of two different axial depths of cut at different feed rates on the surface roughness. In this case, the surface roughness value increases with an increase of the feed rate at a constant cutting speed 15000 rpm.

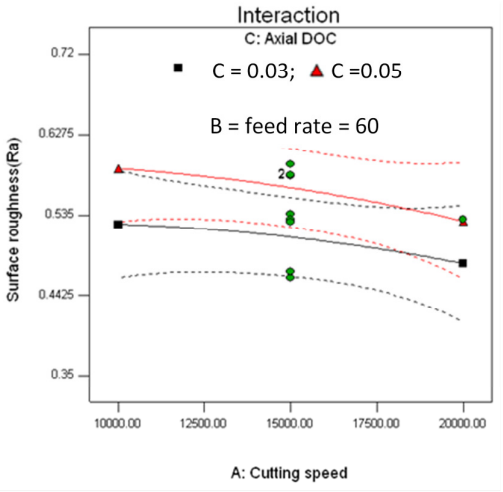

Fig 4.10(c): Interaction plot for A and C

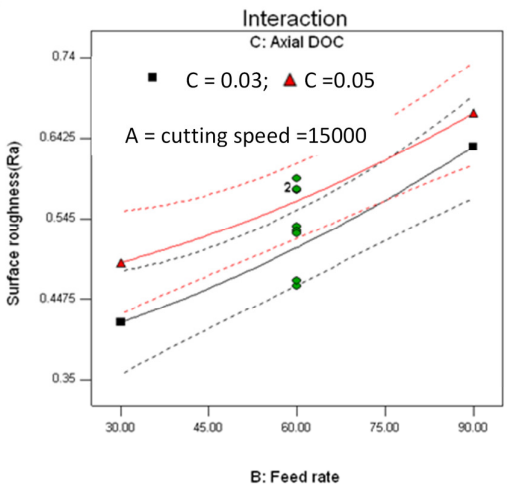

Fig 4.10(d): Interaction plot for B and C

The surface roughness plots are presented in 3-D diagrams in Fig 4.11(a-f). The combined effect of input parameters on the response can be identified here. Figure 4.11(b) is constructed by plotting the cutting speed A and feed rate B against the surface roughness Ra for a given axial depth of cut 0.04 mm. The figures show that a low surface roughness is obtained at feed rates as low as 30 mm/ min and a cutting speed as high as 20000 rpm.

Figures 4.11(c-e) are constructed by plotting the cutting speed A and axial depth of cut C against the surface roughness at three different feed rates 30, 60 and 90 mm/min. It is observed from these figures that the surface finish decreases with decrease in the cutting speed and axial depth of cut at a given feed rate. However, the surface roughness increases with the increase of feed rate (90 mm /min). Based on the results the feed rate is the most influential factor for the studied range of the cutting parameters. These results are consistent with the theories of cutting in end milling of metallic materials [Alauddin et al. 1998, Suresh et al. 2006, Chee et al. 2006, Newby et al. 2007, and Kang et al. 2007].

Figure 4.11(f) is constructed by plotting feed rate B and the axial depth of cut C against surface roughness for the cutting speed of 15000 rpm. It shows that a higher surface roughness value is observed for the combination of a feed rate of 90 mm/min and the axial depth of cut of 0.05 mm.

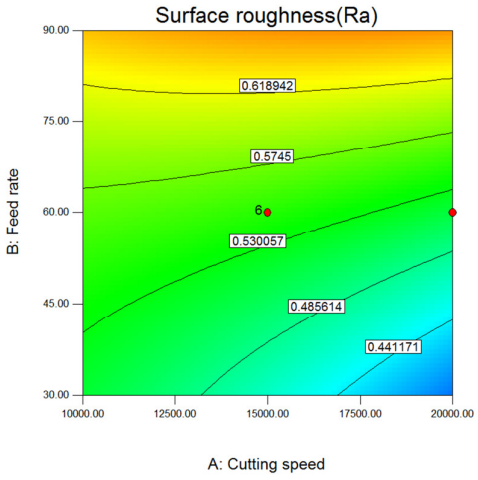

Fig 4.11(a): Contour plot for A and B

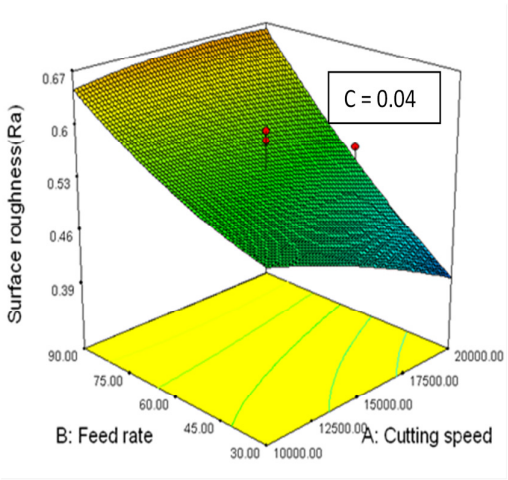

Fig 4.11(b): 3-D Ra plot for A and B

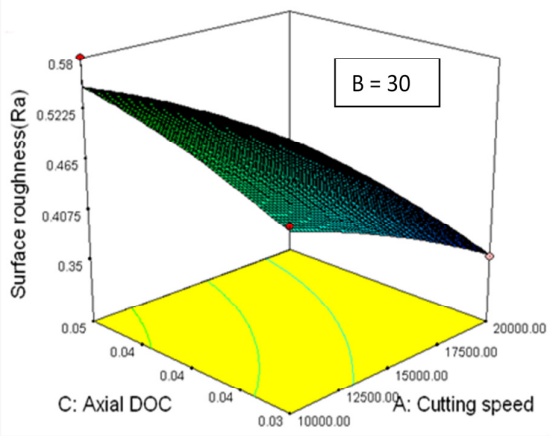

Fig 4.11(c): 3-D Ra plot for A and C

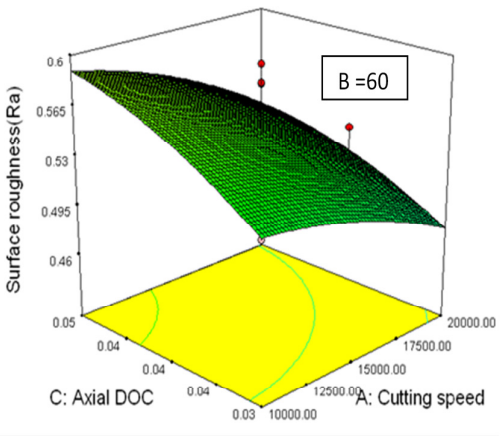

Fig 4.11(d): 3-D Ra plot for A and C

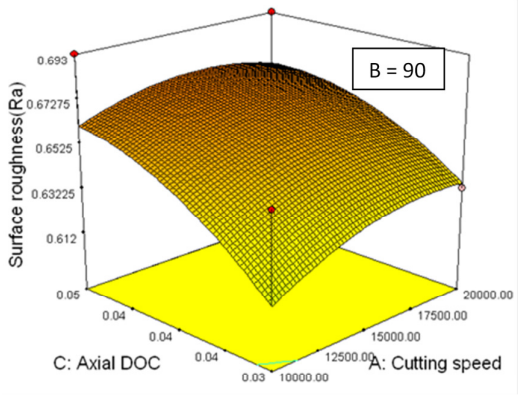

Fig 4.11(e): 3-D Ra plot for A and C

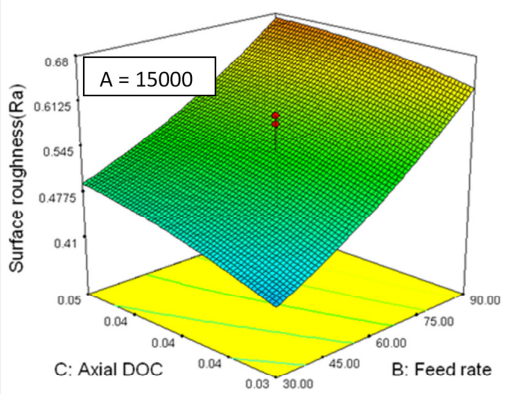

Fig 4.11(f): 3-D Ra plot for B and C

The quadratic model Eqn (4.6) was used for further optimization. Twenty three solutions were obtained and low surface roughness was predicted (0.3548 μm) at a combination of 20000 rpm (cutting speed), 30 mm/min (feed rate), and 0.03 mm (axial depth of cut) in the studied range of cutting parameters.

One can therefore conclude that the surface roughness increases with an increase of the feed rate and axial depth of cut, whilst an increase of the cutting speed decreases the surface roughness. However, the surface roughness increases with the increase in cutting speed at a high feed rate.

4.3.2 Cutting Force Model using Two Flute Square End Micro Grain Solid Carbide End Mill

Cutting Forces in the X, Y and Z were measured using a piezoelectric Kistler dynamometer. The resultant cutting force (resultant of F_X, F_Y and F_z) acting on the work piece was calculated and depicted in Table 4.12, to establish the cutting force model. Based on experimental results, the fit and summary test suggests that the following quadratic Eqn (4.7) for the cutting force F_r:

$$F_r = 158.78 - 7.107 \times 10^{-3} \times A + 0.364 \times B - 5003.26 \times C - 2.419 \times 10^{-5} \times A \times B + 0.0979 \times A \times C - 3.746 \times B \times C - 2.715 \times 10^{-7} \times A^2 + 3.211 \times 10^{-3} \times B^2 + 44057.3 \times C^2 \quad (4.7)$$

To verify the adequacy of the proposed quadratic model, ANOVA was used and the results are shown in the Table 4.14

Table 4.14: ANOVA table for the cutting force (Fr) quadratic model

Source	Sum of Squares	DOF	Mean Square	F-value	P-value	
Model	*4843.87*	*9*	*538.21*	*3.61*	*0.0290*	*significant*
A-Cutting Speed	3268.68	1	3268.68	21.91	0.0009	
B-Feed Rate	690.57	1	690.57	4.63	*0.0569*	
C-Depth of Cut	74.92	1	74.92	0.50	*0.4947*	
AB	105.39	1	105.39	0.71	0.4202	
AC	191.88	1	191.88	1.29	0.2832	
BC	10.10	1	10.10	0.068	*0.7999*	
A^2	416.97	1	416.97	2.80	0.1255	
B^2	121.40	1	121.40	0.81	0.3882	
C^2	282.08	1	282.08	1.89	*0.1991*	
Residual	1491.69	10	149.17			
Lack of Fit	820.88	*5*	164.18	*1.22*	*0.4150*	*Not significant*
Pure Error	670.81	5	134.16			
Cor Total	6335.55	19				

The ANOVA table indicates that the model is significant for 95% confidence level (P value < 0.05). From the table it is observed that the cutting speed A is the most influential factor in the cutting force model (Large F value). From the perturbation plot shown in Fig 4.12, the cutting speed has the most significant effect on the cutting force. The figure clearly indicates that with the increase in the cutting speed and feed rate, the cutting force value increases. In the case of axial depth of cut, the surface roughness decreases with the increase of axial depth of cut.

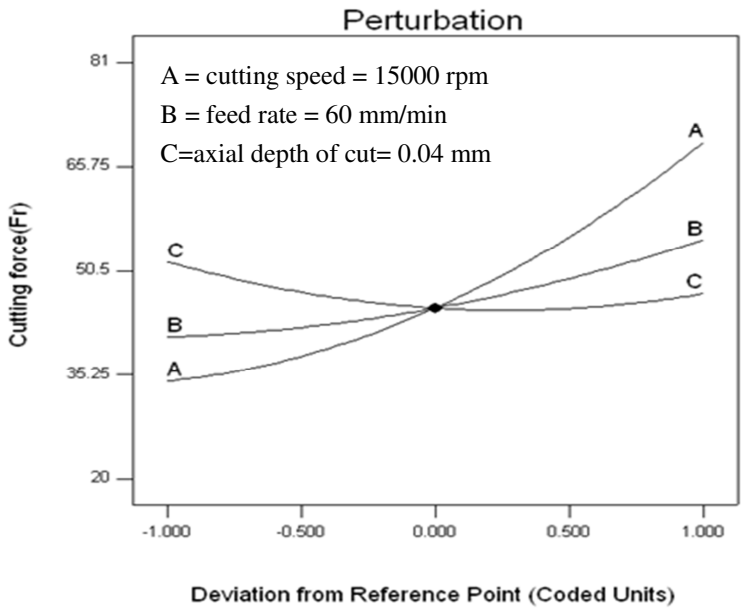

Fig 4.12: Perturbation plot Fr Vs. A, B, and C

The interaction effect of the cutting parameters on the cutting force value is shown in Figs 4.13(a-d).

In Fig 4.13(a), the effect of the cutting speed on the cutting force is shown with two different feed rates. From this figure it follows there is a general trend that an increased feed rate leads to an increase of the cutting force at any particular cutting speed, with an axial depth of cut of 0.04 mm. The cutting force is small at a low cutting speed, but it increases with an increase of the cutting speed. This increase is rapid at a low feed rate of 30 mm/min as compared with a high feed rate. This may be due to high cutting time to complete one slot and it leads to loss in the CBN coating layer on a tool.

The variation of the cutting force against cutting speed A at two different values of the axial depths of cut is shown in Fig 4.13(b). The cutting force increases with increase in the cutting speed. The critical point to note is that, at a low cutting speed, the cutting force is also low even at an high axial depth of cut of 0.05 mm. In

contrast, at a high cutting speed, the cutting force increases rapidly at a high axial depth of cut. This may be due to high chip load at a high cutting speed and a high axial depth of cut.

The variations in the cutting force are different at cutting speeds of 15000 rpm and 20000 rpm as shown in Fig 4.13(c-d). At 15000 rpm, the cutting force is high at a low axial depth of cut, whereas at 20000 rpm, the cutting force is high at a high axial depth of cut. This indicates that the cutting speed is the most dominant factor.

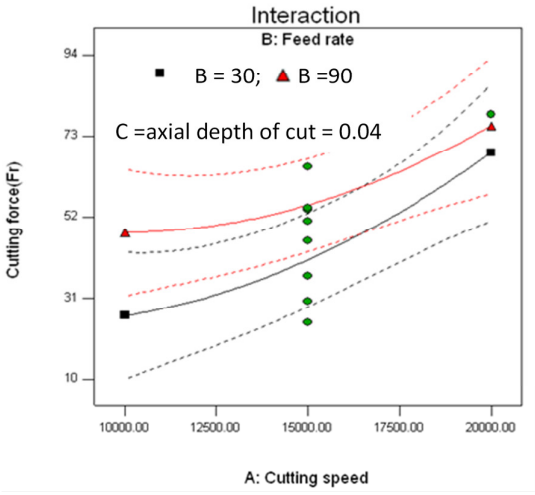

Fig 4.13(a): Interaction plot for A and B

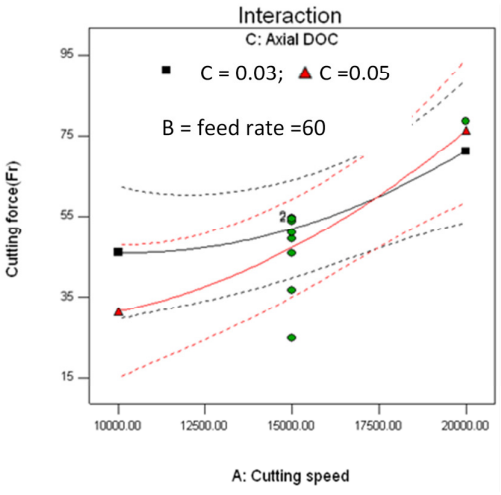

Fig 4.13(b): Interaction plot for A and C

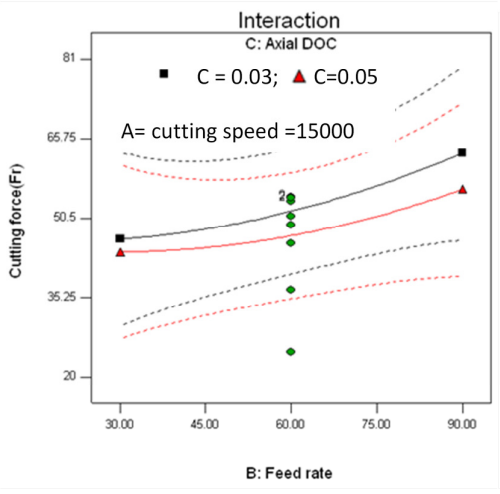

Fig 4.13(c): Interaction plot for B and C

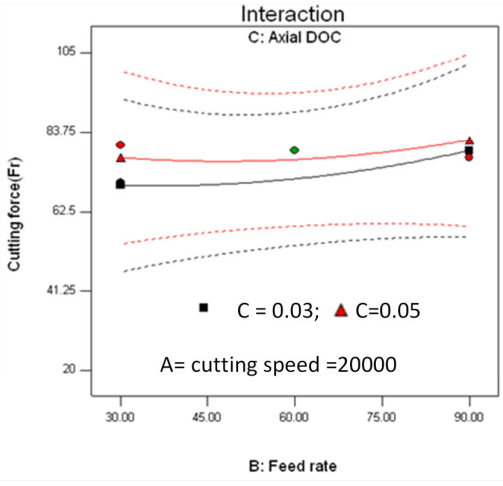

Fig 4.13(d): Interaction plot for B and C

The 3-D and contour plots shown in Fig 4.14(a-d) provide details of the combined effect of the cutting speed, feed rate and axial depth of cut on the cutting force. The cutting force increases rapidly with an increase of the cutting speed compared to the feed rate and axial depth of cut as shown in Fig 4.14(b-c). A low cutting speed and a low feed rate is the right choice to obtain a low cutting force value.

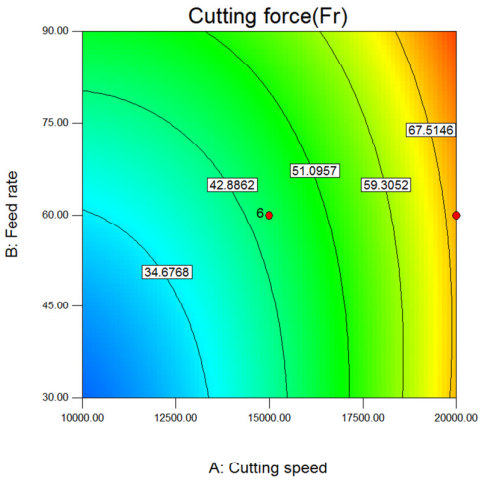

Fig 4.14(a): Contour plot for A and B

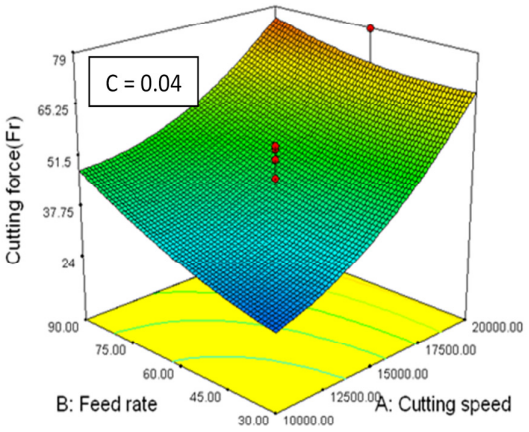

Fig 4.14 (b): 3-D Fr plot for A and B

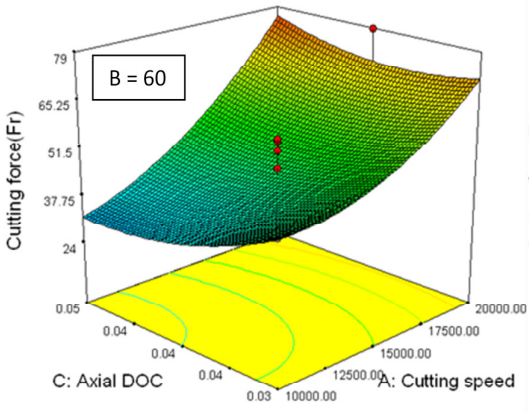

Fig 4.14(c): 3D Fr plot for A and C

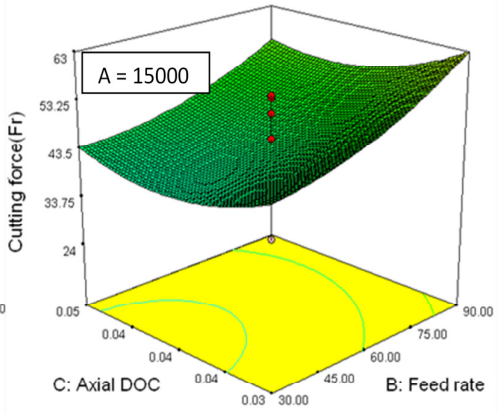

Fig 4.14(d): 3D Fr plot for B and C

The developed quadratic model, Eqn (4.7), was used for the optimization of operating cutting parameters to obtain the minimum cutting force. Twenty solutions were obtained for the low cutting force in the selected range of the cutting

parameters after optimization. Low cutting force was predicted (24.345 N) at a combination of 10000 rpm (cutting speed), 30 mm/min (feed rate), and 0.05 mm (axial depth of cut) in the studied range of cutting parameters.

The optimized cutting parameters (23 solutions obtained) were selected (11590 rpm cutting speed, 30 mm/min feed rate, and 0.03 mm axial depth of cut) based on the minimum surface roughness and low cutting force in the studied range of cutting parameters. The predicted surface roughness and the cutting force values were 0.4765 μm and 33.66 N respectively for the selected combination of cutting parameters.

From the experimental results above, one can conclude that the cutting force is mainly affected by the cutting speed and the feed rate. The value of the cutting force increases with the increase in the cutting speed and feed rate.

4.3.3 Surface Roughness Model using CBN Coated Internal Grinding Tool grit

The cutting experiments were carried out on the V-55 vertical milling machine using a CBN coated internal grinding tool grit. The internal grinding tool grit is considered as a specimen for grinding process in this work. A very low feed rate range (1 to 3 mm/min) is chosen due to the grinding process. Internal grinding tool grit have no sharp cutting edges, so the axial depth of cut is considered as constant (volume of material removal for each cutting is fixed), to reduce the number of experiments. Hence, only two cutting parameters, the cutting speed and the feed rate, are considered for analysis. The independent variables are coded, taking into consideration the preliminary tests, capacity of the CNC milling machine, and cutting tool as depicted in Table 4.15. When considering two factors, a total of 13 tests are needed (8 + 5 at center =13) according to the CCD. The detailed combinations of 13 cutting tests are shown in Table 4.16. TheMitutoyo SJ 301 is used to measure the surface roughness of a machined surface. During all the milling experiments the

surface roughness, Ra, is recorded at three locations (starting place, middle and end) and the averages of three Ra values are represented in Table 4.16 to establish the surface roughness model. The cutting force is measured using the Piezoelectric Kistler dynamometer.

Table 4.15: Range of cutting parameters for the experiment

Factors	Minimum	Central	Maximum
Coded factor	-1	0	1
Spindle Speed (RPM)	10000	15000	20000
Feed Rate (mm/min)	1	2	3

Table 4.16: Cutting conditions and output responses

Standard Order	Spindle Speed (rpm)	Feed Rate (mm/min)	Surface Roughness (μm)	Resultant cutting force (N)
1	20000	1	0.454	35.23
2	20000	3	0.652	56.23
3	15000	2	0.512	44.5
4	20000	2	0.514	43.28
5	15000	2	0.423	48.2
6	7928	2	0.325	38.4
7	15000	2	0.462	40.12
8	15000	0.58	0.412	38.8
9	15000	3.41	0.602	57.23
10	15000	2	0.486	51.2
11	15000	2	0.5	41.23
12	10000	3	0.514	51.5
13	10000	1	0.412	40.24

The experimental results shown in Table 4.24 are used to develop the surface roughness model using the RSM. The Fit and summary tests suggest the following quadratic Eqn (4.8) for the surface roughness (R_a)

$$R_a = 0.2735 + 1.9935 \times 10^{-5} \times A - 0.1046 \times B + 4.8 \times 10^{-6} \times A \times B - 5.995 \times 10^{-1} \times A^2 + 0.0259 \times B^2 \quad (4.8)$$

where A is the cutting speed and B is the feed rate

To verify the adequacy of the proposed quadratic model, ANOVA was used with 95% confidence level and the results are shown in Table 4.17. Based on the ANOVA table, both the cutting speed and the feed rate influence the surface roughness with feed rate (F value = 28.40) being the most dominant factor.

Table 4.17: ANOVA table for surface roughness Ra quadratic model

Source	**Sum of Squares**	**DOF**	**Mean Square**	**F-value**	**P-value**	
Model	0.076	*5*	*0.015*	*10.64*	*0.0036*	*significant*
A-Cutting Speed	0.022	1	0.022	15.20	0.0059	
B-Feed Rate	0.040	1	0.040	28.40	*0.0011*	
AB	2.304×10^{-3}	1	2.304×10^{-3}	1.62	0.2439	
A^2	1.090×10^{-3}	1	1.090×10^{-3}	0.77	0.4105	
B^2	4.740×10^{-3}	1	4.740×10^{-3}	3.33	0.1108	
Residual	9.965×10^{-3}	7	1.424×10^{-3}			
Lack of Fit	4.990×10^{-3}	*3*	1.663×10^{-3}	*1.34*	*0.3803*	*not significant*
Pure Error	4.975×10^{-3}	4	1.244×10^{-3}			
Cor Total	0.086	12				

The perturbation plot in Fig 4.15(a) shows surface roughness increases by increasing the cutting speed and the feed rate value. The interaction plot, Fig 4.15 (b), shows that the surface roughness value increases with an increase in feed rate at two

different speeds (low and high). This increase is rapid at a high cutting speed of 20000 rpm.

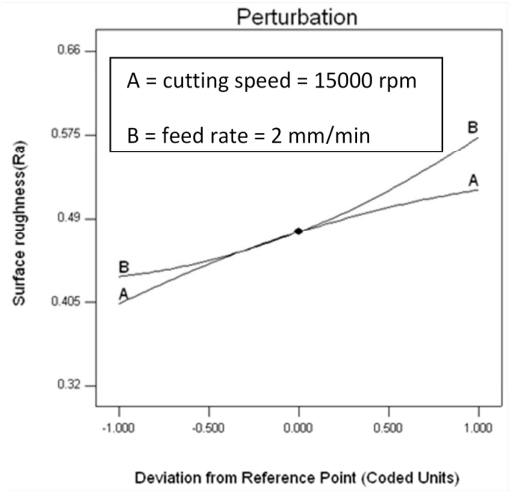

Fig 4.15(a): Perturbation plot for Ra

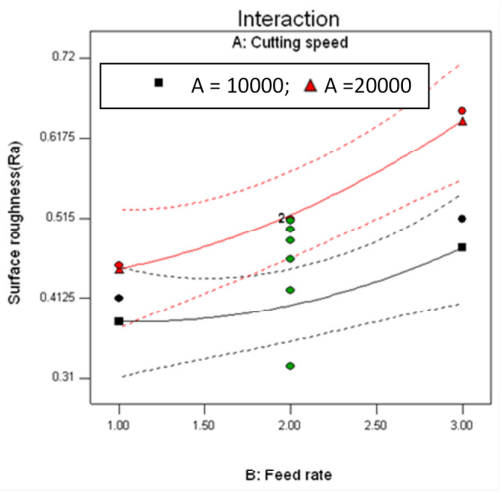

Fig 4.15(b): Interaction plot for A and B

From the 3-D and contour plots in Fig 4.16(a-b), it can be observed that a low feed rate and a low cutting speed is the right choice to achieve a good surface roughness. However, the effect of the cutting speed on the surface roughness is different with this tool. This could be due to the high range of cutting speeds selected for the grinding process, and indicates another speed range may need to study.

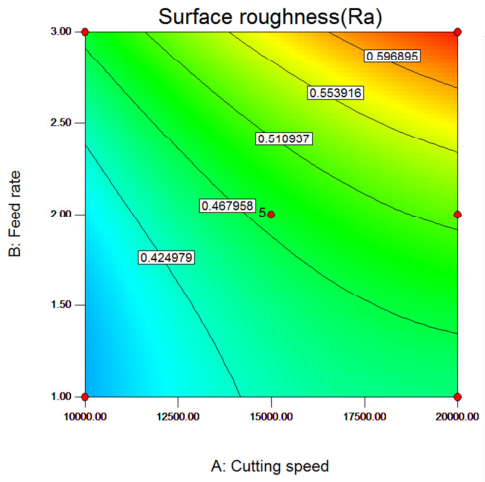

Fig 4.16(a): Ra contour plot for A and B

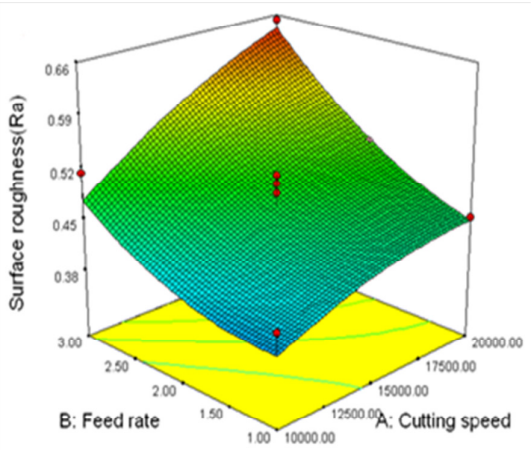

Fig 4.16(b):3D Ra plot for A and B

The developed model, Eqn (4.8), was used for optimization of the cutting parameters. Five solutions were obtained based on the minimum surface roughness in the studied range of cutting parameters. Low surface roughness was predicted (0.382 µm) at a combination of 10000 rpm (cutting speed), 1.1 mm/min (feed rate).

From the study above one can conclude that the minimum surface roughness value is obtained with a low cutting speed and a low feed rate for the selected range of cutting parameters.

4.3.4 Cutting Force Model using CBN Coated Internal Grinding Tool grit

Eqn (4.9) is developed for the cutting force (F_r) by using the experimental results shown in Table 4.24.

$$F_r = 32.519 + 1.636 \times 10^{-3} \times A - 7.80 \times B + 4.87 \times 10^{-4} \times A \times B - 8.364 \times 10^{-8} \times A^2 + 1.946 \times B^2 \quad (4.9)$$

To verify the adequacy of the proposed second order model, ANOVA was used and the results are is shown in Table 4.18.

Table 4.18: ANOVA table for cutting force (Fr) quadratic model

Source	Sum of Squares	DOF	Mean Square	F-value	P-value	
Model	506.76	*5*	*101.35*	*7.02*	*0.0118*	*significant*
A-Cutting Speed	1.65	1	1.65	0.11	0.7456	
B-Feed Rate	425.21	1	425.21	29.44	*0.0010*	
AB	23.72	1	23.72	1.64	0.2408	
A^2	21.22	1	21.22	1.47	0.2648	
B^2	26.73	1	26.73	1.85	0.2159	
Residual	101.10	7	14.44			
Lack of Fit	14.15	*3*	4.72	*0.22*	*0.8801*	*not significant*
Pure Error	86.94	4	21.74			
Cor Total	607.86	12				

The analysis found that the model is adequate with 95% confidence intervals (Model *P*-Value 0.0118 < 0.05, implies that the selected model is significant). The large value of F (29.44) indicates that the feed rate B has the highest influence on the surface roughness.

From the perturbation plot, Fig 4.17(a), the cutting force increases with an increase in cutting speed up to 15000 rpm and then decreases with an increase of the cutting speed. The figure clearly shows that the cutting force increases with the feed rate increase.

Fig 4.17(b) represents the effect of the feed rate on the resultant cutting force at two different cutting speeds, showing an interaction between these two parameters. From this figure, it can be noted that the cutting force value increases with increase in the feed rate; this increase is rapid in the case of a high cutting speed. This figure shows that (for values up to 1.8 mm/min), a low cutting speed generates a high cutting force. At a high feed rate, on the contrary, a high cutting speed generates a high cutting force. This may be due to the operation of the CNC milling machine with a maximum capacity and high feed rate. At high cutting parameters the machine may generate large amount of loads.

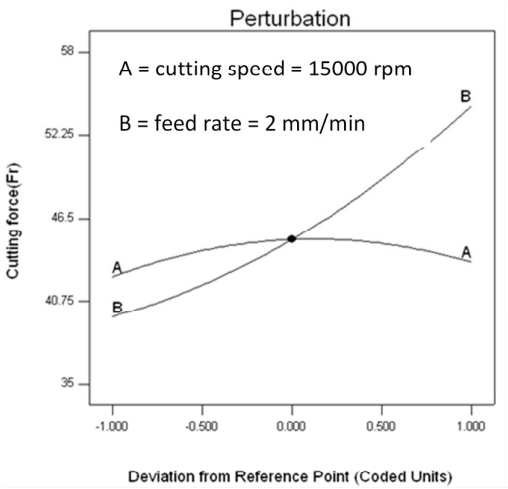

Fig 4.17(a): Perturbation plot for Fr

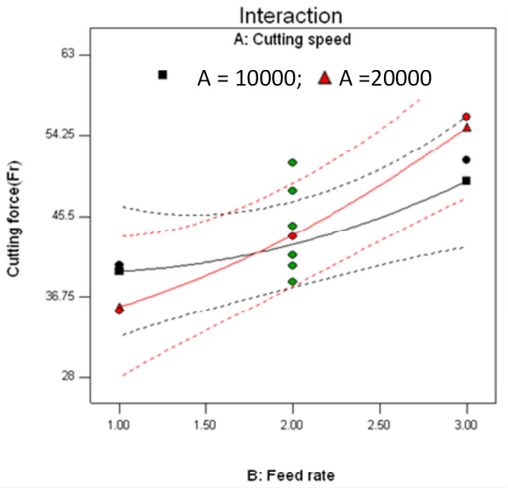

Fig 4.17(b): Interaction plot for A and B

From the 3-D and contour plots shown in Fig 4.18 (a-b), it is observed that the high cutting speed and low feed rate is the right choice to achieve low cutting force. These results are very similar to those in the grinding process of metallic materials.

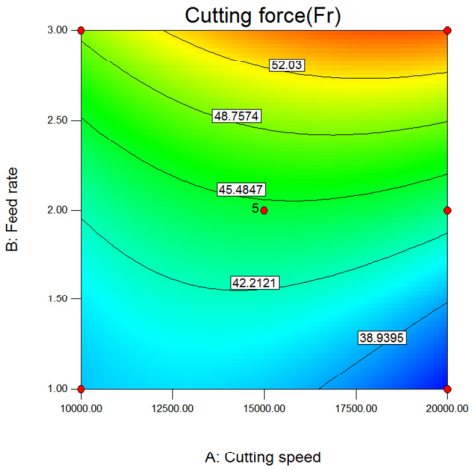

Fig 4.18(a): contour plot for A and B

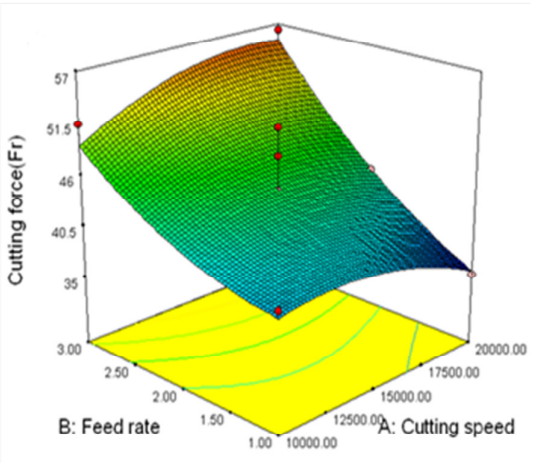

Fig 4.18(b): 3-D plot for A and B

The developed quadratic model, Eqn (4.9), was used further for optimization of operating cutting parameters. Four solutions were obtained after optimization for the minimum cutting force in the selected range of cutting parameters. The predicted cutting force was 35.66 N for the selected combination of 20000 rpm (cutting speed), 1 mm/min (feed rate).

The optimized cutting parameters (11 solutions obtained) were selected (10000 rpm cutting speed, 1 mm/min feed rate) based on the minimum surface roughness and low cutting force in the studied range of cutting parameters. The predicted surface roughness and the cutting force values were 0.3822 µm and 39.53 N respectively for the selected combination of cutting parameters.

From the above experimental results, one can conclude that a low feed rate and a high cutting speed is the right choice to achieve a low cutting force. These results are very similar to the grinding process of metallic materials.

4.4 Summary

This section summarizes the experimental results of the MGC for each tool using low speed and high speed CNC end milling process.

(a) Low speed CNC milling machine

- *Two Flute Square End Micro Grain Solid Carbide end mill*

  The most influential factors on the surface roughness model for the studied range of the cutting parameters are feed rate and axial depth of cut. Surface roughness increased with feed rate and axial depth of a cut increase and this increase was rapid at high cutting speeds. Low surface roughness was predicted (0.4790 μm) at a combination of 4933 rpm (cutting speed), 11.5mm/min (feed rate), and 0.12 mm (axial depth of cut) in the studied range of cutting parameters.

- *TiAlN and TiN Coated Carbide Tool insert*

  The surface roughness decreases with an increase in the cutting speed, and increases with an increase of the feed rate and axial depth of cut. The tool wear increases with an increase in the cutting speed and axial depth of cut. These tendencies in behavior of the cutting parameters are very similar to end milling of metallic materials. Minimum surface roughness (0.3419 μm) and low tool wear (25.81 N) was predicted for a combination of 3000 rpm (cutting speed), 10 mm/min (feed rate), and 0.3 mm (axial depth of cut) in the studied range of cutting parameters

- *CBN Coated Internal Grinding Tool grit*

  Lack of fit was significant on the predicted surface roughness model. This indicates that other factors like radial depth of cut, tool geometry, tool properties, and coolant, not considered as variables for this study, may affect

the model significantly. Low surface finish was predicted (0.2786 µm) at a combination of 3943 rpm (cutting speed), 1.7 mm/min (feed rate), and 0.17 mm (axial depth of cut) in the studied range of cutting parameters.

(b) High speed CNC milling machines

- *Two Flute Square End Micro Grain Solid Carbide end mill*

  The feed rate was the most influential factor on surface roughness model. The surface roughness increased with feed rate increase. The cutting force value increased with the increase in the cutting speed and feed rate. Low value of Surface roughness (0.4765 µm), and low cutting force (33.66 N) was predicted for a combination of 11590 rpm (cutting speed), 30 mm/min (feed rate), and 0.03 mm (axial depth of cut) in the studied range of cutting parameters.

- *CBN Coated Internal Grinding Tool grit*

  The surface roughness increased with an increase in the cutting speed and feed rate. However, compared to the other tool, the effect of the cutting speed on the surface roughness was different. This could be due to the high range of cutting speeds selected for the grinding process, and indicates another speed range could be consider for study. The value of the cutting force increased with feed rate increase. Low surface roughness (0.3822 µm) and low cutting force (39.53 N) was predicted for a combination of 10000 rpm (cutting speed), 1 mm/min (feed rate) in the studied range of cutting parameters.

CHAPTER 5: EXPERIMENTAL RESULTS AND ANALYSIS FOR ALUMINUM NITRIDE CERAMIC (AlN)

5.1 Introduction

Aluminum Nitride Ceramic (AIN) is relatively well suited for engineering applications, and is a very attractive structural ceramic because of the plastic deformation nature identified in this ceramic. This chapter analyses the performance of the end milling of AIN when using the following cutting tools:

a) Two flute square end micro grain solid carbide end mill
b) TiAIN + TiN coated carbide tool insert
c) CBN coated internal grinding tool grit

The ranges of cutting parameters were selected on the basis of preliminary tests [Appendix A], capacity of CNC machines and cutting tools. In this study A (spindle speed), B (feed rate), C (axial depth of cut) were the main factors considered for the experiment. The Response Surface Methodology (RSM) was implemented to conduct the primary experiments (similar to the MGC experimental studies in Chapter 4) and to develop predictive models for surface roughness, cutting force and tool wear in terms of cutting speed, feed rate and axial depth of cut.

5.2 Experimental Results using Low Spindle Speed Vertical Milling Machine

The subsequent sections describe the effect of cutting parameters, cutting speed, feed rate and axial depth of cut on surface roughness and tool wear, utilising three types of tools. The tests for AlN were conducted using the Leadwell V-30 series CNC vertical milling machine.

5.2.1 Surface Roughness Analysis using a Two Flute Square End Micro Grain Solid Carbide End Mill

The influence of the cutting speed (A), feed rate (B) and axial depth of cut (C) for the surface roughness was analyzed by using a two flute square end micro grain solid carbide end mill. The cutting parameters ranges were selected on the basis of preliminary experiments (Appendix A), capacities and limiting cutting conditions of the tool and the machine. The three machining parameters and their selected ranges are shown in the Table 5.1.The upper limit of the factor is coded as +1 and the lower limit as -1.

Table 5.1: Actual coded factors in experiment

Factors	Minimum	Central	Maximum
Coded factor	-1	0	1
Spindle Speed (RPM)	3000	4000	5000
Feed Rate (mm/min)	10	20	30
Depth of Cut (mm)	0.1	0.2	0.3

A CCD approach shown in Table 5.2 consisting of 20 sets (14+6 repeated at center) was generated according to Table 3.11(Chapter 3). The machining test was conducted for all 20 cutting conditions (Table 5.2). After every cutting, the work piece surface roughness was measured, cutting conditions and the measured surface roughness values are presented in Table 5.2. All experimental tests were conducted without lubrication.

Table 5.2 shows the average of three surface roughness values, where the lower surface roughness value is desirable for surface quality. Experiment run 16 gives the lowest surface roughness, 0.411 µm obtained at the lowest cutting speed 2318 rpm, feed rate at 20 mm/min, and 0.2 mm axial depth of cut, while the highest surface roughness 0.881, at large axial depth of cut 0.368 mm, feed rate at 20 mm/min and cutting speed at 4000 rpm.

Table 5.2: Experimental design and corresponding surface roughness results

Standard Order	Spindle Speed (rpm)	Feed Rate (mm/min)	Depth of Cut (mm)	Surface Roughness (μm)
1	5000	10	0.3	0.713
2	4000	20	0.2	0.552
3	5000	30	0.3	0.835
4	4000	20	0.368	0.881
5	3000	10	0.3	0.573
6	5000	30	0.1	0.693
7	4000	36.8	0.2	0.82
8	4000	20	0.2	0.543
9	4000	20	0.0318	0.462
10	4000	20	0.2	0.513
11	3000	10	0.1	0.581
12	5000	10	0.1	0.543
13	4000	20	0.2	0.511
14	3000	30	0.1	0.621
15	3000	30	0.3	0.752
16	2318	20	0.2	0.411
17	4000	3.18	0.2	0.523
18	5681	20	0.2	0.783
19	4000	20	0.2	0.553
20	4000	20	0.2	0.531

The RSM based mathematical model has been developed to correlate the relationship between the response Ra and process parameters. Fit and summary tests have suggested that the following quadratic Eqn (5.1) is significant based on the analysis of surface roughness(R_a) test results:

$$R_a = 1.0597 - 1.920 \times 10^{-4} \times A - 0.0185 \times B - 2.422 \times C + 6.625 \times 10^{-7} \times A \times B + 2.362 \times 10^{-4} \times A \times C + 0.0139 \times B \times C + 2.452 \times 10^{-8} \times A^2 + 5.086 \times 10^{-4} \times B^2 + 5.086 \times C^2 \quad (5.1)$$

A is the cutting speed, B is the feed rate, and C is the axial depth of cut respectively. To verify the adequacy of the proposed second order quadratic model, ANOVA was used and the results are shown in the Table 5.3. The analysis was performed to achieve the contribution of individual factors and to establish the best or the optimum condition for a product or a process.

Table 5.3: ANOVA table for surface roughness quadratic model

Source	**Sum of Squares**	**DOF**	**Mean Square**	**F-value**	**P-value**	
Model	*0.30*	*9*	*0.034*	*7.50*	*0.0021*	*significant*
A-Cutting Speed	0.057	1	0.057	12.76	0.0051	
B-Feed Rate	0.072	1	0.072	16.07	*0.0025*	
C-Depth of Cut	0.095	1	0.095	21.27	*0.0010*	
AB	3.511×10^{-4}	1	3.511×10^{-4}	0.079	0.7850	
AC	4.465×10^{-3}	1	4.465×10^{-3}	1.00	0.3412	
BC	1.540×10^{-3}	1	1.540×10^{-3}	0.34	*0.5703*	
A^2	8.664×10^{-3}	1	8.664×10^{-3}	1.94	0.1941	
B^2	0.037	1	0.037	8.34	0.0162	
C^2	0.037	1	0.037	8.34	*0.0162*	
Residual	0.045	10	4.471×10^{-3}			
Lack of Fit	0.0043	*5*	8.593×10^{-3}	*24.62*	*0.016*	*significant*
Pure Error	1.745×10^{-3}	5	3.490×10^{-4}			
Cor Total	0.35	19				

The values of column "P" which are less than 0.0500 indicate that the model is significant. Significant lack of fit is not desirable i.e. indicating other cutting parameters and conditions, not considered for the analysis in this study may influence significantly.

The parametric analysis was carried out to study the influence of the process parameters on surface roughness during the end milling. To evaluate the change of response surface, contour plots and three-dimensional response surface plots were formed, based on the RSM quadratic models. These plots also produced further correlation assessment between the input process parameters and output response.

Figure 5.1(a) shows the trends of each cutting parameter on the surface roughness, Ra, which increases with increasing the cutting speed, feed rate and the axial depth of cut.

Equation (5.1) has been plotted in Fig 5.1(b-d) for Ra, at studied levels of cutting conditions. Figure 5.1(b) represents the effects of cutting speed on the surface roughness at two different feed rate values. Surface roughness increases with the cutting speed increase. At low feed rate value the surface roughness value is low compared to high feed rate value. The rate of the surface roughness increase remains almost the same for both low and high feed rates.

Figure 5.1(c) shows the effects of the cutting speed with a different axial depth of cut on the surface roughness. Here, it can be observed that surface roughness increases as the cutting speed increases. The trend shows that an increased axial depth of cut leads to an increase in the surface roughness at a given cutting speed. The surface roughness increases rapidly at a high axial depth of cut, and this reveals that improved surface roughness is achieved at a low axial depth of cut 0.1mm.

The surface roughness is plotted against feed rate for two different axial depths of cut values as shown in Fig 5.1(d). It is clear that the surface roughness increases as the feed rate increases, and this can be attributed to the increase in the cutting force as the feed rate increases. The surface roughness value is higher at larger axial depth of cut even in this case. Improved surface roughness is, thus, possible at low axial depth of cut.

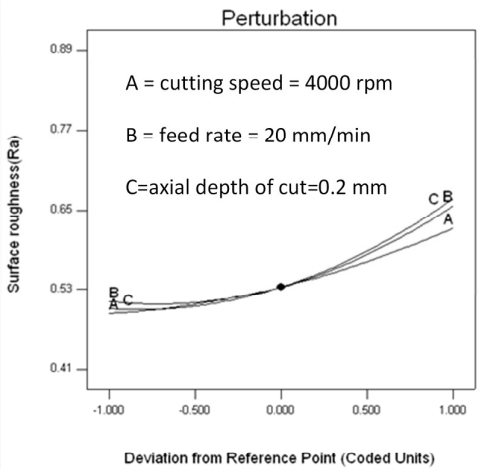

Fig 5.1(a): Perturbation plot for Ra

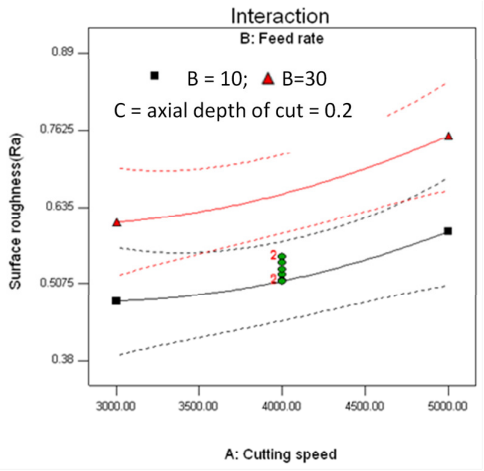

Fig 5.1(b): Interaction plot for A and B

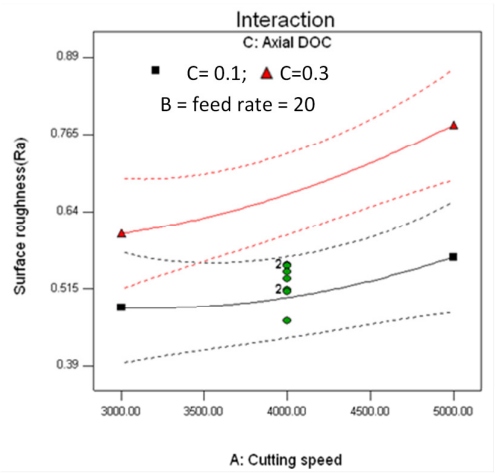

Fig 5.1(c): Interaction plot for A and C

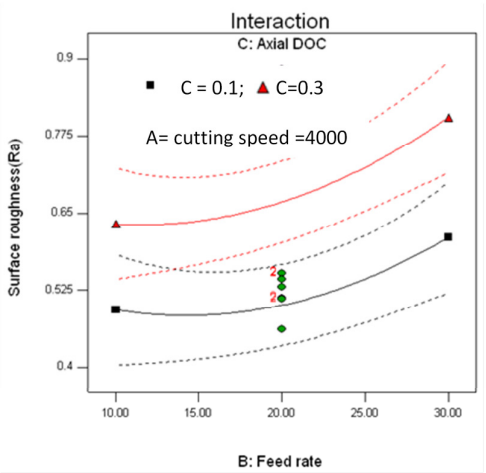

Fig 5.1(d): Interaction plot for B and C

Three-dimensional response surface plots give further assessment of the correlation between the cutting parameters and the surface roughness. Figure 5.2(a) has been constructed by plotting cutting speed A and feed rate B against surface roughness, at a selected level of axial depth of cut (0.2mm). It clearly shows that surface roughness increases with an increase in feed rate and the cutting speed. Figure 5.2(b) also shows that the surface roughness value increases with an increase in axial depth of cut and the cutting speed.

Figure 5.2(c) shows the interaction between feed rate B and axial depth of cut C on the surface roughness at a cutting speed of 4000 rpm. It shows a noticeable higher surface roughness value at maximum values of the cutting parameters. Based on these results all the three cutting parameters are significant.

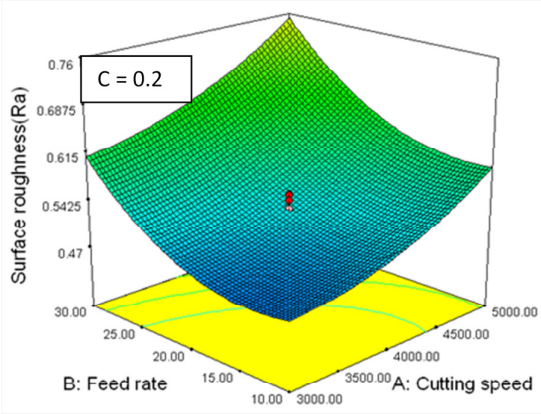

Fig 5.2(a): 3-D surface plot for A and B

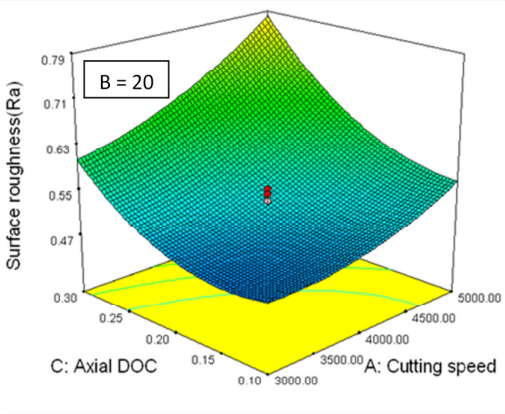

Fig 5.2(b): 3-D surface plot for A and C

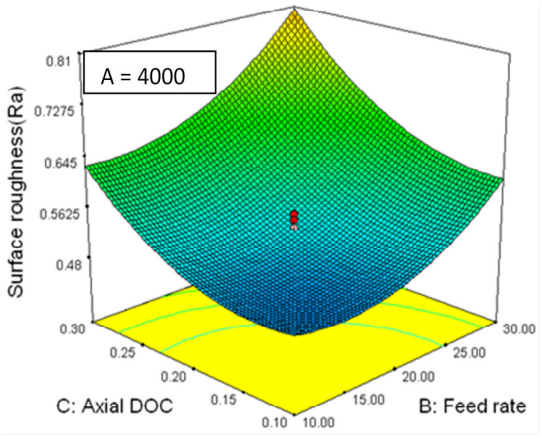

Fig 5.2(c): 3-D surface plot for B and C

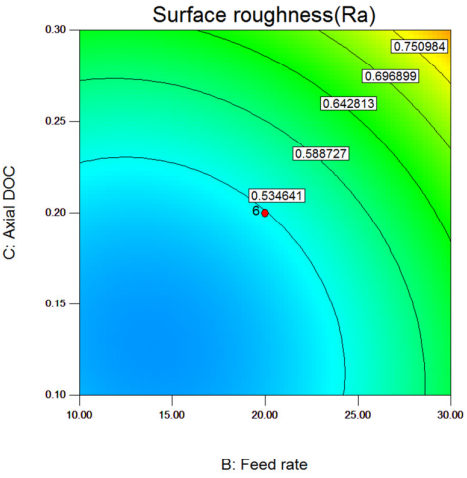

Fig 5.2(d): Contour plot for B and C

The developed quadratic model Eqn (5.1) has been utilized to optimize the parameters. Only one solution for the minimum surface roughness in the selected range of the cutting parameters was obtained after optimization. After identifying the most effective parameters, experimental tests were conducted for optimal combination. Experimental test results show that surface roughness value 0.4820 µm was close to the predicted surface roughness value 0.4591 µm for the selected

combination of 3006 rpm (cutting speed), 14.2 mm/min (feed rate), and 0.15 mm (axial depth of cut).

A better surface finish was obtained at a combination of 3006 rpm (cutting speed), 14.2 mm/min (feed rate), and 0.15 mm (axial depth of cut). Hence it is clear from the experimental studies that surface roughness Ra increases with increase in the cutting speed, feed rate, and the axial depth of cut. However, in order to reduce machining time and increase the material removal rate, the feed rate and axial depth of cut should be as high as possible.

5.2.2 Surface Roughness Analysis using Coated Carbide Tool inserts

The end milling operation was carried out on a V-30 CNC vertical milling machine, while the cutting tests were carried out under dry conditions using a combined TiAlN and TiN coated carbide tool insert.

The levels of independent variables and coding identifications used in this design are presented in Table 5.4. The values of the range of cutting parameters were selected based on preliminary experiments, limitations of CNC end milling machine speed and tool capacity.

Table 5.4: Actual coded factors for experiment

Factors	Minimum	Central	Maximum
Coded factor	-1	0	1
Spindle Speed (RPM)	3000	4000	5000
Feed Rate (mm/min)	10	20	30
Depth of Cut (mm)	0.1	0.2	0.3

Table 5.5: Cutting conditions and output responses

Standard Order	Spindle Speed (rpm)	Feed Rate (mm/min)	Depth of Cut (mm)	Surface Roughness (µm)	Tool Wear (µm)
1	4000	20	0.2	0.581	11.43
2	5681	20	0.2	0.482	73.6
3	4000	20	0.2	0.495	36.3
4	5000	10	0.3	0.486	53.6
5	4000	3.18	0.2	0.528	14.2
6	3000	30	0.1	0.891	29.8
7	4000	20	0.2	0.513	35.6
8	3000	30	0.3	0.982	29.8
9	2318	20	0.2	0.862	1.52
10	5000	30	0.1	0.484	53.1
11	4000	36.81	0.2	0.618	43.6
12	5000	30	0.3	0.564	63.5
13	4000	20	0.03	0.496	13.2
14	5000	10	0.1	0.447	43.4
15	4000	20	0.2	0.523	42.3
16	3000	10	0.1	0.698	19.6
17	4000	20	0.2	0.552	39.6
18	4000	20	0.368	0.658	5.36
19	3000	10	0.3	0.791	37
20	4000	20	0.2	0.567	32.5

Twenty runs were conducted using the CCD approach. After each cutting process, the surface roughness parameter (Ra) was measured, using the stylus-type surface roughness tester, and the tool wear was measured using a Leica microscope (shown in Fig 3.15, Chapter 3). The surface roughness was recorded at three places (starting point, middle and end) and an average of the three Ra values was tabulated. After

each cutting process, the cutting tool insert was examined to verify the tool wear. The measurements were taken at the location where the highest tool wear had occurred. The details of the cutting conditions and measured surface roughness values are shown in Table 5.5. The model (Eqn 5.2) was developed to predict surface roughness by using the least square statistical method with the help of design expert software.

$$R_a = 1.778 - 5.372 \times 10^{-4} \times A + 7.6 \times 10^{-3} \times B - 0.371 \times C - 3.362 \times 10^{-6} \times A \times B - 8.125 \times 10^{-5} \times A \times C + 4.875 \times 10^{-3} \times B \times C + 5.909 \times 10^{-8} \times A^2 + 2.409 \times 10^{-4} \times B^2 + 2.551 \times C^2 \quad (5.2)$$

Table 5.6: ANOVA table for surface roughness quadratic model

Source	**Sum of Squares**	**DOF**	**Mean Square**	**F-value**	**P-value**	
Model	*0.42*	*9*	*0.047*	*14.57*	*0.0001*	*significant*
A-Cutting Speed	0.30	1	0.30	92.49	<0.0001	
B-Feed Rate	0.031	1	0.031	9.59	*0.0113*	
C-Depth of Cut	0.024	1	0.024	7.51	*0.0208*	
AB	9.045×10^{-3}	1	9.045×10^{-3}	2.80	0.1252	
AC	5.281×10^{-4}	1	5.281×10^{-4}	0.16	0.6945	
BC	1.901×10^{-4}	1	1.901×10^{-4}	0.059	*0.8132*	
A^2	0.050	1	0.050	15.58	0.0027	
B^2	8.365×10^{-3}	1	8.365×10^{-3}	2.59	0.1387	
C^2	9.376×10^{-3}	1	9.376×10^{-3}	2.90	*0.1193*	
Residual	0.032	10	4.471×10^{-3}			
Lack of Fit	0.027	*5*	8.593×10^{-3}	*4.79*	*0.0554*	*Not significant*
Pure Error	5.583×10^{-3}	5	3.490×10^{-4}			
Cor Total	0.46	19				

To check the adequacy of the proposed model, ANOVA analysis was carried out (Table 5.6) utilizing the Design expert software. From the F-value the adequacy of the model was established. Table 5.6 also depicts the effect of the cutting speed, feed rate, axial depth of cut, and combined effect between cutting speed, feed rate, and

axial depth of cut on the proposed model.

It can be seen from Table 5.6 that the second order model is adequate with 95% confidence intervals (Model *P*-Value" of 0.0001 implies that the selected model is significant). The F value 92.59(Table 5.7) indicates that the cutting speed A has the highest influence on the surface roughness. The following results and analysis has been published in the Conference [Reddy et al. 2012]

The perturbation plot Fig 5.3(a) shows that the cutting speed has a significant effect on the surface roughness. The effect of the feed rate and the axial depth of cut are minimal. The surface roughness decreases with an increase in the cutting speed and an increase in the feed rate and axial depth of cut increases the surface roughness.

It is clear From Fig 5.3(b) that the surface roughness decreases with increases in the cutting speed; also this decrease in surface roughness was rapid at a high feed rate of 30 mm/min.

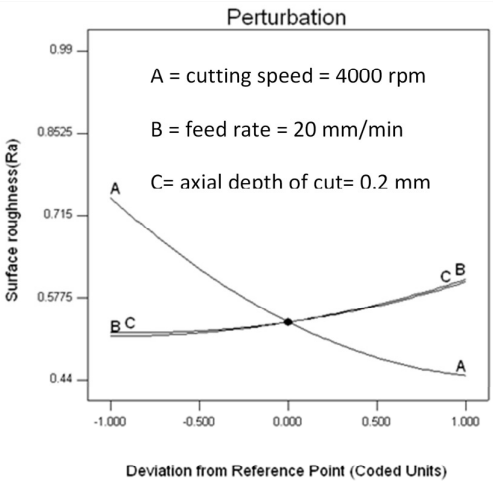

Fig 5.3(a): Perturbation plot for Ra

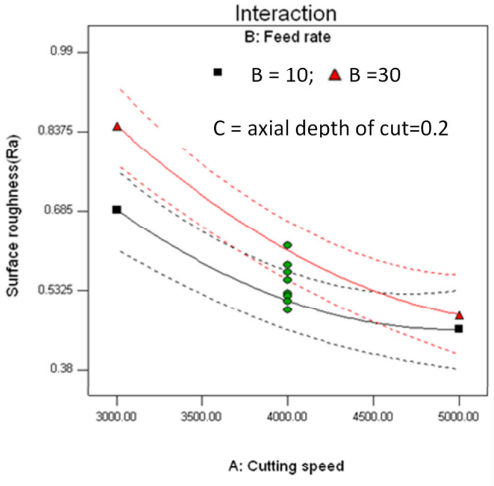

Fig 5.3(b): Interaction plot for A and B

Figure 5.3(c) explains the variation of surface roughness at low and high axial depths of cut value against the cutting speed. The rate of the surface roughness decrease remains almost the same for both low and high axial depth of cut against the cutting speed. Figure 5.3(d), shows that surface roughness improves a little if cutting is

performed at lower feed rates. It is noticeably high at a high axial depth of cut value. The rate of increase of surface roughness is similar at low and high axial depths of cut value against the feed rate.

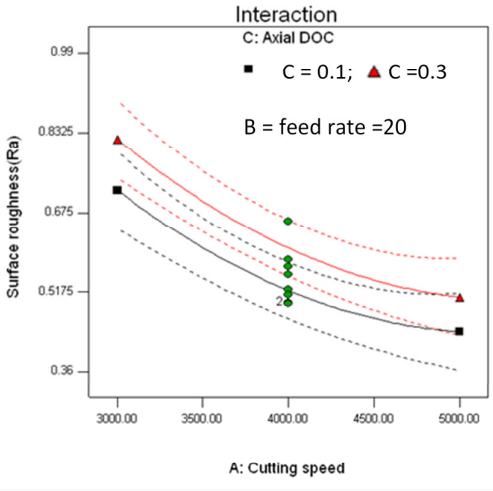

Fig 5.3(c): Interaction plot for A and C

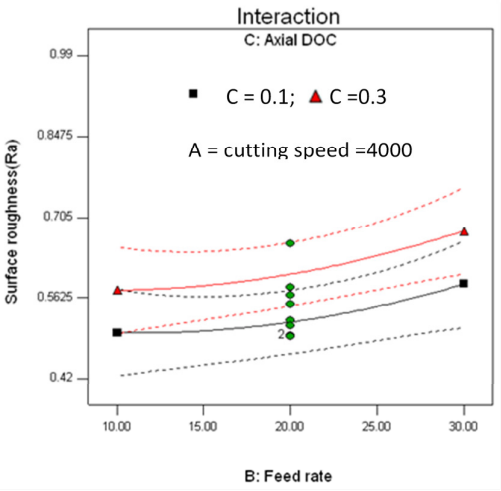

Fig 5.3(d): Interaction plot for B and C

The effect of the cutting parameters on the surface roughness in 3-D and contour plots is shown in Fig 5.4(a-d). Figure 5.4(a-b) shows the interactions between cutting speed A and feed rate B, on the surface roughness, at 0.2mm axial depth of cut. The surface roughness value is lower at lower feed rates and higher cutting speeds.

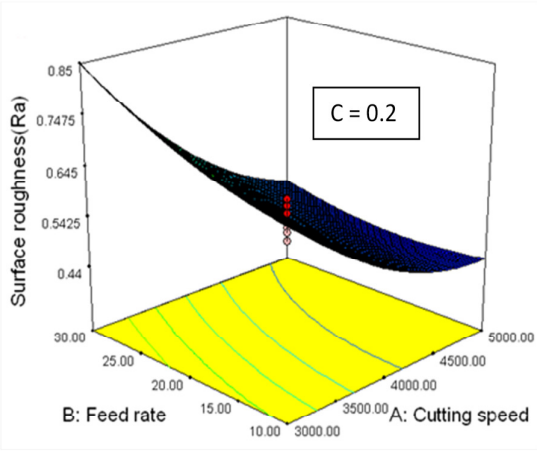

Fig 5.4(a): 3-D Ra plot for A and B

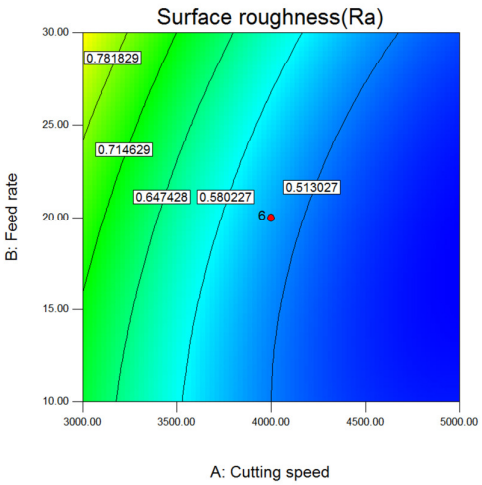

Fig 5.4(b): Contour plot for A and B

Figure 5.4(c) constructed the cutting speed A, and the axial depth of cut C against the surface roughness for the invariable feed rate 20 mm/min. It shows that the surface roughness value increases by increasing the axial depth of cut, and decreases by increasing the cutting speed.

The effect of feed rate B and the axial depth of cut C on surface roughness plot at a particular cutting speed 4000 rpm are illustrated in Fig 5.4 (d). The figure shows that better surface roughness is observed at minimum values of the cutting parameters.

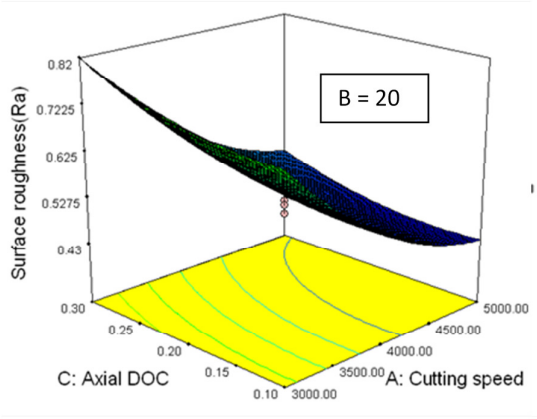

Fig 5.4(c): 3-D Ra plot for A and C

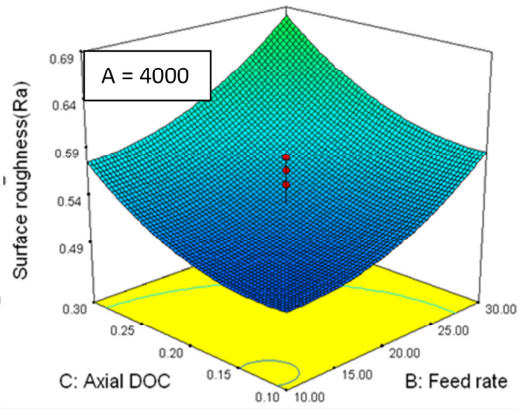

Fig 5.4(d): 3-D Ra plot for B and C

Equation (5.2) was used for further optimization, where 39 solutions were obtained. Low surface roughness was predicted (0.4369 μm) at a combination of 4970 rpm (cutting speed), 17.7 mm/min (feed rate), and 0.16 mm (axial depth of cut) in the studied range of cutting parameters. Experimental tests were conducted based on a selected combination of parameters. The experimental value 0.4623 concurred with the predicted surface roughness value of 0.4369.

From the experimental studies, one can conclude that, lower surface roughness is achievable with high cutting speed, lower feed rate, and low axial depth of cut. The observation is similar to that obtained for metallic materials [Ozcelik and Bayramoglu 2006, Bao and Tancel 2000, Chee et al. 2006]. However, in order to

reduce machining time and increase material removal rate, both the feed rate and axial depth of cut should be as high as possible.

5.2.3 Tool Wear Analysis using Carbide Tool insert Coated with Multiple Layers of TiAlN and TiN

The RSM based mathematical model was developed to relate the relationship between the tool wear and the process parameters. The fit and summary tests suggest that the following quadratic model is significant:

$$Tool\ wear = 35.53 - 0.0297 \times A - 0.687 \times B + 241.166 \times C + 2.075 \times 10^{-4} \times A \times B + 4.0 \times 10^{-3} \times A \times C - 2.150 \times B \times C + 5.098 \times 10^{-6} \times A^2 + 0.0204 \times B^2 - 489.989 \times C^2 \quad (5.3)$$

To verify the adequacy of the proposed quadratic model, ANOVA was used and the results are shown in the Table 5.7. The table indicates that the tool wear model is not significant; therefore, it cannot be concluded from these experiments with 95% confidence level that the proposed model Eqn (5.3) is suitable. Other factors besides the three selected cutting parameters might have to be considered for areas of further research.

The data also shows that the cutting speed has the most significant effect (F-value 16.81) on tool wear as shown in Table 5.7, while the effect of feed rate and the axial depth of cut are minimal.

Table 5.7: ANOVA table for tool wear quadratic model

Source	Sum of Squares	DOF	Mean Square	F-value	P-value	
Model	4857.49	9	539.72	2.59	*0.0770*	*Not significant*
A-Cutting Speed	3499.80	1	3499.80	16.81	0.0021	
B-Feed Rate	380.06	1	380.06	1.83	*0.2064*	
C-Depth of Cut	45.09	1	45.09	0.22	*0.6516*	
AB	34.44	1	34.44	0.17	0.6927	
AC	1.28	1	1.28	6.149×10^{-3}	0.9390	
BC	36.98	1	36.98	0.18	*0.6823*	
A^2	374.63	1	374.63	1.80	0.2094	
B^2	59.79	1	59.79	0.29	0.6037	
C^2	346.00	1	346.00	1.66	*0.2263*	
Residual	2081.64	10	208.16			
Lack of Fit	1468.44	*5*	293.69	*2.39*	*0.1799*	*Not significant*
Pure Error	613.20	5	122.64			
Cor Total	6939.13	19				

At a high cutting speed, more heat is generates due to friction and this might have caused the insert to wear faster. The perturbation plot, in Fig 5.5 (a), shows that tool wear, increases when increasing the cutting speed and the feed rate. It initially increases with increased axial depth of cut and then decreases slowly with increased axial depth of cut. At lower feed rates, it could be that machining takes more time and leads to higher tool wear.

The interaction plot, Fig 5.5(b), shows the effect of the cutting speed on tool wear at low and high feed rate values at a particular axial depth of cut 0.2 mm. The decrease in surface roughness is not influenced by changes in feed rate. At a low feed rate the value of the surface roughness is less than that of a high feed rate.

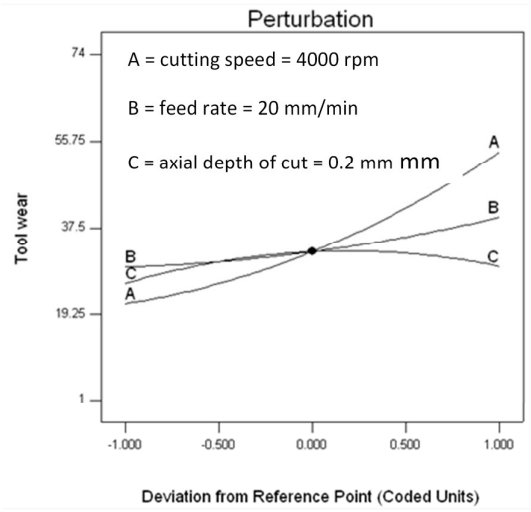

Fig 5.5(a): Perturbation plot on Tool wear

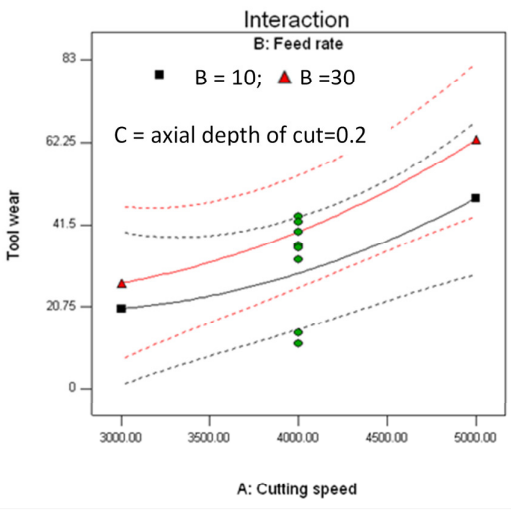

Fig 5.5(b): Interaction plot for A and B

Figure 5.5(c) shows, the effect of the axial depth of cut on tool wear at low and high cutting speed values at a feed rate 60 mm/min. The effect of the axial depth of cut is very minimal on the tool wear. Figure 5.5(d) depicts the fact that the tool wear value increases slightly with increase in the feed rate. The rate of the tool wear is higher at lower axial depth of cut, but it is small at low feed rate and low axial depth of cut in the studied range of cutting parameters.

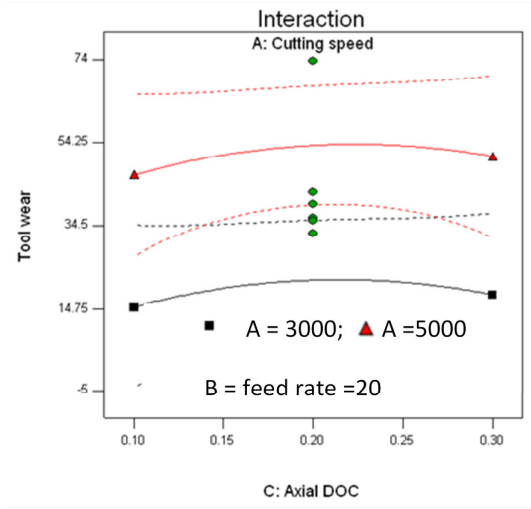

Fig 5.5(c): Interaction plot for A and C

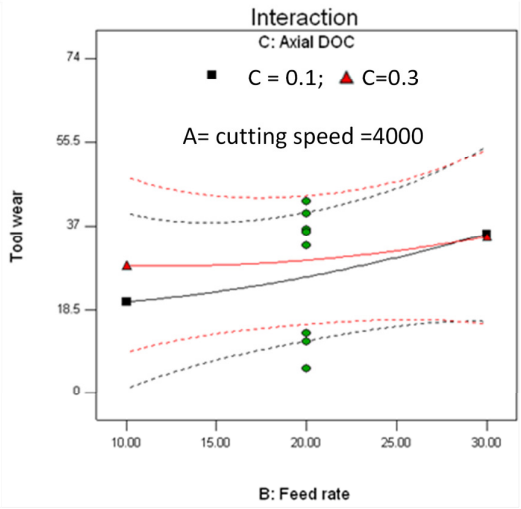

Fig 5.5(d): Interaction plot for B and C

The 3-D and contour plots shown in Fig 5.6(a-d) represent the effect of the cutting speed, feed rate and axial depth of cut against the tool wear. The cutting speed has a significant effect on the tool wear compared to the other two cutting parameters. In Fig 5.6(a), as increase of the cutting speed shows rapid increase in tool wear compared to increase in feed rate. At high speeds, temperatures may increase and lead to damaging of the cutting tool materials. Higher cutting temperatures may be further generated under dry machining and this leads to higher tool wear.

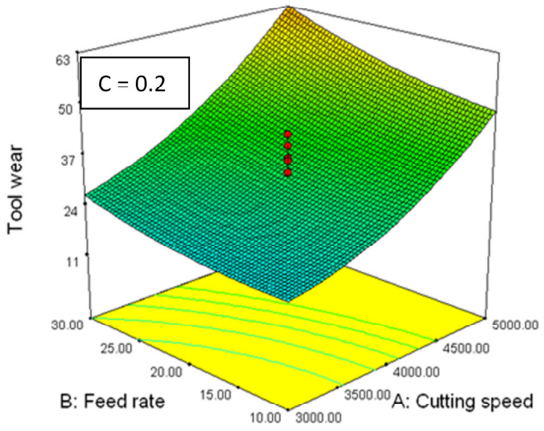

Fig 5.6(a): 3-D plot for B and A

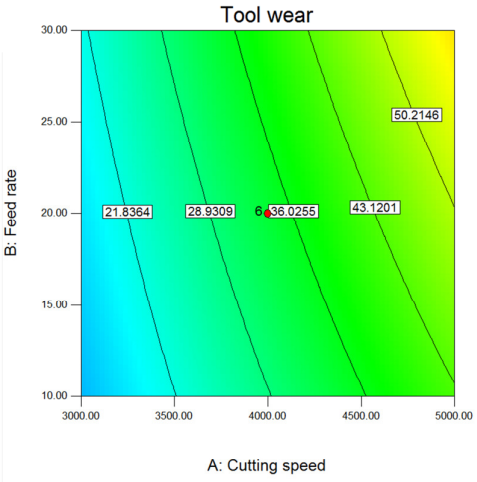

Fig 5.6(b): Contour plot for B and A

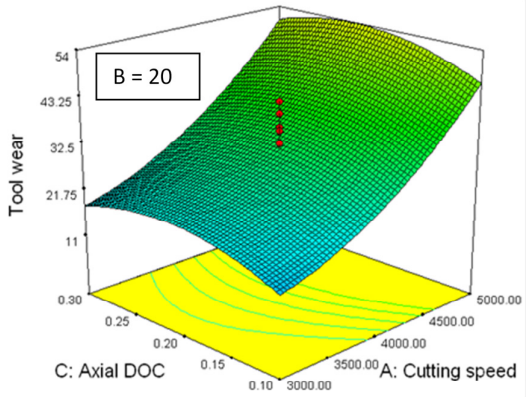

Fig 5.6(c): 3-D plot for A and C

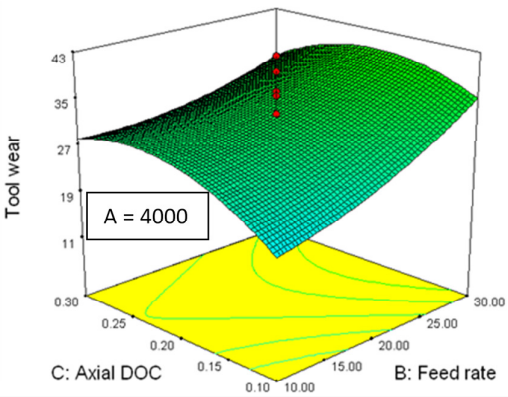

Fig 5.6(d): 3-D plot for B and C

In Figure 5.6(c), a similar trend can be seen for the cutting speed and the axial depth of cut on tool wear, i.e. increase in the cutting speed shows rapid increase in tool wear compared to the increase in axial depth of cut. This suggests that the cutting speed is the most significant variable in the tool wear model for this case. Smaller tool wear value is possible with low cutting parameters like the lower cutting speed, lower axial depth of cut, and the lower feed rate in the selected range. The above discussed results has been published in conference [Reddy et al. 2012].

The developed mathematical model, Eqn (5.3), was used for further optimization of the operating cutting parameters for the minimum tool wear, where 25 solutions were obtained. Experimental test was conducted for the selected combination of 3000 rpm (cutting speed), 10 mm/min (feed rate), and 0.1 mm (axial depth of cut). Experimental test were show that the tool wear value of 13.56 was close to the predicted tool wear value of 11.1754 at the selected combination.

Nine solutions were obtained based on the minimum surface roughness and the minimum tool wear. Minimum surface roughness (0.5189 μm) and low tool wear (22.74 μm) were predicted for a combination of 3855 rpm (cutting speed), 10 mm/min (feed rate), and 0.1 mm (axial depth of cut) in the studied range of cutting parameters. The experimental values were (surface roughness 0.4920 μm and tool wear 26.41 μm), close to the predicted ones for the above selected combination.

One can therefore conclude that the tool wear is mainly affected by cutting speed. Tool wear increases with increases in the cutting speed, feed rate and axial depth of cut.

5.2.4. Surface Roughness Model using CBN Coated Internal Grinding Tool grit

The end milling operation was conducted using CBN coated internal grinding tool grit on the V-30 vertical CNC milling machine.

Table 5.8: Actual coded factors for experiment

Factors	Minimum	Central	Maximum
Coded factor	-1	0	1
Spindle Speed (RPM)	3000	4000	5000
Feed Rate (mm/min)	1	2	3
Depth of Cut (mm)	0.1	0.2	0.3

The independent variables are coded in Table 5.8 on the basis of preliminary tests, limitation of the tool, and capacity of the milling machine. Twenty experiments were conducted by varying all the three identified cutting parameters based on CCD.

The surface roughness was measured at three locations and the average surface roughness was analyzed. Cutting conditions and measured average surface roughness values are shown in Table 5.9.

The experimental results of Table 5.9 are used to develop a second order surface roughness model (Eqn 5.4) using RSM.

$$R_a = 0.117 - 4.456 \times 10^{-6} \times A + 0.106 \times B + 0.379 \times C - 3.725 \times 10^{-5} \times A \times B - 9.75 \times 10^{-5} \times A \times C - 0.562 \times B \times C + 1.118 \times 10^{-8} \times A^2 + 0.072 \times B^2 + 3.593 \times C^2 \quad (5.4)$$

Table 5.9: Cutting conditions and surface roughness value

Standard Order	Spindle Speed (rpm)	Feed Rate (mm/min)	Depth of Cut (mm)	Surface Roughness (μm)
1	3000	1	0.1	0.326
2	5000	3	0.3	0.626
3	4000	2	0.031	0.354
4	4000	0.3182	0.2	0.314
5	4000	3.68	0.2	0.72
6	5681	2	0.2	0.314
7	4000	2	0.368	0.474
8	4000	2	0.2	0.26
9	5000	1	0.1	0.38
10	3000	3	0.1	0.766
11	3000	1	0.3	0.476
12	4000	2	0.2	0.374
13	5000	3	0.1	0.74
14	4000	2	0.2	0.494
15	4000	2	0.2	0.354
16	5000	1	0.3	0.56
17	3000	3	0.3	0.76
18	2318	2	0.2	0.374
19	4000	2	0.2	0.48
20	4000	2	0.2	0.46

To verify the adequacy of the proposed second order model, ANOVA was used and the results shown in the Table 5.10.

Table5.10: ANOVA table for surface roughness quadratic model

Source	Sum of Squares	DOF	Mean Square	F-value	P-value	
Model	*0.38*	*9*	*0.043*	*3.53*	*0.0312*	*significant*
A-Cutting Speed	1.106×10^{-3}	1	1.106×10^{-3}	0.091	0.7686	
B-Feed Rate	0.25	1	0.25	20.32	*0.0011*	
C-Depth of Cut	0.012	1	0.012	1.03	*0.3350*	
AB	0.011	1	0.011	0.92	0.3608	
AC	7.605×10^{-4}	1	7.605×10^{-4}	0.063	0.8072	
BC	0.025	1	0.025	2.09	*0.1788*	
A^2	1.802×10^{-3}	1	1.802×10^{-3}	0.15	0.7077	
B^2	0.075	1	0.075	6.23	0.0317	
C^2	0.019	1	0.019	1.54	*0.2434*	
Residual	0.12	10	0.012			
Lack of Fit	0.080	*5*	0.016	*1.94*	*0.2419*	*Not significant*
Pure Error	0.041	5	8.229×10^{-3}			
Cor Total	0.51	19				

The F-value of 3.53 ($P < 0.05$) implies that the model is significant. From the perturbation plot shown in Fig 5.7(a), the effect of cutting speed and axial depth of cut on the surface roughness is negligible. The feed rate was found to have the maximum influence on the surfaces roughness which increases with the increase of feed rate.

From the interaction plot shown in Fig 5.7(b), the effect of cutting speed on surface roughness are opposite at low and high feed rate values. At a low feed rate value 1 mm/min the surface roughness increases by increasing the cutting speed at 0.2 mm axial depth of cut. At the high feed rate of 3 mm/min, surface roughness decreases by increasing the cutting speed. These results suggest that a combined effect of the cutting parameters may be influencing the model.

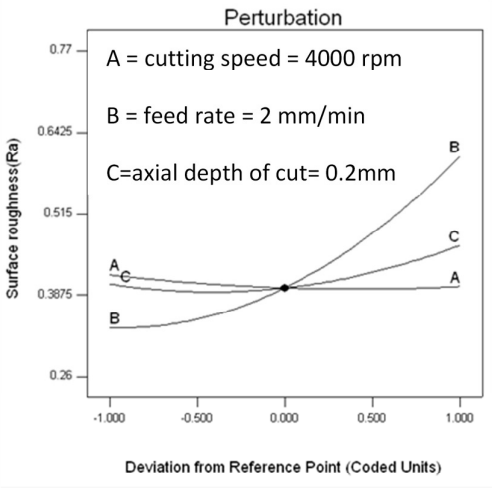

Fig 5.7(a): Perturbation plot for Ra

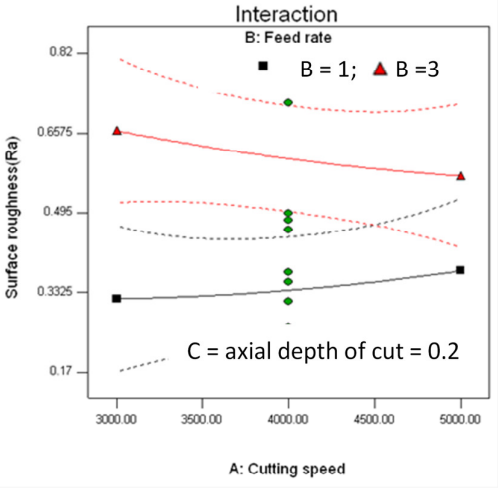

Fig 5.7(b): Interaction plot for A and B

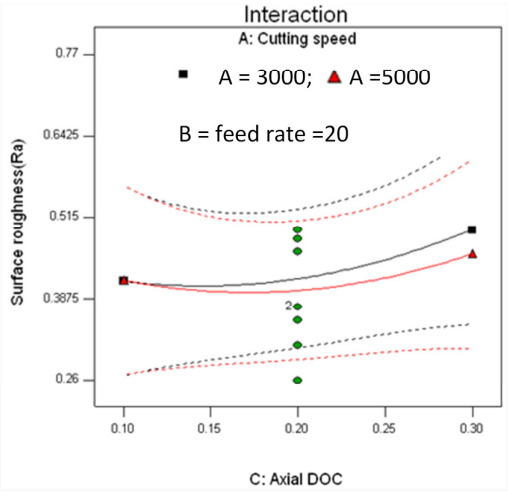

Fig 5.7(c): Interaction plot for A and C

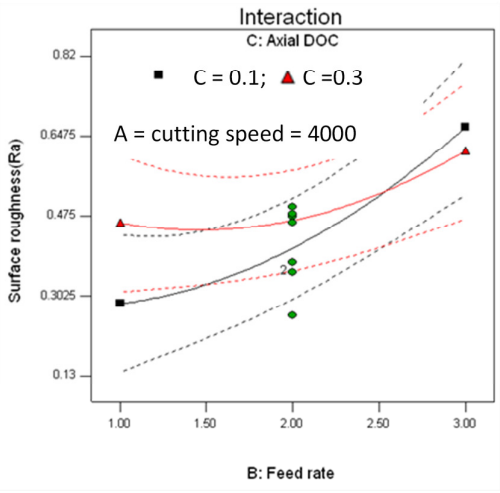

Fig 5.7 (d): Interaction plot for A and B

One can conclude from the interaction plot, Fig 5.7(c), that the value of the surface roughness is more or less the same at low and high cutting speeds in all the axial depth of cut values. In other words, increasing the cutting speed does not result in much improvement in surface roughness. Also, the surface roughness value increases insignificantly by increasing the axial depth of cut.

In Figure 5.7(d), the effect of the feed rate on the surface roughness is shown at low and high axial depth of cut value at a particular cutting speed 4000 rpm. The surface roughness value increases by increasing the feed rate. It is interesting to note that the

surface roughness has been increasing rapidly with an increase in feed rate at a low axial depth of cut, compared to that of a high axial depth of cut. One can choose a high feed rate at a high axial depth of cut without sacrificing the surface finish. This reduces the machining time since the material removal rate is high at high cutting parameters (feed rate and axial depth of cut).

The 3-D and contour plots, Fig 5.8(a-d), gives a clear picture about the interaction effect of the cutting speed, feed rate, and the axial depth of cut on the surface roughness. Figures 5.8(a) and 5.8(c) shows that the surface roughness increases rapidly with an increase of the feed rate compared to cutting speed and axial depth of cut. These figures provide the evidence that the feed rate is the most significant factor compared to the cutting speed and the axial depth of cut.

The most interesting observation at the high cutting speed of 5000 rpm is that the surface roughness slightly decreases even at a high feed rate and the high axial depth of cut. This indicates that the cutting speed may be dominant some specified range of parameters. In this case the minimal surface roughness value is achievable with the low cutting parameter values.

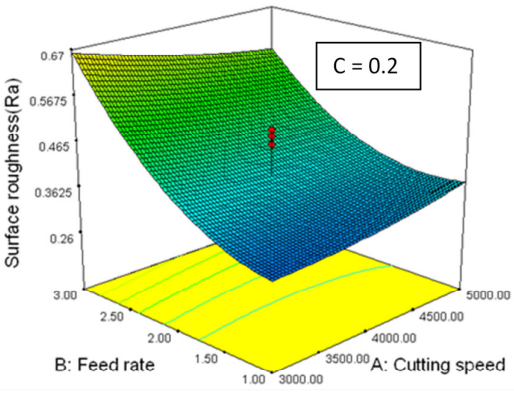

Fig 5.8(a): 3-D Ra plot for A and B

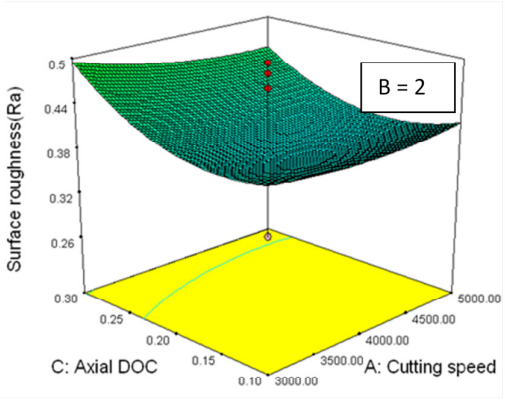

Fig 5.8(b): 3-D Ra plot for A and C

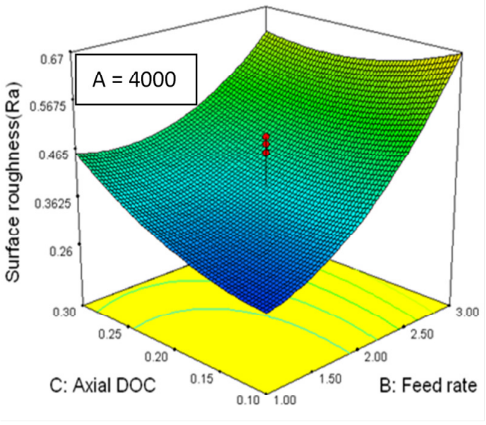

Fig 5.8(c): 3-D Ra plot for B and C

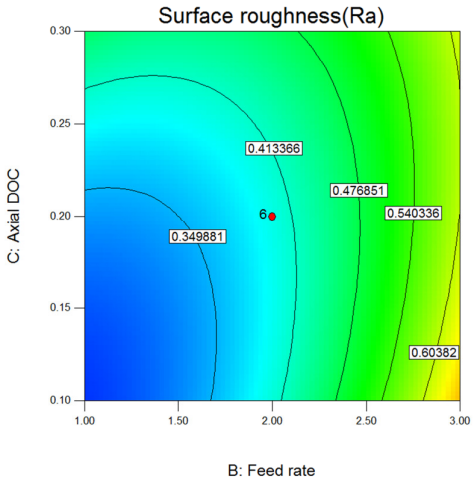

Fig 5.8(d): Contour plot for B and C

Fourteen solutions were obtained after optimization based on the minimum surface roughness in the selected range of cutting parameters. Experimental test show that the surface roughness value of 0.2880 was close to the predicted surface roughness value of 0.2598 for the selected combination of 3001 rpm (cutting speed), 1 mm/min (feed rate), and 0.1 mm (axial depth of cut).

From the results one can conclude that minimal surface roughness is achievable with low cutting parameter values. It is also possible to achieve high material removal rate (at high feed rate and high depth of cut) with little compromise on the surface roughness.

5.3 Experimental Results using High Spindle Speed Vertical Milling Machine

The cutting experiments were carried out on the V-55 vertical milling machine (20000 rpm capacity), using the two flute square end micro grain solid carbide end mill and the CBN coated internal grinding tool grit. The influence of the cutting speed, feed rate and the axial depth of cut on the surface roughness and the cutting force were analyzed. By using RSM, surface roughness, and cutting force models were developed in terms of the cutting speed, feed rate and axial depth of cut. For

each case the total number of experiments were planned based on the CCD, which states that twenty tests are required for three parameters (Table 3.11, Chapter 3). The Mitutoyo SJ 301 Surface tester was used to measure the surface roughness (Ra). The measurement of the cutting forces in the X, Y and Z directions during the machining process was carried out using the Piezoelectric Kistler dynamometer, and the resultant cutting force was then used to analyze the effect of the cutting parameters.

5.3.1 Surface Roughness Analysis by using Two Flute Square End Micro Grain Solid Carbide End Mill

The cutting experiments were carried out on the V-55 vertical milling machine using a two flute square end micro grain solid carbide end mill. The independent variables were coded in Table 5.11, taking into consideration the preliminary tests, limitations of cutting tool and capacity of the machine.

Table 5.11: Actual coded factors for experiment

Factors	Minimum	Central	Maximum
Coded factor	-1	0	1
Spindle Speed (RPM)	10000	15000	20000
Feed Rate (mm/min)	30	60	90
Depth of Cut (mm)	0.03	0.04	0.05

During all the milling experiments the Ra was recorded at three places and an average of the three Ra was tabulated (Table 5.12) to establish a surface roughness model. The values of resultant cutting force was also tabulated (Table 5.17) to establish cutting force model.

Table 5.12: Cutting conditions and output responses

Standard Order	Spindle Speed (rpm)	Feed Rate (mm/min)	Depth of Cut (mm)	Surface Roughness (μm)	Resultant cutting force (N)
1	15000	60	0.056	0.5633	41.2
2	10000	90	0.05	0.78	34.65
3	15000	60	0.023	0.533	14.95
4	20000	30	0.05	0.53	37.2
5	20000	30	0.03	0.533	15.58
6	15000	110	0.04	0.78	21.77
7	15000	60	0.04	0.605	14.34
8	10000	30	0.03	0.59	17.7
9	15000	60	0.04	0.543	22.4
10	15000	60	0.04	0.57	23.67
11	10000	30	0.05	0.5967	30.4
12	15000	60	0.04	0.5866	22.66
13	20000	60	0.04	0.513	14.56
14	15000	60	0.04	0.523	13.87
15	15000	9.5	0.04	0.5167	46.17
16	6591	60	0.04	0.5566	24.93
17	20000	90	0.05	0.736	50.02
18	15000	60	0.04	0.603	14.2
19	20000	90	0.03	0.65	20.7
20	10000	90	0.03	0.623	25.4

Based on the results, the fit and summary test suggests the following quadratic Equation (5.5) for surface roughness(R_a):

$$R_a = 0.808 - 3.07 \times 10^{-6} \times A - 8.105 \times 10^{-3} \times B - 3.514 \times C + 8.892 \times 10^{-8} \times A \times B - 2.018 \times 10^{-4} \times A \times C + 0.0997 \times B \times C + 9.843 \times 10^{-11} \times A^2 + 4.316 \times 10^{-5} \times B^2 + 34.222 \times C^2 \quad (5.5)$$

To verify the adequacy of the proposed quadratic model, ANOVA was used with 95% confidence level and the results are shown in the Table 5.13

Table 5.13: ANOVA table for the surface roughness quadratic model

Source	Sum of Squares	DOF	Mean Square	F-value	P-value	
Model	*0.11*	*9*	*0.012*	*7.02*	*0.0027*	*significant*
A-Cutting Speed	2.169×10^{-3}	1	2.169×10^{-3}	1.24	0.2918	
B-Feed Rate	0.071	1	0.071	40.33	*<0.0001*	
C-Depth of Cut	6.488×10^{-3}	1	6.488×10^{-3}	3.70	*0.0832*	
AB	1.423×10^{-3}	1	1.423×10^{-3}	0.81	0.3885	
AC	8.141×10^{-4}	1	8.141×10^{-4}	0.46	0.5109	
BC	7.158×10^{-3}	1	7.158×10^{-3}	4.09	*0.0708*	
A^2	5.481×10^{-5}	1	5.481×10^{-5}	0.031	0.8631	
B^2	0.022	1	0.022	12.52	0.0054	
C^2	1.702×10^{-4}	1	1.702×10^{-4}	0.097	*0.7616*	
Residual	0.018	10	1.751×10^{-3}			
Lack of Fit	0.012	*5*	2.401×10^{-3}	*2.18*	*0.2064*	*Not significant*
Pure Error	5.509×10^{-3}	5	1.102×10^{-3}			
Cor Total	0.13	19				

Table 5.13 shows that the model is significant with 95% confidence level. The feed rate is very significant and dominant in the proposed model.

The perturbation plot in Fig 5.9(a) shows that the feed rate has the most significant effect on surface roughness. The figure clearly indicates that with the increase in the

feed rate and the axial depth of cut, the surface roughness value increases. In the case of the cutting speed, the surface roughness decreases by increasing the cutting speed. The interaction plot in Fig 5.9(b) indicates that the effect of the cutting speed is not significant on surface roughness. However, at low feed rate (30 mm/min) surface roughness reduces slightly with increase of the cutting speed.

As seen from Fig 5.9(c), the surface roughness slightly increases by increasing the axial depth of cut. This increase is less at the high cutting speed of 20000 rpm, and this speed is preferable to get a low surface roughness.

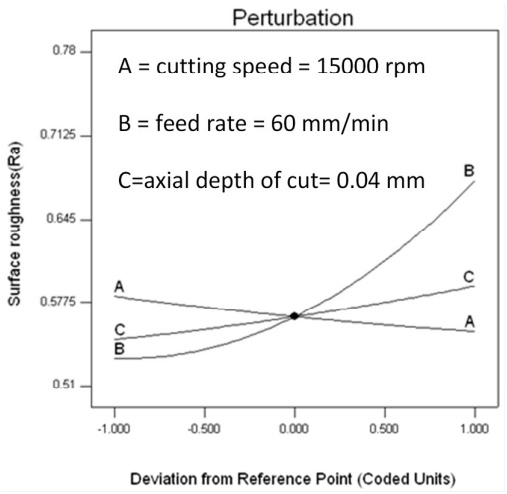

Fig 5.9(a): Perturbation plot for Ra

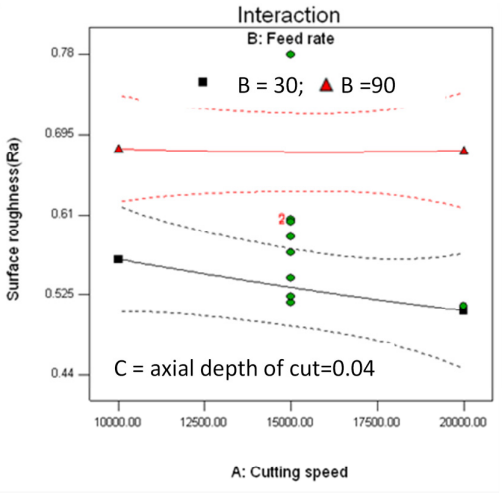

Fig 5.9(b): Interaction plot for A and B

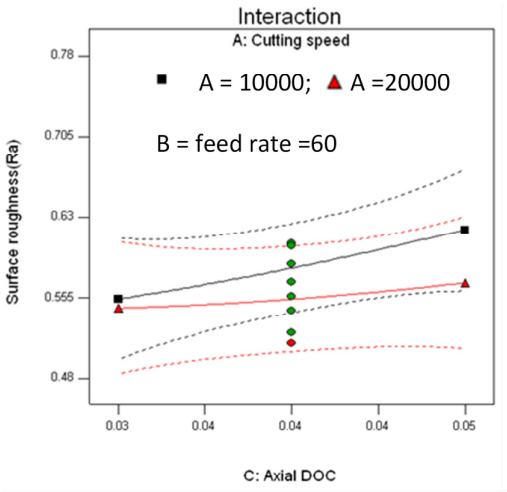

Fig 5.9(c): Interaction plot for A and C

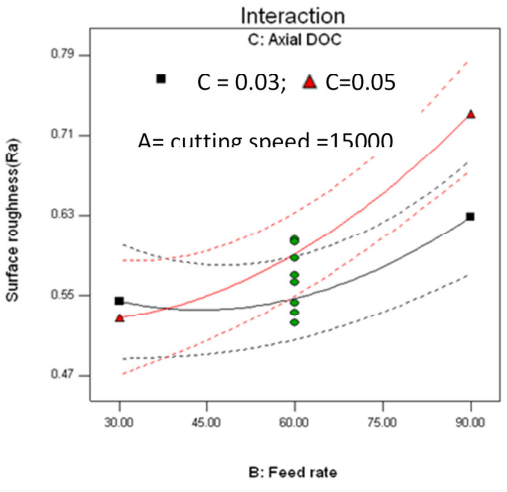

Fig 5.9(d): Interaction plot for B and C

Figure 5.9(d) shows the effect of the feed rate on the surface roughness at two different values of the axial depth of cut. The surface roughness Ra increases by increasing the feed rate and this increase is rapid at a higher axial depth of cut value of 0.05mm. However, at a low feed rate of 30 mm/min, surface roughness is small at a high axial depth of cut than a low axial depth of cut.

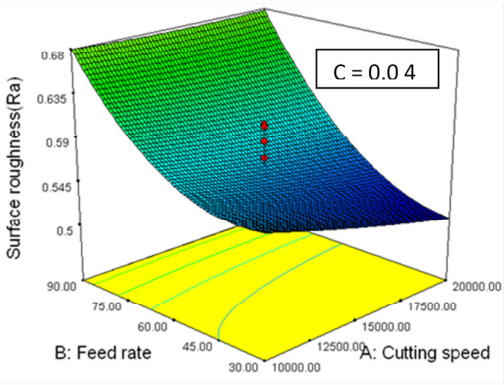

Fig 5.10(a): 3-D Ra plot for A and B

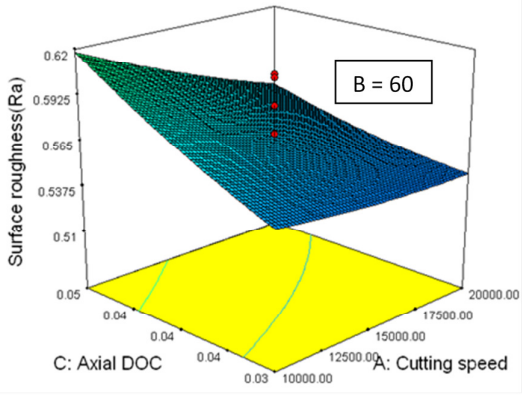

Fig 5.10(b): 3-D Ra plot for A and C

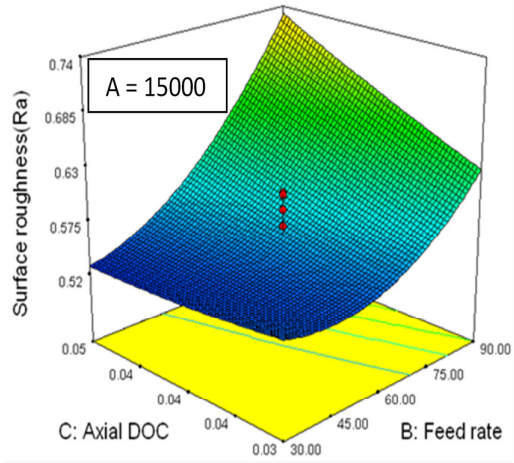

Fig 5.10(c): 3-D Ra plot for B and C

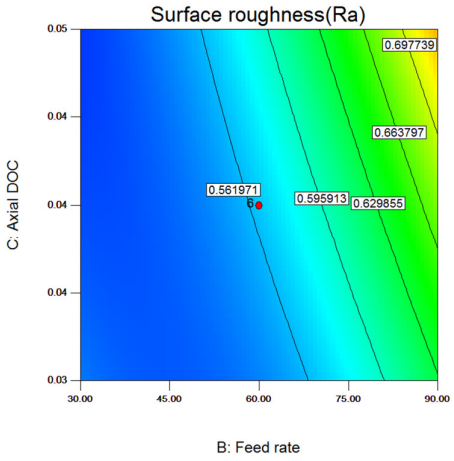

Fig 5.10(d): Contour plot for B and C

5.10(a) shows that the surface roughness increases rapidly with increase of the feed rate, and the effect of the cutting speed is not significant. A similar trend is observed between the axial depth of cut and the cutting speed in Fig 5.10(b). This demonstrates that the feed rate and axial depth of cut is the most significant factor in the surface roughness model for this case.

Figure 5.10(c) shows the highest surface roughness when machining at a high feed rate of 90 mm /min, at a high axial depth of cut 0.05 mm, and at a particular cutting speed of 15000 rpm. It clearly shows that surface roughness increases with an increase in feed rate and axial depth of cut. All the 3-D and contour plots conclude that the lowest surface roughness is achieved when machining with a higher cutting speed, a lower feed rate, and a lower axial depth of cut.

The developed quadratic model Eqn (5.5) was used for optimization of the operating cutting parameters. Forty solutions were obtained after optimization for the minimum surface roughness in the studied range of cutting parameters. Low surface roughness was predicted (0.4928 μm) at a combination of 2000 rpm (cutting speed), 30 mm/min (feed rate), and 0.05 mm (axial depth of cut) in the studied range of cutting parameters.

One can conclude that feed rate is the most dominant factor affecting the surface roughness, where the value is less at a high cutting speed, low feed rate, and low axial depth of cut value in the selected range of cutting parameters. However, at a low feed rate of 30 mm/min, surface roughness is small at a high axial depth of cut than a low axial depth of cut.

The behavior of the cutting parameters on surface roughness of these experiments is same as that of the metallic materials

5.3.2 Cutting Force Model by using Two Flute Square End Micro Grain Solid Carbide End Mill

Cutting forces in the X, Y and Z directions were measured using a Kistler Dynamometer. The resultant cutting force (resultant of F_X, F_Y and F_z) acting on the work piece is represented in Table 5.12. The second order model shown in Eqn (5.6) was developed to describe the relationship between the cutting force (F_r) and the

investigated independent variables using experimental results.

$$F_r = 132.83 - 5.484 \times 10^{-3} \times A - 0.923 \times B - 3171.08 \times C + 4.992 \times 10^{-6} \times A \times B + 0.0725 \times A \times C + 1.771 \times B \times C + 8.055 \times 10^{-8} \times A^2 + 6.253 \times 10^{-3} \times B^2 + 35433.0 \times C^2 \quad (5.6)$$

The ANOVA analysis was carried out to check the adequacy of the second order model. Table 5.14, shows that the second order model is adequate with 95% confidence intervals and it clearly shows that the individual variable axial depth of cut C is more significant.

Table 5.14 in next page shows that, the model F-value of 3.28 implies that the model is significant (0.05>P). The effect of the axial depth of cut is significant, while the cutting speed and feed rate is insignificant (values of P> 0.0500).

Table 5.14: ANOVA table for cutting force quadratic model

Source	**Sum of Squares**	**DOF**	**Mean Square**	**F-value**	**P-value**	
Model	*1759.55*	*9*	*195.51*	*3.28*	*0.0389*	*significant*
A-Cutting Speed	4.57	1	4.57	0.077	0.7872	
B-Feed Rate	9.09	1	9.09	0.15	*0.7041*	
C-Depth of Cut	1003.01	1	1003.01	16.85	*0.0021*	
AB	4.49	1	4.49	0.075	0.7893	
AC	105.06	1	105.06	1.77	0.2135	
BC	2.26	1	2.26	0.038	*0.8494*	
A^2	36.71	1	36.71	0.62	0.4505	
B^2	460.23	1	460.23	7.73	0.0194	
C^2	182.46	1	182.46	3.07	*0.1105*	
Residual	595.20	10	59.52			
Lack of Fit	478.78	*5*	95.76	*4.11*	*0.0734*	*Not significant*
Pure Error	116.42	5	23.28			
Cor Total	2354.76	19				

From the perturbation plot in Fig 5.11(a), one can see that the cutting force decreases initially with the increase of cutting speed A and the feed rate B, until a minimum is reached. The cutting force value then increases with the increase of feed rate and cutting speed. The axial depth of cut C value shows a dominant effect on the cutting force where the cutting force increases by increasing axial depth of cut. Figure 5.11(a) explains the effect of each cutting parameter on the cutting force.

The interaction effect of the cutting parameters on the cutting force is shown in Fig 5.11(b-d). Fig 5.11(b) presents the effect of the cutting speed on the cutting force at two different feed rates, showing an interaction between these two parameters. Although the cutting speed does not affect the cutting force significantly, it can be seen from this figure that the general trend is that the cutting force decreases with an increase of the feed rate at a given axial depth of cut 0.04 mm.

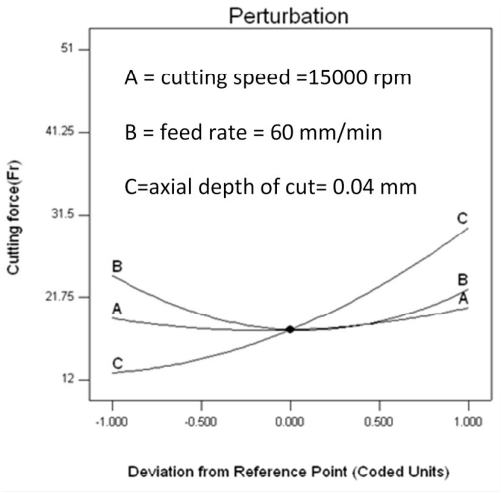

Fig 5.11(a): Perturbation plot for Fr

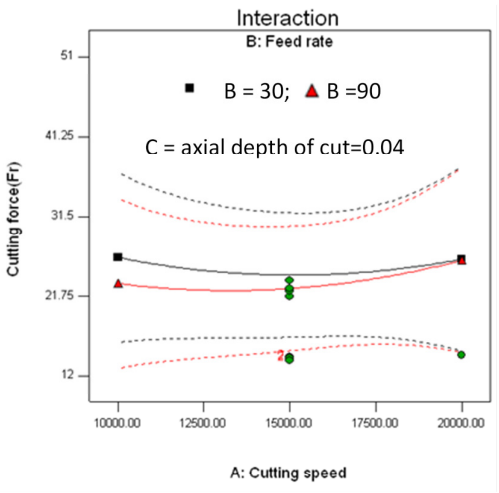

Fig 5.11(b): Interaction plot for A and B

The variations of surface roughness with two different axial depths of cut are shown in Fig 5.11(c). This figure reveals that for a given feed rate, the cutting force increases by increasing the cutting speed, when the axial depth of cut is 0.05mm and the cutting force decreases by increasing the cutting speed when the axial depth of cut 0.03mm. This indicates that the effect of the axial depth of cut is significant.

Figure 5.11(d) also shows the effects of the feed rate with two different axial depths of cut values on the cutting force. This figure shows that the cutting force decreases by increasing the feed rate up to a moderate value, and then increases for both low and high axial depth of cut value at a given cutting speed of 15000 rpm. This increase is very small and hence the effect of the feed rate is also not significant. The cutting force is high at a high axial depth of cut of 0.05 mm irrespective of the other two cutting parameters. One can observe clearly from Fig 5.11(c-d) that the cutting force decreases with the increase of cutting speed and feed rate at low axial depth of cut. At a high axial depth of cut the cutting force increases with an increase of cutting speed and feed rate. This may be due to the large amount of material removal rate at high axial depth of cut, and it can certainly lead to chattering and high load on cutting edges.

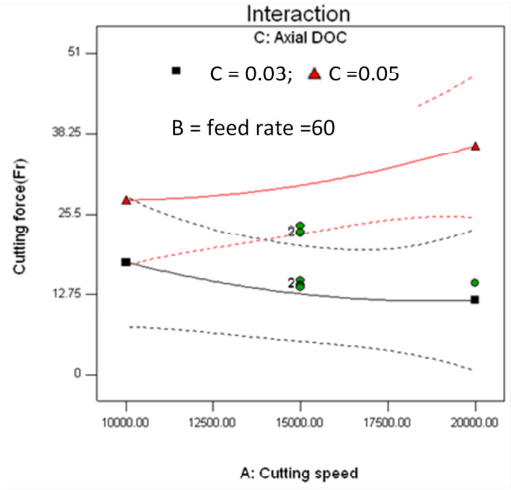

Fig 5.11(c): Interaction plot for A and C

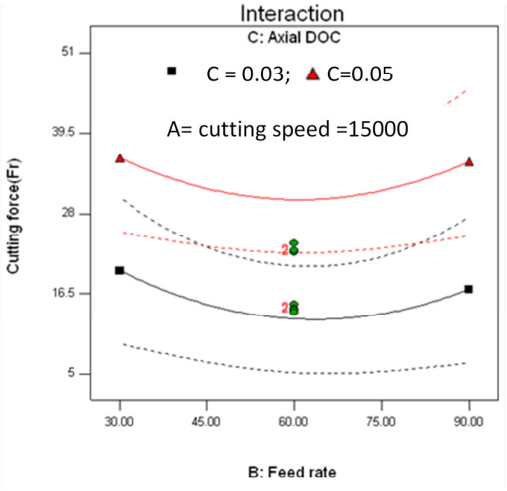

Fig 5.11(d): Interaction plot for B and C

The 3-D and contour plots shown in Fig 5.12(a-d) gives a clearer picture about the combined effect of the cutting speed, feed rate and the axial depth of cut on the resultant cutting force.

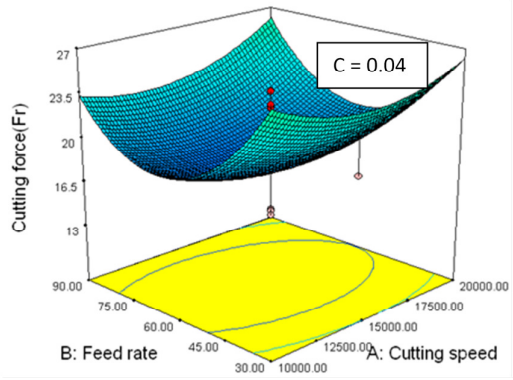

Fig 5.12(a): 3-D Fr plot A and B

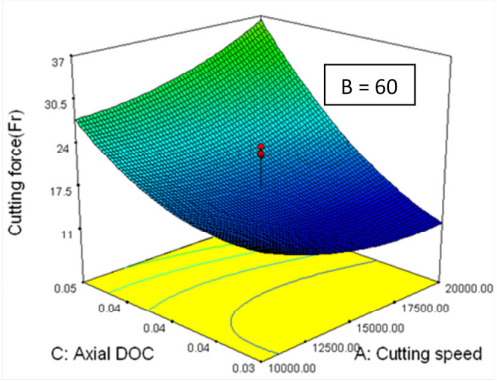

Fig 5.12(b): 3-D Fr plot A and C

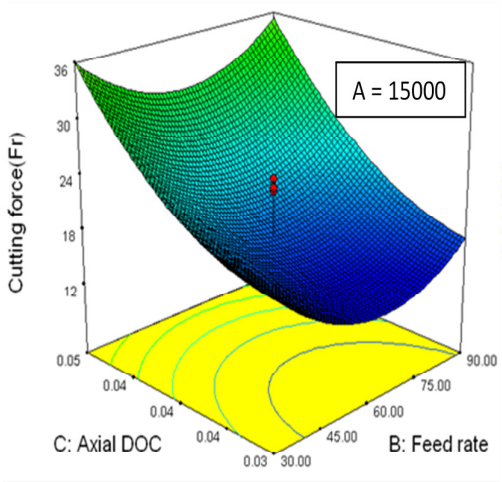

Fig 5.12(c): 3-D Fr plot B and C

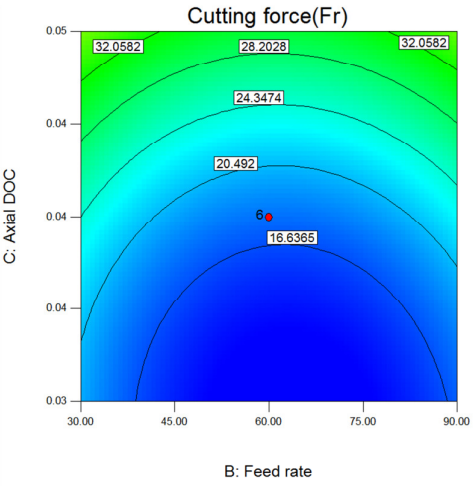

Fig 5.12(d): Contour plot for Fr

Figure 5.12(a) shows the combined effect of the cutting speed A and the feed rate B on the cutting force at the particular axial depth of cut 0.04mm. The figure shows that cutting force value is low at moderate feed rate and lower cutting speed. It is clear from these figures that the cutting force increases with the increase of axial depth of cut, irrespective of the feed rate and cutting speed in the selected range of cutting parameters.

Figure 5.12(b) represents the effect of cutting speed A and the axial depth of cut C on the cutting force for the feed rate 60 mm/min. The figure shows that the cutting force

value increases by increasing the axial depth of cut, and decrease by increasing the cutting speed. Figure 5.12(c-d) shows the combined effect of feed rate B and axial depth of cut C on the cutting force at the particular cutting speed 15000 rpm. The lower cutting force appears at moderate feed rate and low axial depth of cut value.

The developed quadratic model Eqn (5.6) was used for further optimization of the operating cutting parameters for the minimum cutting force. Forty solutions were obtained based on the minimum cutting force in the selected range of cutting parameters. Low cutting force was predicted (12.1217 N) at a combination of 18807 rpm (cutting speed), 54.7 mm/min (feed rate), and 0.03 mm (axial depth of cut).

Seven solutions were obtained after optimization based on the minimum surface roughness and minimum cutting force in the selected range. The minimum surface roughness (0.5271 μm) and low cutting force (13.87 N) were predicted for a combination of 20000 rpm (cutting speed), 44 mm/min (feed rate), and 0.03 mm (axial depth of cut). The above discussed results has been published in the Journal [Reddy et al. 2011].

From the experimental studies, one can conclude that a combination of low axial depth of cut, moderate feed rate and high cutting speed is the right choice to achieve low cutting forces in the selected range of cutting parameters. The most dominant factor is the axial depth of cut compared to the other two factors.

5.3.3 Surface Roughness Model using CBN Coated Internal Grinding Tool grit

The cutting experiments were carried out on a V-55 vertical milling machine using a CBN coated internal grinding tool grit. In this case only the effect of cutting speed and feed rate on the surface roughness and the cutting force was analyzed. The independent variables were coded taking into consideration the preliminary tests, the limitation of tool and capacity of the milling machine as depicted in Table 5.15.

Table 5.15: Actual coded factors for experiment

Factors	Minimum	Central	Maximum
Coded factor	-1	0	1
Spindle Speed (RPM)	10000	15000	20000
Feed Rate (mm/min)	1	2	3

Table 5.16: Cutting conditions and output responses

Standard Order	Spindle Speed (rpm)	Feed Rate (mm/min)	Surface Roughness (μm)	Resultant cutting force (N)
1	15000	2	0.71	51.1
2	15000	2	0.74	57.2
3	15000	2	0.76	55.2
4	15000	2	0.77	55.6
5	15000	0.58	0.5	35.8
6	15000	3.41	0.966	63.82
7	10000	3	1.07	65.2
8	7928	2	0.84	58.4
9	20000	1	0.52	33.21
10	10000	1	0.64	50.34
11	20000	2	0.67	50.52
12	20000	3	0.96	61.2
13	15000	2	0.75	51.6

When considering only two factors, a total number of thirteen tests are required (8 + 5 at center =13) according to CCD. The Mitutoyo SJ 301 was used to measure the surface roughness of the work piece. During all thirteen experiments the surface roughness was recorded at three places and the averages of three Ra values expressed in Table 5.16, to establish the surface roughness model. The cutting force was measured using Piezoelectric Kistler dynamometer.

The experimental results were used to develop the surface roughness model by using the RSM. The fit and summary test suggests that the following quadratic model for the surface roughness(R_a) holds:

$$R_a = 0.786 - 4.0467 \times 10^{-5} \times A + 0.153 \times B + 5.0 \times 10^{-7} \times A \times B + +9.368 \times 10^{-10} \times A^2 + 7.608 \times 10^{-3} \times B^2 \quad (5.7)$$

where A is cutting speed and B is the feed rate

Table 5.17: ANOVA table for surface roughness Ra quadratic model

Source	Sum of Squares	DOF	Mean Square	F-value	P-value	
Model	*0.32*	*5*	*0.064*	*32.97*	*0.0001*	*significant*
A-Cutting Speed	0.021	1	0.021	10.72	0.0136	
B-Feed Rate	0.29	1	0.29	149.58	*<0.0001*	
AB	2.500×10^{-5}	1	2.500×10^{-5}	0.013	0.9131	
A^2	2.662×10^{-3}	1	2.662×10^{-3}	1.36	0.2813	
B^2	4.084×10^{-4}	1	4.084×10^{-4}	0.21	0.6614	
Residual	0.014	7	1.954×10^{-3}			
Lack of Fit	0.012	*3*	3.852×10^{-3}	*7.27*	*0.0427*	*significant*
Pure Error	2.120×10^{-3}	4	5.300×10^{-4}			
Cor Total	0.34	12				

ANOVA was carried out to investigate the effect of each parameter on the surface roughness. Table 5.17 shows the results of ANOVA for the surface roughness Ra. The F-value and probability value indicate that the model is significant. From the table one can conclude that the feed rate is the most dominant factor to affect the surface roughness. The effect of the cutting speed on the surface roughness is also significant in this case.

The Model F-value of 32.97 implies that it is significant (P value < 0.05). There is only a 0.01% chance that a "Model F-Value" this large could occur due to noise. In this case A, and B are significant parameters. The F value 149.58 indicates that feed rate B has the highest influence on the surface roughness Ra. Significant lack of fit indicates that other cutting conditions could influence the surface roughness model significantly.

In this case only two cutting parameters were considered, the perturbation plot (Fig 5.13(a)), shows that the surface roughness decreases when increasing the cutting speed, and increases when increasing the feed rate. It is apparent from the interaction plot, Fig 5.13(b), that the surface roughness value increases by increasing the feed rate. At a high cutting speed of 20000 rpm the surface roughness is low as compared to 10000 rpm cutting speed.

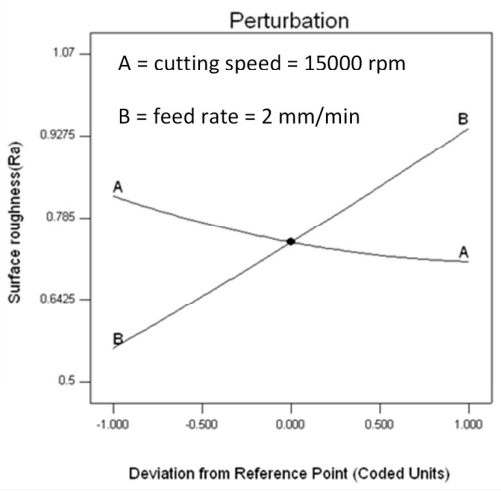

Fig 5.13(a): Perturbation plot for Ra

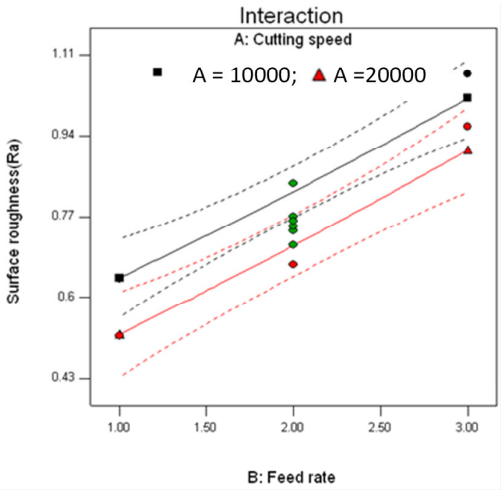

Fig 5.13(b): Interaction plot for A and B

In the 3-D and contour plots shown in Fig 5.14(a-b), it is clear that to achieve good surface roughness, a low feed rate and a high cutting speed is the right choice. These results concur with previous experiments.

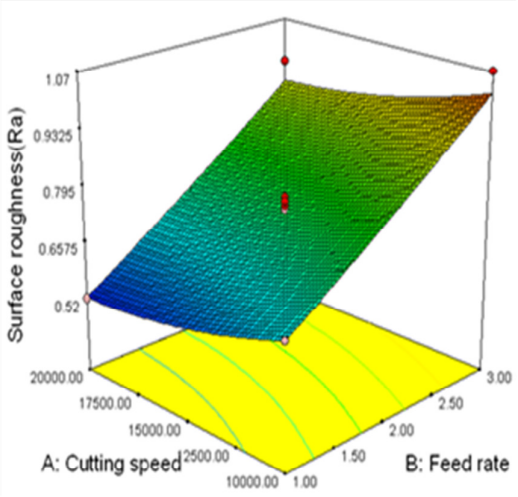

Fig 5.14(a): 3-D Fr plot for A and B

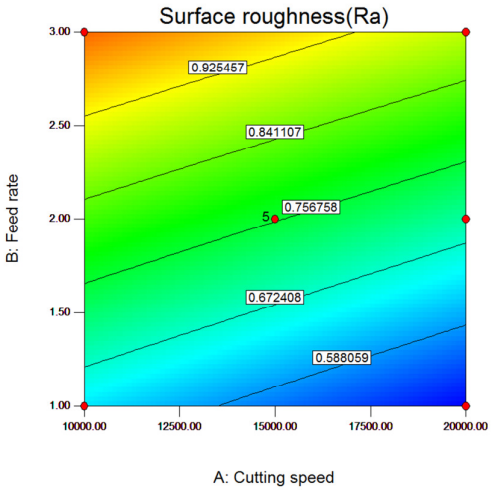

Fig 5.14(b): Contour plot for A and B

The developed quadratic model, Eqn (5.7), was used for further optimization of the operating cutting parameters. Six solutions were obtained for the minimum surface roughness optimization in the studied range of the cutting parameters. Low surface roughness was predicted (0.5037 µm) at a combination of 20000 rpm (cutting speed), 1 mm/min (feed rate).

The effect of the cutting parameters on the surface roughness is very similar to that for metallic materials. The lack of fit indicates a significant effect, implying that other cutting conditions, which are not considered here, may have a significant effect.

5.3.4 Cutting Force Model using CBN Coated Internal Grinding Tool grit

The experimental results were used to develop the cutting force model by using the RSM. The fit and summary tests suggest that the following second order model for the cutting force (F_r) holds.

$$F_r = 56.11 - 1.837 \times 10^{-3} \times A + 8.308 \times B + 6.565 \times 10^{-4} \times A \times B - 1.2335 \times 10^{-8} \times A^2 - 1.9616 \times B^2 \quad (5.8)$$

ANOVA (Table 5.18) was used to investigate the effect of each cutting parameter on the cutting force. The F-value and the probability values indicate that the model is significant. These results (Table 5.18), clearly show that the cutting parameters have significant effects, and also the interaction effect is considerable on the cutting force.

Table 5.18: ANOVA table for cutting force Fr quadratic model

Source	Sum of Squares	DOF	Mean Square	F-value	P-value	
Model	*1060.44*	*5*	*212.09*	*39.70*	*<0.0001*	*significant*
A-Cutting Speed	129.72	1	129.72	24.28	0.0017	
B-Feed Rate	850.29	1	850.29	159.18	*<0.0001*	
AB	43.10	1	43.10	8.07	0.0250	
A^2	0.46	1	0.46	0.086	0.7773	
B^2	27.15	1	27.15	5.08	0.0588	
Residual	37.39	7	5.34			
Lack of Fit	9.08	*3*	3.03	*0.43*	*0.7444*	*Not significant*
Pure Error	28.31	4	7.08			
Cor Total	1097.83	12				

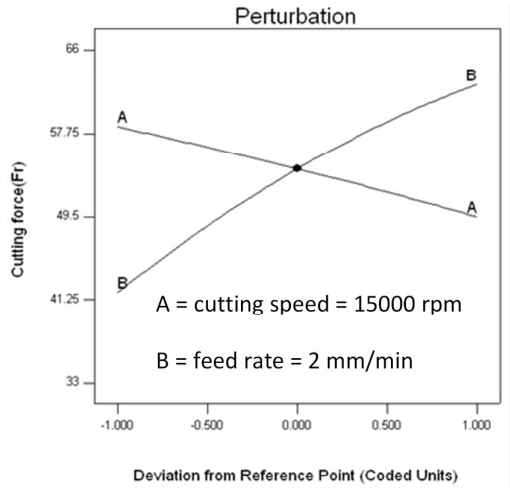

Fig 5.15(a): Perturbation plot for Ra

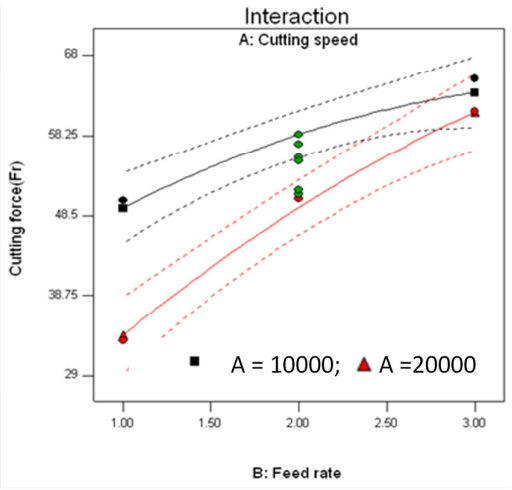

Fig 5.15(b): Interaction plot for A and B

The perturbation plot in Fig 5.15(a) indicates that the cutting force decreases by increasing the cutting speed, and increases by increasing the feed rate for the studied range of cutting parameters. Figure 5.15(b) clearly shows that the cutting force value increases by increasing the feed rate, this increase is rapid at a high cutting speed value. At this speed, the high feed rate generates more friction and this may lead to large cutting forces.

It can be observed from the 3-D and contour plots in Fig 5.16(a-b), that to achieve a low cutting force, a low feed rate and high cutting speed would be required.

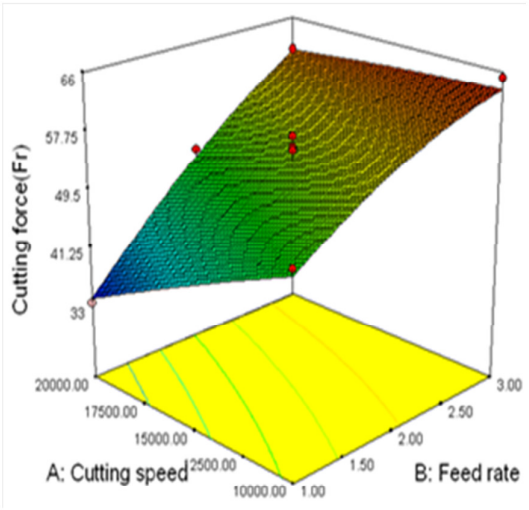

Fig 5.16(a): 3-D Fr plot for A and B

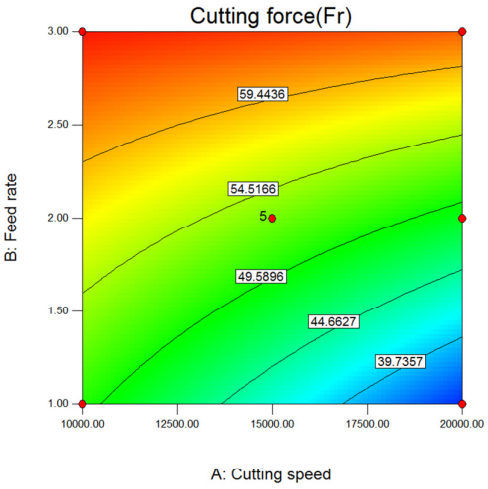

Fig 5.16(b): Contour plot for A and B

operating cutting parameters for the minimum cutting force. Four solutions were obtained based on the minimum cutting force and the predicted value of 34.81N for the selected combination of 20000 rpm (cutting speed), 1 mm/min (feed rate).

Only one solution was obtained based on the minimum surface roughness and cutting force in the studied range. The predicted surface roughness and cutting force values were 0.5037 and 34.81 respectively.

To achieve low cutting force, experimental studies suggesting, low feed rate and high cutting speed would be suitable for the studied range of cutting parameters.

5.4 Summary

The experimental results of the Aluminum Nitride Ceramic (AlN) for each tool, using low speed and high speed CNC end milling process are summarized below:

(a) Low speed CNC milling machine

- *Two Flute Square End Micro Grain Solid Carbide end mill*

  The surface roughness Ra increased with increase in the cutting speed, feed rate and the axial depth of cut. Lack of fit was significant for the predictive surface roughness model and this implies that other cutting parameters and range of parameters, which are not considered for this study may influence significantly. Low surface finish was predicted (0.4591 μm) at a combination of 3006 rpm (cutting speed), 14.2 mm/min (feed rate), and 0.15 mm (axial depth of cut), in the selected range of cutting parameters

- *TiAlN and TiN Coated Carbide Tool insert*

  The surface roughness decreased with increase in the cutting speed, while increased with increase in the feed rate and the axial depth of cut. Tool wear increased with an increase in the cutting speed, feed rate, and the axial depth of cut. Low surface finish (0.4369 μm) was predicted at a combination of 4970 rpm cutting speed, 17.7 mm/min feed rate, and 0.16 mm axial depth of cut. Also low tool wear 11.1754 μm was predicted at a combination of 3000 rpm cutting speed, 10 mm/min feed rate, and 0.1 mm axial depth of cut in the studied range of cutting parameters.

- *CBN Coated Internal Grinding Tool grit*

  The feed rate was found to have the maximum influence on the surface roughness, which increased with the increase of feed rate. The effect of cutting speed and axial depth of cut on the surface roughness was negligible.

A minimum surface roughness of 0.2598 μm is could be achieved at a combination of the cutting speed of 3001 rpm, the feed rate of 1 mm/min, and the axial depth of cut of 0.1 mm within the studied range of cutting parameters.

(b) High speed CNC milling machine

- *Two Flute Square End Micro Grain Solid Carbide end mill*

  The feed rate had the most significant effect on surface roughness. The surface roughness Ra increased by increasing the feed rate, and this increase is rapid at a higher axial depth of cut value. The axial depth of cut C value showed a dominant effect on the cutting force, where the cutting force increased by increasing axial depth of cut. Low surface roughness (0.527 μm) and low cutting force (13.87 N) was predicted at a combination of 20000 rpm (cutting speed), 44 mm/min (feed rate), and 0.03 mm (axial depth of cut) in the studied range of cutting parameters.

- *CBN Coated Internal Grinding Tool grit*

  The surface roughness and cutting force decreased when increasing the cutting speed, and increased when increasing the feed rate. The lack of fit is significant on the surface roughness model, indicating that other factors not considered for study (radial depth of cut, tool geometry, and tool properties) might be of significant influence. Low surface finish (0.5037 μm) and low cutting force (34.81 N) was predicted at a combination of 20000 rpm (cutting speed), 1 mm/min (feed rate) in the studied range of cutting parameters.

CHAPTER 6: CONCLUSIONS AND RECOMMENDATIONS

This chapter summarizes the key findings on the performance of the machining of advanced ceramics by using the end milling. It also provides the recommendations for future research in this area.

6.1 Major Conclusions

- The results of the experimental tests with both low speed and high speed CNC machines, that cover a wide range of applications and products required for manufacturers, show that the end milling process of advanced ceramics can be applied successfully with the proper selection of cutting parameters.
- The cutting parameters profoundly affect the surface roughness, cutting force and the tool wear; a proper selection of the cutting parameters improves surface quality (good surface finish, minimal edge chips and surface cracks), reduces cutting forces and tool wear. Models based on the RSM approach for finding the cutting parameters (cutting speed, feed rate, axial depth of cut) that yield the minimum surface roughness, low cutting forces and the least expected tool wear for each given tool and set of cutting parameters have been developed. The optimization results have been validated experimentally with a good surface roughness.
- This study suggests that the surface finish on Machinable Glass Ceramic (MGC) and Aluminum Nitride Ceramic (AlN) generated by end mills is comparable to internal grinding tool grits. Ultimately, one can significantly improve the productivity and manufacturing cost of advanced ceramic components by reducing the involvement of the grinding process for finishing purposes.

Findings specific for each tool which can be used as a guideline for low and high speed CNC milling machines for both studied types of materials are given in the following paragraph.

6.1.1 Specific Findings for Machinable Glass Ceramic (MGC)

(a) Low speed CNC milling machine

- *Two Flute Square End Micro Grain Solid Carbide end mill*

  All the three cutting parameters have been chosen to have low values within the selected range in order to produce a smooth surface finish. The effect of the cutting speed has not been very significant. The surface roughness is predicted to be as low as 0.4790 µm at the following combination of the cutting parameters values: the cutting speed is 4933 rpm, the feed rate is 11.5 mm/min, and the axial depth of cut is 0.12 mm within the studied range of the parameters. However, in order to reduce machining time and increase material removal rate, the feed rate and axial depth of cut should be as high as possible.

- *TiAlN and TiN Coated Carbide Tool insert*

  The minimal surface roughness has been obtained with a higher cutting speed, lower feed rate, and the value of moderate depth of cut for the studied range of cutting parameters. These results are very similar to those obtained for machining metallic materials. The surface finish is predicted to be as low as 0.3136 µm at the following combination of the cutting parameters values: the cutting speed is 4998 rpm, the feed rate is10 mm/min, and the axial depth of cut is 0.33 mm within the studied range of the parameters. However, in order to reduce the machining time and increase the material removal rate, both the feed rate and axial depth of cut should be as high as possible.

The cutting speed and the axial depth of cut are the most influential parameters on the tool wear for the selected range conditions. At the low cutting speed and the axial depth of cut, one can choose a high feed rate without scarifying the tool life; this reduces the machining time since the material removal rate is high. The tool wear is predicted to be as low as 23.12 µm µm at the following combination of the cutting parameters values: the cutting speed is 3007 rpm, the feed rate is19 mm/min, and the axial depth of cut is 0.3 mm within the studied range of the parameters.

The cutting speed of 3000 rpm, the feed rate of 10 mm/min, and the axial depth of cut 0.3 mm represent the optimal combination within the studied range of cutting parameters to achieve the surface roughness as low as 0.3419 µm and the minimal tool wear of 25.81 N as it follows from the model prediction.

- *CBN Coated Internal Grinding Tool grit*

  The moderate cutting parameters gives better results for the surface roughness in the studied range of cutting parameters. A minimum surface roughness of 0.2786 µm is predicted to be achieved at a combination of the cutting speed of 3943 rpm, the feed rate of 1.7 mm/min, and the axial depth of cut of 0.17 mm within the studied range of cutting parameters.

(b) High speed CNC milling machines

- *Two Flute Square End Micro Grain Solid Carbide end mill*

  The surface roughness increases with an increase in the feed rate and axial depth of cut, whilst increasing cutting speed decreases the surface roughness. However, the surface roughness increases with the cutting speed increase at high feed rate. The predicted combination of optimal cutting parameters to achieve the surface finish as low as 0.3548 µm is represented by the cutting

speed of 20000 rpm, the feed rate of 30 mm/min, and the axial depth of cut of 0.03 mm in the studied range of the cutting parameters.

The cutting force is mainly affected by the cutting speed and feed rate. The values of the cutting force increase with the increase in the cutting speed and feed rate. The model predicts the cutting force as low as 23.345 N at the cutting speed of 10000 rpm, the feed rate of 30 mm/min, and the axial depth of cut of 0.05 mm in the studied range of cutting parameters.

The lowest values of the surface roughness (0.4765 μm) and the cutting force (33.66 N) are achieved at the cutting speed of 11590 rpm, the feed rate of 30 mm/min, and axial depth of cut of 0.03 mm in the studied range of cutting parameters.

- *CBN Coated Internal Grinding Tool grit*

  A minimum surface roughness value of 0.382 μm is predicted at as low as 10000 rpm the cutting speed and as low as 1.1 mm/min the feed rate for studied range of the cutting parameters.

  In order to achieve a low cutting force, a low feed rate and high cutting speed are necessary. A minimum cutting force of 35.67 N is predicted at a combination of 20000 rpm cutting speed and 1 mm/min feed rate in the studied range of the cutting parameters.

  The model predicts that within the studied range of the cutting parameters an optimal combination of 10000 rpm cutting speed and 1 mm/min feed rate achieves a minimum surface roughness of 0.3822 μm and a minimum cutting force of 39.53 N.

6.1.2 Specific Findings for Aluminum Nitride Ceramic

(a) Low speed CNC milling machine

- *Two Flute Square End Micro Grain Solid Carbide end mill*

  The surface roughness increases with an increase of the cutting speed, feed rate, and axial depth of cut. The surface roughness is predicted to be as low as 0.4591 μm at the following combination of the cutting parameters values: the cutting speed is 3006 rpm, the feed rate is14.2 mm/min, and the axial depth of cut is 0.15 mm within the studied range of the parameters. However in order to reduce machining time and increase material removal rate, the feed rate and axial depth of cut should be as high as possible.

- *TiAlN and TiN Coated Carbide Tool insert*

  An improved surface roughness can be achieved with a high cutting speed, lower feed rate, and low axial depth of cut. The effect of these parameters is similar to that found during end milling metallic materials. However, in order to reduce machining time and to increase material removal rate both the feed rate and axial depth of cut should be as high as possible. The surface finish is predicted to be as low as 0.4369 μm at the following combination of the cutting parameters values: the cutting speed is 4970 rpm, the feed rate is 17.7 mm/min, and the axial depth of cut is 0.16 mm within the studied range of the parameters.

  The tool wear is mainly affected by the cutting speed. The values of tool wear increase with increasing the cutting speed, feed rate and axial depth of cut. A minimum tool wear of 11.1754 μm is predicted at an optimal combination of 3000-rpm-cutting speed, 10-mm/min-feed rate, and 0.1-mm-axial depth of cut in the studied range of cutting parameters.

- *CBN Coated Internal Grinding Tool grit*

  The minimum surface roughness value was achieved with low cutting parameter values. It was possible to achieve a high material removal rate (at high feed rate and high depth of cut) with little compromise on the surface roughness. A minimum surface roughness of 0.2598 μm is predicted to be achieved at a combination of the cutting speed of 3001 rpm, the feed rate of 1 mm/min, and the axial depth of cut of 0.1 mm within the studied range of cutting parameters.

(b) High speed CNC milling machine

- *Two Flute Square End Micro Grain Solid Carbide end mill*

  The feed rate is the most dominant factor affecting surface roughness. The surface roughness value is less at a high cutting speed, low feed rate, and low axial depth of cut value in the studied range of cutting parameters. The effect of the cutting parameters on the surface roughness is very similar to that for metallic materials. Experiments also show that at a low feed rate of 30 mm/min, surface roughness was low even at high axial depth of cut; as a result it achieves high materials removal rate. The predicted combination of optimal cutting parameters to achieve the surface finish as low as 0.4928 μm is represented by the cutting speed of 20,000 rpm, the feed rate of 30 mm/min, and the axial depth of cut of 0.05 mm in the studied range of the cutting parameters.

  A low cutting force was obtained at a low axial depth of cut, medium feed rate and high cutting speed. The most dominant factor is the axial depth of cut. The model predicts the cutting force as low as 12.12 N at the cutting speed of 18,807 rpm, the feed rate of 54.7 mm/min, and the axial depth of cut of 0.03 mm in the studied range of cutting parameters.

The lowest values of the surface roughness (0.527 μm) and the cutting force (13.87 N) are achieved at the cutting speed of 20,000 rpm, the feed rate of 44 mm/min, and axial depth of cut of 0.03 mm in the studied range of cutting parameters.

- *CBN Coated Internal Grinding Tool grit*

  The effect of the cutting parameters on the surface roughness is very similar to that for metallic materials. A high cutting speed and a low feed rate is the right combination to obtain a minimum surface roughness.

  A minimum surface roughness value of 0.5037 μm is predicted at an optimal combination of 20,000-rpm-cutting speed and 1.0-mm/min-feed rate for studied range of the cutting parameters.

  In order to achieve a low cutting force, a low feed rate and a high cutting speed are the right choice for the studied range of the cutting parameters. A minimum cutting force of 34.81 N is predicted at a combination of 20,000 rpm cutting speed and 1.0 mm/min feed rate in the studied range of the cutting parameters.

6.2 Future Work

This study has indicated a number of challenging problems that need further investigations.

Even though the surface roughness is successfully improved by the end milling process, during the cutting tests, at some critical combination of the cutting parameters (with higher values than the studied range of the cutting parameters) edge chips and brittle fractures are observed. Experiments need to be conducted to extend the range of the cutting parameters beyond the studied ones. It is advisable to run these tests on high speed CNC machines (up to 100000 rpm) to avoid edge chips and

brittle fracture completely.

At high speed CNC machines, a cutting zone of work piece may undergo plastic deformation due to a high temperature and this may prevent brittle fracturing. This effect requires a special investigation.

To examine the rate of production for machining complex shapes more experiments on high speed machines on machining complex objects should be carried out. To recommend the process for specific industrial applications, in-depth investigations are required.

Most applications of advanced ceramics are for very small devices. It is advisable to conduct experiments with micro tools on high speed machines.

In this study only three cutting parameters have been considered. Future work should consider other parameters like radial depth of cut, various cutting tool geometries, and tool materials in order to improve the limitations of the proposed in this research models.

REFERENCES

Every reasonable effort has been made to acknowledge the owners of copyright material. I would be pleased to hear from any copyright owner who has been omitted or incorrectly acknowledged.

Abou, El H. K.A., and Yahya, Z., [2005]. "High-speed end-milling of AISI 304 stainless steels using new geometrically developed carbide inserts", Journal of Materials Processing Technology, 162–163, pp. 596-602.

Abou, El H. K.A., Kadirgama, K., Hamdi, M., and Benyounis, K.Y., [2007]. "Prediction of cuttingforce in end milling operation of modified AISI P20 tool steel", Journal of MaterialsProcessing Technology 182, pp. 241-247.

Agarwal, S., and Rao, P.V.,[2008]. "Experimental investigation of surface/subsurface damage formation and material removal mechanisms in SiC grinding", International Journal of Machine Tools and Manufacture, 48, pp. 698–710.

Alagumurthi, N., Palaniradja, K., and Soundararajan, V., [2006]. "Optimization of grinding process through design of experiment (DOE): a comparative study", Materials Manufacturing Process, 21 (1), pp. 19–21.

Alam, S., Nurul, AKM., Konneh, M., and Anayet U.P., [2009]. "Surface roughness prediction in high speed flat end milling of Ti-6Al-4V and optimization by desirability function of RSM", Advanced Materials Research, 264 – 265, pp. 1166-1173.

Alauddin, M., EI Baradie, M.A., and Hashmi, M.S.J., [1995]. "Computer aided analysis of a surface roughness model for end milling", Journal of Material Processing Technology, 55, pp. 123-127.

Alauddin, M., EI Baradie, M.A., and Hashmi. M.S.J., [1996]. “Modelling of cutting force in end milling Inconel 718”, Journal of Material Processing Technology, 58, pp. 100-108.

Alauddin, M., EI Baradie, M.A., and Hashmi, M.S.J., [1998]. “Cutting forces in the end milling Inconel 718”, Journal of Material Processing Technology, 77, pp. 153-159.

Allor, R.L., Whalen, T.J., Baer, J.R., and Kumar, K.V., [1993]. “Machining of silicon nitride: experimental determination of process/property relationships”, Proceedings of International Conference on Machining Advanced Materials, U. S. Government Printing Office, Washington, NIST SP847, pp. 223–234.

Allor, R.L and Jahanmir, S, [1996]. “Current problems and future directions for ceramic machining”, American Society Bulletin, 75(7), pp. 40–43.

Baik, D.S., No, K.S, Chun, J.S., and Yoon, Y.J., [1995]. “Mechanical properties of mica glass–ceramics”, Journal of the American Ceramic Society 78 (5), pp. 1217–1222.

Baik, D.S., No, K.S., Chun, J.S., Yoon, Y.J., and Cho, H.Y, [1995]. “A Comparative evaluation for mica-based glass ceramics”, Journal of Material Science, 30, pp. 1801-1806.

Baik, Y., and Drew, R.A.L., [1996]. “Aluminum nitride: processing and applications”, Advanced Ceramic Materials, 122, pp. 553–570.

Balda, R., Fernández, J., Iparraguirre, I., Azkargorta, J., Garcia-Revilla, S., Pena, JI., Merino, R.I., and Orera, V.M., [2009]. “Broadband laser tunability of Nd3+ ions in 0.8CaSiO3-0.2Ca3(PO4)2 eutectic glass”, Optics Express 17(6), pp. 4382–4387.

Bao, W.Y., and Tansel, I.N., [2000]. “Modeling micro end milling operations, Part 1: analytical cutting force model”, International Journal of Machine Tools & Manufacture, 40 , pp. 2155-2173.

Beck, S.Y., Bong, C.S., Myeong, W.C., Lee, E.S., Dong, S.P., Jin, D.Y., and Won, S.E., [2008]. “Machining characteristics of AlN-hBN composites in end-milling and precision lapping processes”, Key Engineering Materials, 368-372, pp. 947-950.

Bernados, P.G., and Vosniakos, G.C., [2003]. “Predicting surface roughness in machining: a review”, International Journal of Machine Tools and Manufacture, 43(8), pp. 833-944.

Bianchi, E.C., Aguiar, P.R., Aguiar, C.E., DaSilva Jr., and Fortulan, C.A., [2003]. “Advanced ceramics: evaluation of the ground surface”, Ceramica, pp. 49,174-177.

Black, J. T., DeGarmo, E.P., and Kohser, R.A., [2007]. “Materials and processes in manufacturing”, Singapore: John Wiley & Sons Ltd.

Boch, P., and Niepce, J.C., [2007]. “Ceramic materials: processes, properties and applications”, London: ISTE Ltd.

Byrne, G., and Scholta, E., [1993]. “Environmentally clean machining processes, a strategic approach”, Annals of the CIRP 42 (1), pp. 471–474.

Cao, Y.Q., [2001]. “Failure analysis of exit edges in ceramic machining using finite element analysis”, Engineering Failure Analysis, 8 (4), pp. 325-338.

Chang, C. W., and Kuo, C. P., [2007]. “An investigation of laser-assisted machining of Al_2O_3 ceramics planning”, International Journal of Machine Tools & Manufacture, 47, pp. 452–461.

Chee, K. Ng., Shreyes, M.NW.Y, Rahman.M., Senthil, K, [2006]. “Experimental study of micro-and nano-scale cutting of aluminum 7075-T6”, International Journal of Machine tools & Manufacture, 46, pp. 929-936.

Chen, L., Siores, E., and Wong, W. C. K., [1996]. “Keft characteristics in abrasive water jet cutting of ceramics materials”, International Journal of Machine tools & Manufacture, 36, pp. 1201−1206.

Cho, M.W., Kim, D.W., and Cho, W.S., [2007]. “Analysis of micro-machining characteristics of Si3N4 – Hbn composites”, Journal of European Ceramic Society, 27, pp. 1259-1265.

Chryssolouries, G., Anifantis, N., and S. Karagiannis, S., [1997]. “Laser assisted machining: An Overview”, Journal of Manufacturing Science and Engineering, 119(4B), pp. 766–769.

Chwan, H.T., and Chen, H.W., [2003]. “Laser cutting of thick ceramic substrates by controlled fracture technique”, Journal of Materials Processing Technology, 136, pp. 166–173.

Copley, S.M., [1985]. “Laser applications. In: Handbook of High Speed Machining Technology”, New York: Chapman and Hall.

Corning incorporated, “Lighting and Materials, MACOR”, New York: Corning <http://www.technicalproductsinc.com/pdf/macor.pdf>

Dabnun, M.A., Hashmi, M.S.J., and El-Baradie, M.A., [2005]. “Surface roughness prediction model by design of experiments for turning machinable glass–ceramic”, Journal of Materials Processing Technology, 164–165, pp. 1289–1293.

Daniels, W.H., [1989]. “Super abrasives for ceramic grinding and finishing”, SME Technical Paper, Society of Manufacturing Engineers.

Davim, J. P. [2010]. “Surface Integrity in Machining”, New York : Springer.

Daudin, B., and Martin, P., [1989]. “Mega-electron volt ion beam polishing of anodically grown alumina”, Materials Science and Engineering, 115, pp. 63-66.

Derflinger, V., Brandle, H., and Zimmermann, H., [1999]. “New hard/lubricant coating for dry machining”, Surface and Coating Technology, 113 (3), pp. 286–292.

Du, X., Mingli Q., Abdur R., Zhihao Y., Yang, B., and Xuanhui Q., [2008]. “Structure and properties of AlN ceramics prepared with spark plasma sintering”, Materials Science and Engineering, A 496, pp. 269-272.

Duangrudee, C., Krongkarn, S., Kanchana, K., Greg, H., and Kimihiro, Y., [2011]. “Machinable glass-ceramics forming as a restorative dental material”, Dental Materials Journal, 30(3), pp. 358–367.

Dudzinski, D., Devillez, A., Moufki, A., Larrouque`re, D., Zerrouki, V., and Vigneau, J., [2004]. “A review of developments towards dry and high speed machining of Inconel 718 alloy”, International Journal of Machine Tools and Manufacture 44, pp. 439-456.

Eckert, C., and Weatherall, J., [1990]. “Advanced ceramics: 90’s global business outlook”, Ceramics Industry, 134(4), pp. 53–57.

Frei, H., and Grathwohl, G. [1993]. “Microstructure and strength of advanced ceramics after machining”, Ceramics International, 19(2), pp. 93–104.

Fussell, B., and Srinivasan, K., [1989]. “An investigation of the end milling process under varying machining conditions”, Transactions of the ASME, Journal of Engineering for Industry, 111, pp. 27–36.

Ghani, J.A., Choudhury, I.A., and Masjuki, H.H., [2004]. “Wear mechanism of TiN coated carbide and uncoated cermets tools at high cutting speed applications”, Journal of Materials Processing Technology, 153–154 , pp. 1067–1073.

Goodfellow, “Machinable glass ceramic and Aluminum Nitride , Material information”, Huntingdon: Goodfellow Cambridge Ltd.

Guangli, H., Ramesh, K.T., Buyang, C., and McCaule, J.W., [2011]. “The compressive failure of aluminum nitride considered as a model advanced ceramic”, Journal of the Mechanics and Physics of Solids, 59, pp. 1076–1093

Hamatani, G., and Ramulu, M., [1990]. “Machinability of high temperature composites by abrasive water jet”, Journal of Engineering Materials and Technology, Transactions of the ASME, 112(4), pp. 381-386.

Han, F.Z., Wang, Y.X., Zhou, M., [2009]. “High-speed EDM milling with moving electric arcs”, International Journal of Machine Tools & Manufacture, 49, pp. 20–24.

Hocheng, H., Tai, N.H., and Liu, C.S., [2000]. “Assessment of ultrasonic drilling of C/SiC composite material”, Composites, Part A, 31, pp. 133– 142.

Hockin, H.K., and Jahanmir S., [1995]. “Micro fracture and material removal in scratching of alumina”, Journal of Materials Science, 30, pp. 2235-2247.

Huang, H., and Liu, Y.C., [2003]. “Experimental investigations of machining characteristics and removal mechanisms of advanced ceramics in high speed deep

grinding", International Journal of Machine Tools and Manufacture, 43 (8), pp. 811-823.

Hwang, T. W., Evans, C.J, Whitenton, E.P., and Malkin, S., [2000]. "High speed grinding of silicon nitride with electroplated diamond wheels, Part 1: Wear and wheel life", Journal of Manufacturing Science and Engineering 122 (1), pp. 32-41

Hwang, T.W., Evans, C.J., Whitenon, E.P., and Malkin, S., [1999]. "High speed grinding of silicon nitride with electroplated diamond wheels.1.wear and wheel life", Manufacturing Science and Engineering, ASME, 10, pp. 431-441.

Hwang, T.W., Evans, C.J., Whitenon, E.P., and Malkin, S., [1999]. "High speed grinding of silicon nitride with electroplated diamond wheel topography and grinding mechanisms", Manufacturing Science and Engineering, ASME, 10, pp. 443-452.

Hwang, T.W., Evans, C.J., and Malkin, S., [2000]. "An investigation of high speed grinding with electroplated diamond wheels", Annals of CIRP 49(1), pp. 245-248.

Inasaki, I., [1987]. "Grinding of hard and brittle materials", Annals of CIRP 36 (2), pp. 463-471.

Ishikawa, K., Suwabe, H., Nishide, T., and Uneda, M., [1998]. "A study on combined vibration drilling by ultrasonic and low-frequency vibrations for hard and brittle Materials", Precision Engineering, 22, pp. 196-205.

Jahanmir, S., and Ives, L.K., [1995]. "Machining of advanced ceramics, Laboratory report", Tribology International, 28(6), pp. 415-420.

Jahanmir, S., Xu, H.H.K., and Ives, L.K., [1999]. "Mechanisms of material removal in abrasive machining of ceramics", Machining of Ceramics and Composites, New

York: Marcel Dekker.

Jain, V.K., Choudhury, S.K., and Ramesh, K.M., [2002]. “On the machining of alumina and glass”, International Journal of Machine Tools & Manufacture, 42, pp. 1269-1276.

Janssen, R., Scheppokat, S., and Claussen, N., [2008]. “Tailor made ceramic based components advantages by reactive processing and advanced shaping techniques”, Journal of the European Ceramic Society, 28, pp. 1369-1379.

Jia, Z. Z., Yong, G.P., Liu, Y., Zhang, J., Ai, X.Z., and Liu, J., [1996]. “The state of machining of ceramics in China”, Journal of Materials Processing Technology, 62, pp. 20-23.

Jin, H.,Wang, W.,Gao, J., Qiao, G., and Jin, Z., [2006]. “Study of machinable AlN/BN ceramic composites”, Materials Letters, 60 (2), pp. 190-193.

Jingwen, X., Lee, K.J., Si, Y.B., Seok, J.H.,, Bong, C.H., Myeong, W.C., and Won, S.C., [2009]. “Mechanical properties and machinability of AlN- hBN ceramics prepared by spark plasma sintering”, Journal of Ceramic Society of Japan, 117(9), pp. 1028-1031.

Jurgen, R., Alain, B.N.K., Marion, W.E., Daniel, K., Antje, B., Wolfgang, R., Michael, J., Hoffmann, Robert, D., Gerhard, S., [2009]. “Development of a roadmap for advanced ceramics: 2010–2025”, Journal of the European Ceramic Society, 29, pp. 1549–1560

Kalpakjian, S., and Schmid, S.R., [2005]. “Manufacturing engineering and technology”, New Jersey: Prentice Hall.

Kang, I.S, Kim, J.S, Kim, J.H, Kang, M.C, and Seo, Y.W, [2007]. "A mechanistic model of cutting force in the micro end milling process", Journal of Materials Processing Technology, 187-188, pp. 250-255.

Katahira, K., Ohmori, H., Uehara, Y., and Azuma, M., [2005]. "ELID grinding characteristics and surface modifying effects of aluminum nitride (AlN) ceramics", International Journal of Machine Tools & Manufacture, 45, pp. 891-896.

Kishawy, H.A., Elbestawi, M.A., [1998]. "Effects of edge preparation and cutting speed on surface integrity of die materials in hard machining", Proceedings of the ASME, MED, 8, pp. 269-276

Klocke, F., and Eisennblatter, G., [1997]. "Dry cutting", Annals of the CIRP, 46 (2), pp. 519–526.

Klocke, F., [1997]. "Modern approaches for the production of ceramic components", Journal of the European Ceramic Society, 17, pp. 457–465.

Klocke, F., Verlemann, E., and Schippers, C., [1999]. "High speed grinding of ceramics", Machining of Ceramics and Composites, New York: Marcel Dekker.

Konig, W., and Sinhoff, V., [1992]. "Lens and Optical Systems Design", SPIE, pp. 778-788.

Kovach, J.A, Laurich, M.A., Malkin, S., Srinivasan, S., Bandyopadyay, B., and Ziegler, K.R., [1993]. "A feasibility of investigation of high speed, low damage grinding for advanced ceramics", SME, 5th international grinding process conference, Vol. 1, Cincinnati, United states.

Kramer, B.M., and Hartung, P.D., [1981]. “Theoretical consideration on the machining of nickel-based alloys”, International. Conference on Cutting Tool Materials, pp. 57-74, Metals Park, Ohio, United States.

Kumashiro, Y., [2000]. “Electric Refractory Materials” New York: Marcel Dekker.

Kunieda, M., Miyoshi, Y., Takaya, T., Nakajima, N., Bo Y.Z., Yoshida M., [2003]. “High speed 3D milling by dry EDM”, CIRP Annals Manufacturing Technology, 52, pp. 147-150

Landolt, D., Chauvy, R.F., Zinger, O., [2003]. “Electrochemical micromachining, polishing and surface structuring of metals: Fundamentals aspects and new developments”, Electrochimica Acta, 48, pp. 3185-3201

Lee, T.C., and Lau, W.S., [1991]. “Some characteristics of electrical discharge machining of conductive ceramics”, Materials and Manufacturing Processes, 6(4), pp. 635-648.

Lei, S., Liu, W., and Deines, T. , [2006]. “A feasibility study on laser assisted milling of silicon nitride ceramic by integrating experimental study with FEA”, Proceedings of the 2006 NSF Design, Service, and Manufacturing Grantees and Research Conference, St. Louis, MO, pp. 24-27.

Li, K., and Liao, W., [1996]. “Surface/subsurface damage and the fracture strength of ground ceramics”, Journal of Materials Processing Technology, 57, pp. 207-220.

Li, Y., and Liang, S.Y., [1999]. “Cutting force analysis in transient state milling processes”, The International Journal of Advanced Manufacturing Technology, 15, pp. 785-790.

Li, H.Z., Zeng, H., and Chen, X.Q., [2006]. "An experimental study of tool wear and cutting force variation in the end milling of Inconel 718 with coated carbide inserts", Journal of Materials Processing Technology 180, pp. 296-304.

Liu, YH.,Ji, RJ., Li, QY., Yu, LL., and Li, XP., [2009]. "An experimental investigation for electric discharge milling of SiC ceramics with high electrical resistivity", Journal of Alloys and Compounds, 472, 406-410.

Lo, S.P., [2003]. "An adaptive-network based fuzzy inference system for prediction of work piece surface roughness in end milling", Journal of Materials Processing Technology, 142, pp. 665-675.

Luis, C. J., Puertas, I, and Villa, G., [2005]. "Material removal rate and electrode wear study on the EDM of silicon carbide", Journal of Materials Processing Technology, 164-165, pp. 889-896.

Ma, L.J., and Yu, A.B., [2007]. "Influencing of technological parameters on tool wear during turning fluorophlogopite glass-ceramics", Journal of Rare Earths, 25, pp. 330-333.

Malkin, S., and Ritter, J.E., [1989]. "Grinding mechanisms and strength degradation for ceramics", ASME, Journal of Engineering for Industry, 111, pp. 2111-2118.

Mansour, A., and Addalla, H., [2002]. "Surface roughness model for end milling: a semi-free cutting carbon case hardening steel (EN32) in dry condition", Journals of Materials Processing Technology, 124, pp. 183-191.

Marinescu, I., Rowe, B., Yin, L., and Wobker, H.G., [2000]. "Abrasive processes, handbook of ceramics grinding and polishing", New Jersey : Noyes Publications.

Mason, M., Yong, H., Ted K.H., [2007]. "Machinability of ultra-grained copper using tungsten carbide and polycrystalline diamond tools", International Journal of Machine Tools & Manufacture, 47, pp. 286-293.

Matsumoto, Y, Hashimoto, F, and Lahoti, G, [1999]. "Surface integrity generated by precision hard turning", Annals of the CIRP, 48/1, pp. 55-62.

Matsumura, T., Hiramatsu, T., Shirakashi, T., and Muramatsu, T., [2006]. "A study on cutting force in the milling process of glass", Journal of Manufacturing Process, 7 (2), pp. 102-108.

Mayer, Jr. J.E., Fang, G.P., [1993]. "Diamond grinding of silicon nitride", NIST Special Publication, 647, pp. 205-222

Mayer, Jr.J.E.,Fang.G.P., [1995]. "Effect of grinding parameters on surface finish of ground Ceramics", Annals of the CIRP 44 (1), pp. 279-282.

Moche, M.E., Eades, J.A., Metgger, M., Meyer, J.I., and Mochel, J.M., [1984]. "Electron beam cutting in amorphous alumina sheets", Applied Physics Letters, 44, pp. 502–504.

Montgomery, D.C., [2004]. Design and Analysis of Experiments", New York: John Wiley and Sons, Inc.

Myers, R. H., Montgomery, D. C., and. Anderson-Cook, C. M., [2009], "Response Surface methodology:process and product optimization using designed experiments", New York: WiLEY.

Newby, G., Venkatachalam, S., and Liang, S.Y., [2007]. "Empirical analysis of cutting force constants in micro end milling operations", Journal of Materials

Processing Technology, 192-193, pp. 41-47.

Ng, S., Le, D., Tucker, S., and Zhang, G., [1996]. "Control of machining induced edge chipping on glass ceramics", Proceedings of the 1996 ASME International Mechanical Engineering Congress and Exposition, Manufacturing Engineering Division, MED (4), pp. 229-236, Atlanta, United States.

Oktem, H, T. Erzurumlu, T., and Erzincali, F., [2006]. "Prediction of minimum surface roughness in end milling old parts using neural network and generic algorithm", Materials and Design, 27, pp. 735-744.

Ozcelik, B., and Bayramoglu, M., [2006]. "The statistical modelling of surface roughness in high speed end milling", International Journal of Machine Tools & Manufacture, 46, pp. 1395-1402.

Padmanabhan, K.K., and Murthy, A.S., [1991]. "Evaluation of frictional damping by response surface methodology", International Journal of Machine Tools & Manufacture, 31, pp. 95-105.

Prabhakar, D., Pei, Z.J., Ferreira, P.M., and Haselkorn, M., [1993]. "A Theoretical Model for Predicting Material Removal Rates in Rotary Ultrasonic Machining of Ceramics", Transactions of the North American Manufacturing Research Institution of SME, 21, pp. 167–172.

Puertas, I., and Luis, C.J., [2004]. "A study of optimization of machining parameters for electrical discharge machining of boron carbide", Materials Manufacturing Process, 19 (6), pp. 1041-1070.

Rahaman, M., Senthil, A.K., and Prakash, J.R.S, [2001]. "Micro milling of pure Copper", Journal of Materials Processing Technology, 116, pp. 39-43.

Raj, R., [1993]. "Fundamental research in structural ceramics for service near 2000^0 C", Journal of American Ceramic Society, 76, pp. 2147-2174.

Raju, K., Janardhana, G., Kumar, P., and Rao, V., [2011]. "Optimization of cutting conditions for surface roughness in CNC end milling", International Journal of Precision Engineering and Manufacturing, 12 (3), pp. 383-391.

Rajurkar, K.P., Wang, Z.Y., and Kuppattan, A., [1999]. "Micro removal of ceramic material (AL_2O_3) in the precision ultrasonic machining", Precision Engineering, 23, pp. 73-78.

Reddy, M.M., Alexander. G., and Abou El H.K.A., [2011]. "Development of cutting force model for aluminum nitride ceramic processed by micro end milling", Applied Mechanics and Materials, 87, 223-229.

Reddy, M.M., Alexander, G., and Abou El H.K.A., Sujan, D., Ali, M.Y., and Malique, M.A., (2012). "Tool wear analysis in end milling of advanced ceramics with TiAlN and TiN coated carbide insert", Advanced Materials Research, 576, 76-79.

Reddy, M.M., Alexander, G., and Abou El H.K.A., and Sujan, D., (2012). "Performances of aluminum nitride ceramic in end milling using coated carbide tool", 15th International Conference on Advances in Materials & Processing Technologies, AMPT 2012, Sydney, Australia.

Reen, O.W., [1977]. "Modern developments in powder metallurgy", New Jersey: MPIF Publishers

Robert, B. Heimann, [2010]. "Introduction to Advance Ceramics: In Classic and Advanced Ceramics", New Yark: WiLEY-VCH.

Sahin, Y.,, and Riza M.A., [2005]. “Surface roughness model for machining mild steel with coated carbide tool”, Materials and Design, 26, pp. 321-326.

Sahoo, P., Davim, J.P., and Barman, T., [2011]. “Fractal Analysis in Machining”, New York: Springer-Verlag.

Saito, K., Shikida, M., and Tokora, K., [2004]. “Wet-chemical etching and cleaning of Silicon”, Thin Solid Films, 462/463, pp. 205-256.

Sanchez, J.A, Cabanes, I., Lopez, D.L.N., and Lamikiz, A., [2001]. “Development of optimum electro discharge machining technology for advanced ceramics”, International Journal of Advanced Manufacturing Technologies, 18, pp. 897-905.

Sandvik Coromant, [1994]. “Modern metal cutting”, A Practical Handbook, Sweden: Sandvik Coromant.

Sandvik Coromant, [2007]. “New cutting tools”, Main Catalogue, Sweden: Sandvik Coromant.

Schixlir, W.L., [1994]. “Conventional machining of green aluminum/aluminum nitride ceramics”, The Ohio Journal of Science, 94 (5), pp. 151-154.

Schulz, H., Dorr, J., Rass, I.J., Schulze, M., Leyendecker, L., and Erkens, G., [2001]. “Performance of oxide PVD-coatings in dry cutting operations”, Surface and Coatings Technology, 146-147, pp. 480-485

Shaw, M.C., [1986]. “Metal Cutting Principles”, New York: Oxford University Press.

Sheppard, L.M., [1990]. “Aluminum nitride: a versatile but challenging material”, American Ceramic Society Bulletin, 69, pp. 108-112.

Shumyacher, V.M., Dushko, O.V., and Pushkarev, D.O., [2009]. "Predicting the grinding efficiency of hard ceramics in terms of surface brittleness", Russian Engineering Research, 29, pp. 623-624.

Sinan, F., Caroline, M. C., Mathew, B.W., and Burak, O.O., [2007]. "An experimental investigation of micro-machinability of Copper 101 using tungsten carbide micro-end mills", International Journal of Machine Tools and Manufacture, 47, pp. 1088-1100.

Spur, G., Uhlmann, E., Holl, S.E., and Daus, N.A., [1999]. "Influences on surface and subsurface during ultrasonic assisted grinding of advanced ceramics", Proceedings of the 14th Annual Meeting, American Society for Precision Engineering, pp. 481-484, Raleigh, North Carolina.

Sreejith, P.S., [2008]. "Machining of 6061 aluminium alloy with MQL dry and flooded lubricant conditions", Materials Letters, 62, pp. 276-278.

Suhaily, M., Nurul, A.K.M., and Patwari, M.A.U., [2011]. "Prediction of surface roughness in high speed machining of Inconel 718", Advanced Materials Research, 264-265, pp. 1193-1198.

Suresh, K., Reddy, N., and Rao, P.V., [2006]. "Experimental investigation to study the effect of solid lubricants on cutting forces and surface quality in end milling", International Journal of Machine Tools & Manufacture 46, pp. 189-198

Taira, M., and Yamaki, M., [1994]. "Ranking machinability of nine machinable ceramics by dental high speed cutting tests", Journal of Material Science Letters, 13, pp. 480-482.

Takeuchi, Y., Sawada, K., and Sata, T., [1996]. “Ultra precision 3D micromachining of glass”, Annals of CIRP, 45 (1), pp. 401-404.

Takacs, M., Vero. B., and Meszaros, I., [2003]. “Micro milling of metallic materials”, Journal of Materials Processing Technology, 138, pp. 152-155.

Taylor, D.A., [2001]. “Advanced Ceramics-The Evolution, classification, properties, production, firing, finishing and Design”, Materials Australia, 33, No. 1, pp. 20-22.

Thoe, T.B., Aspinwall, D.K., and Wise, M.L.H., [1998]. “Review on Ultrasonic Machining”, International Journal of Machine Tools and Manufacture, 38(4), pp. 239–255.

Tian, Y., Wu, B., Anderson, M., and Shin, Y.C., [2008]. “Laser-assisted milling of silicon nitride and Inconel 718”, Transactions of the ASME, Journal of Manufacturing Science and Engineering, 130, 031013-1-9.

Topal, E.S., [2009]. “The role of step over ratio in prediction of surface roughness in flat end milling”, International Journal of Mechanical Sciences 51, pp. 782-789

Treadwell, C., and Pei, Z.J., [2003]. “Machining ceramics with rotary ultrasonic machining, Ceramic Industry, June, pp. 39-42.

Tuersley, I.P., Jawaid, A., and Pashby, I.R., [1994]. “Review: Various methods of machining advanced ceramic materials”, Journal of Materials Processing Technology, 42, pp. 377-390.

Vermeulen, J.P., Rosielle, M.B., and Schellekens, P.H.J., [2000]. “An advanced ceramics optical diamond turning machine design and prototype development”, Annals of the CIRP, 49, pp. 201-204.

Wang, Z.Y., Rajarkar. K.P, and Murugappan, M., [1996]. “Cryogenic PCBN turning of ceramic (Si3Ni4)”, Wear, 195, pp. 1-6.

Wang, W., Kweon, S.H., and Yang, S.H., [2005]. “A study on roughness of the micro-end-milled surface produced by a miniatured machine tool”, Journal of Materials Processing Technology 162-163, pp. 702-708.

Xu, H.H.K., and Jahanmir, S., [1994]. “Simple Technique for observing subsurface damage in machining of ceramics”, Journal of American Ceramics Society, 77, pp. 1388-1390.

Yan, B.H., Huang, F.Y, and Chow. H. M., [1995]. “Study on the turning characteristics of alumina-based ceramics”, Journal of Materials Processing Technology, 54, pp. 341-347.

Yang, Y.K., [2006]. “Optimization of a photo resists coating process for photolithography in wafer manufacturing via design of experiments method”, Microelectronics International, 23 (3), pp. 26-32.

Yang, X.H., Zhang, Y.M., and Han, J.C., [2007]. “High speed lapping of SiC ceramic material with fixed abrasive”, Key Engineering Materials, 336–338, pp. 1458-1460.

Yang, B., and Lei, S., [2008]. “Laser-assisted milling of silicon nitride ceramic: a machinability study”, International Journal of Mechatronics and Manufacturing Systems 1, pp. 116-130.

Yang, B., Deines, T., Geist, C., and Lei, S., [2007]. “An experimental study of laser assisted milling of silicon nitride ceramic”, Transactions of the North American Manufacturing Research Institution of SME, 35, pp. 473-480.

Yang, B., Shen, X., and Lei, S., [2009]. "Mechanisms of edge chipping in laser-assisted milling of silicon nitride ceramics", International Journal of Machine Tools & Manufacture 49, pp. 344-350

Zeng, W.M., Li, Z.C., Pei, Z.J., and Treadwell, C., [2005]. "Experimental observation of tool wear in rotary ultrasonic machining of advanced ceramics", International Journal of Machine Tools & Manufacture 45, pp. 1468-1473.

Zhang, J.Z, Chen, J.C and Kirby, E.D., [2007]. "Surface roughness optimization in an end-milling operation using the Taguchi design method", Journal of Materials Processing Technology, 184, pp. 233-239.

Zhong, Z., [2002]. "Surface finish of precision machined advanced materials, Journal of Materials Processing Technology", 122, 2-3, pp. 173-178.

APPENDIX A

Preliminary Experimental Results

The results acquired from preliminary experiments are presented in the following Tables (1-10), these were utilized to choose the range of cutting parameters. The V-30 CNC vertical milling machine was used for low spindle speed experiments (Table A1 – Table A6) and the V-55 CNC vertical milling machine was used for high spindle speed experiments (Table A7 – Table A10)

Table A1: Preliminary test results on MGC using solid carbide end mill

Runs	Cutting Speed rpm	Feed Rate (mm/min)	Depth of Cut (mm)	Surface Roughness (µm)
1	1000	10	0.1	0.52
2	3000	10	0.1	0.36
3	6000	10	0.1	0.99
4	3000	30	0.1	0.41
5	1000	30	0.3	0.53
6	3000	30	0.3	0.39
7	6000	30	0.3	1.14
8	1000	40	0.5	0.98
9	4000	40	0.5	1.28
10	5000	40	0.5	1.22
11	5000	30	0.5	0.82
12	5000	30	0.3	0.52
13	6000	40	0.5	1.31
14	5000	10	0.6	1.28
15	5000	30	0.6	1.33

Table A2: Preliminary experimental results on MGC using coated tool insert

Runs	Cutting Speed rpm	Feed Rate (mm/min)	Depth of Cut (mm)	Surface Roughness (µm)
1	1000	10	0.1	0.43
2	3000	10	0.1	0.55
3	6000	10	0.1	0.83
4	3000	30	0.1	0.48
5	1000	30	0.3	0.54
6	3000	30	0.3	0.62
7	6000	30	0.3	0.86
8	1000	40	0.5	0.89
9	4000	40	0.5	0.92
10	5000	40	0.5	0.89
11	5000	30	0.5	0.74
12	5000	30	0.3	0.66
13	6000	40	0.5	1.12
14	5000	10	0.6	1.04
15	5000	30	0.6	0.97

Table A3: Preliminary results on MGC using CBN coated internal tool grit

Runs	Cutting Speed rpm	Feed Rate (mm/min)	Depth of Cut (mm)	Surface Roughness (µm)
1	1000	1	0.1	0.28
2	3000	1	0.1	0.34
3	6000	1	0.1	0.78
4	3000	2	0.1	0.42
5	6000	2	0.2	0.82
6	3000	3	0.2	0.56
7	6000	3	0.3	0.87
8	1000	4	0.3	0.92
9	4000	4	0.1	0.86
10	5000	4	0.3	0.79
11	5000	3	0.5	0.83
12	5000	3	0.3	0.68
13	6000	4	0.5	0.94
14	5000	1	0.5	0.82
15	5000	3	0.5	0.94

Table A4: Preliminary test results on AlN using solid carbide end mill

Runs	Cutting Speed rpm	Feed Rate (mm/min)	Depth of Cut (mm)	Surface Roughness (µm)
1	1000	10	0.1	0.52
2	3000	10	0.1	0.40
3	6000	10	0.1	0.78
4	3000	30	0.1	0.46
5	1000	30	0.3	0.51
6	3000	30	0.3	0.42
7	6000	30	0.3	0.88
8	1000	40	0.5	1.12
9	4000	40	0.5	1.18
10	5000	40	0.5	1.15
11	5000	30	0.5	0.98
12	5000	30	0.3	0.58
13	6000	40	0.5	1.22
14	5000	10	0.6	1.12
15	5000	30	0.6	1.21

Table A5: Preliminary experimental results on AlN using coated tool insert

Runs	Cutting Speed rpm	Feed Rate (mm/min)	Depth of Cut (mm)	Surface Roughness (µm)
1	1000	10	0.1	0.41
2	3000	10	0.1	0.58
3	6000	10	0.1	0.88
4	3000	30	0.1	0.51
5	1000	30	0.3	0.51
6	3000	30	0.3	0.59
7	6000	30	0.3	0.92
8	1000	40	0.5	0.87
9	4000	40	0.5	0.97
10	5000	40	0.5	0.78
11	5000	30	0.5	0.88
12	5000	30	0.3	0.66
13	6000	40	0.5	1.23
14	5000	10	0.6	1.09
15	5000	30	0.6	1.10

Table A6: Preliminary results on AlN using CBN coated internal tool grit

Runs	Cutting Speed rpm	Feed Rate (mm/min)	Depth of Cut (mm)	Surface Roughness (µm)
1	1000	1	0.1	0.31
2	3000	1	0.1	0.37
3	6000	1	0.1	0.84
4	3000	2	0.1	0.39
5	6000	2	0.2	0.72
6	3000	3	0.2	0.58
7	6000	3	0.3	0.91
8	1000	4	0.3	0.71
9	4000	4	0.1	0.81
10	5000	4	0.3	0.79
11	5000	3	0.5	0.88
12	5000	3	0.3	0.72
13	6000	4	0.5	0.96
14	5000	1	0.5	0.81
15	5000	3	0.5	0.99

Table A7: Preliminary results on MGC using solid carbide end mill

Runs	Cutting Speed rpm	Feed Rate (mm/min)	Depth of Cut (mm)	Surface Roughness (µm)
1	10000	10	0.2	1.12
2	15000	10	0.2	1.08
3	20000	10	0.1	0.82
4	10000	30	0.1	0.93
5	15000	30	0.05	0.69
6	20000	30	0.05	0.68
7	10000	60	0.03	0.67
8	15000	60	0.03	0.51
9	20000	60	0.03	0.47
10	10000	90	0.05	0.73
11	15000	90	0.05	0.56
12	20000	30	0.03	0.49
13	10000	30	0.03	0.56
14	15000	110	0.03	1.12
15	20000	110	0.04	1.21

Table A8: Preliminary results on MGC using CBN coated internal tool grit

Runs	Cutting Speed rpm	Feed Rate (mm/min)	Surface Roughness (µm)
1	10000	1	0.31
2	15000	1	0.37
3	20000	1	0.42
4	10000	2	0.39
5	15000	2	0.43
6	15000	3	0.58
7	20000	3	0.56
8	10000	4	0.71
9	15000	4	0.81
10	20000	4	0.79
11	20000	3	0.66
12	15000	3	0.68
13	20000	4	0.96
14	15000	5	0.98
15	20000	5	1.15

Table A9: Preliminary test results on AlN using solid carbide end mill

Runs	Cutting Speed rpm	Feed Rate (mm/min)	Depth of Cut (mm)	Surface Roughness (µm)
1	10000	10	0.2	0.88
2	15000	10	0.2	1.18
3	20000	10	0.1	0.78
4	10000	30	0.1	0.91
5	15000	30	0.05	0.67
6	20000	30	0.05	0.68
7	10000	60	0.03	0.67
8	15000	60	0.03	0.61
9	20000	60	0.03	0.49
10	10000	90	0.05	0.76
11	15000	90	0.05	0.66
12	20000	30	0.03	0.53
13	10000	30	0.03	0.49
14	15000	110	0.03	1.32
15	20000	110	0.04	1.36

Table A10: Preliminary results on AlN using CBN coated internal tool grit

Runs	Cutting Speed rpm	Feed Rate (mm/min)	Surface Roughness (µm)
1	10000	1	0.38
2	15000	1	0.36
3	20000	1	0.67
4	10000	2	0.48
5	15000	2	0.52
6	15000	3	0.55
7	20000	3	0.59
8	10000	4	0.74
9	15000	4	0.87
10	20000	4	0.89
11	20000	3	0.62
12	15000	3	0.66
13	20000	4	0.78
14	15000	5	1.12
15	20000	5	0.98

From the preliminary results, the cutting parameter values were not considered in the main tests, if the value of the surface roughness exceeded 0.8 µm for the solid carbide end mill and coated carbide tool inserts. In the case of the CBN coated internal grinding tool grit, the cutting parameters were selected for the main tests, only when the surface roughness value was below 0.7 µm.

APPENDIX B

Pictures of Surface finish and Tool Wear

The following diagrams (Fig B1- B9) show the locations of tool wear, surface roughness, damage of tool wear, good and poor surface finish.

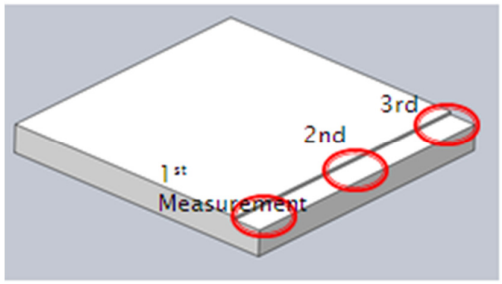

Fig B1: Locations of surface roughness measurements
Three roughness measurements were taken.

- Average value was considered

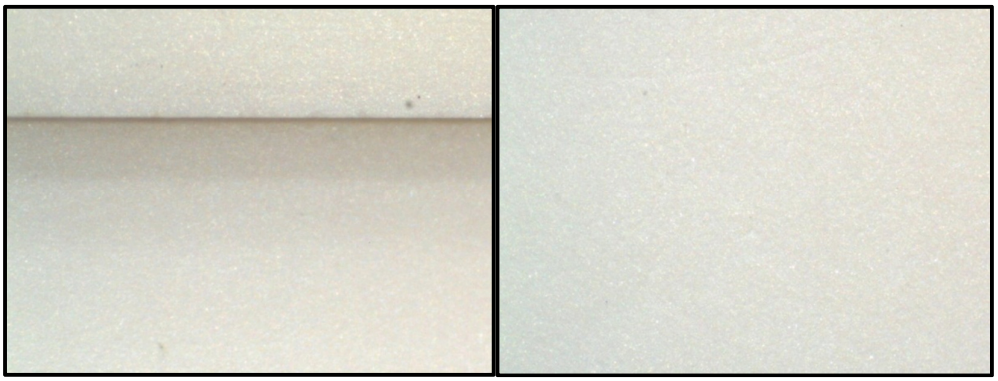

Fig B2: Surface finish of AlN generated by two flute solid carbide end mill

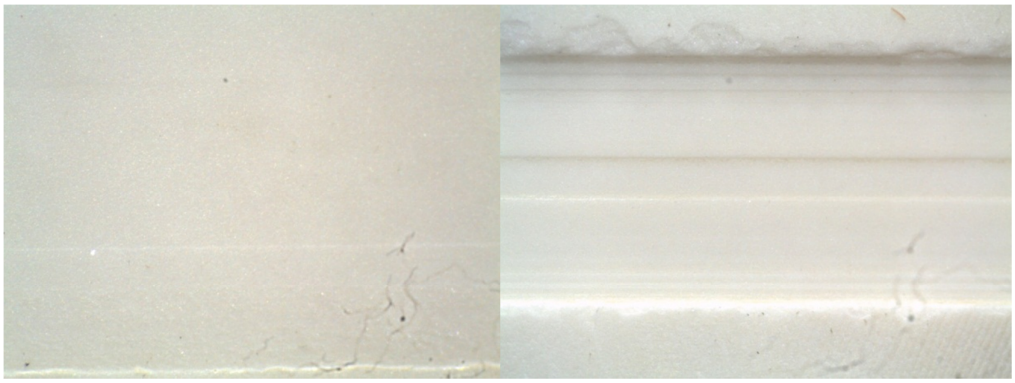

Fig B3: Micro cracks and edge chips at high critical parameters

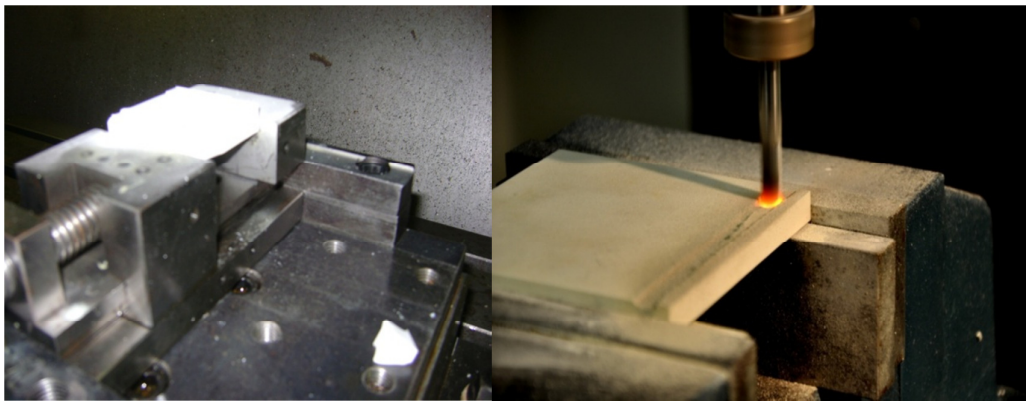

Fig B4: Brittle fracture and tool failure at high critical cutting parameters

Tool wear to be viewed under a microscope:

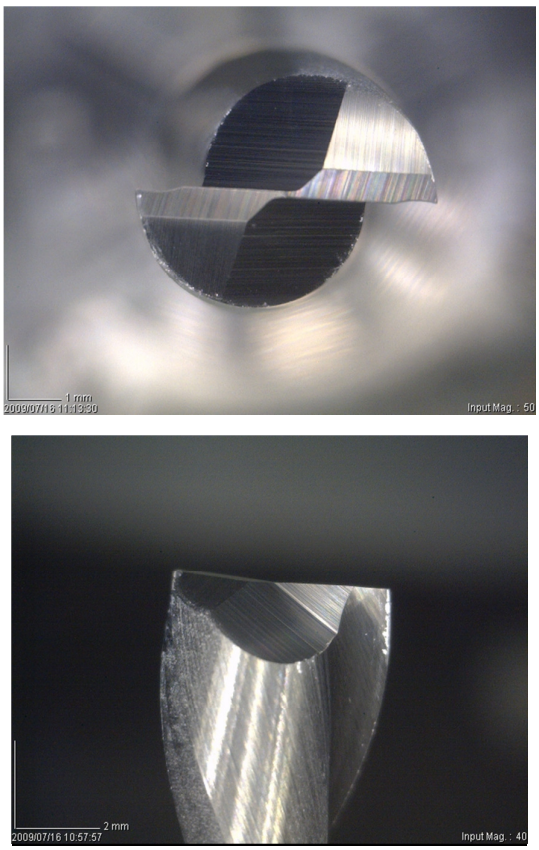

Fig B5: Two flute solid carbide end mill wear

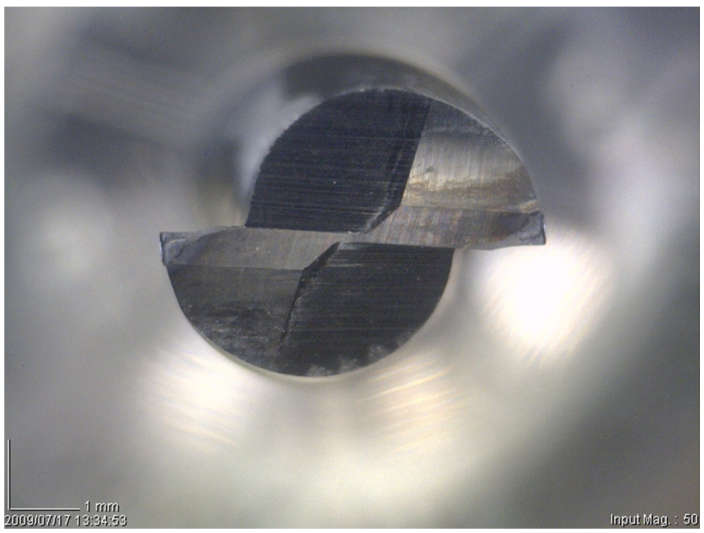

FigB6: Tool damage at high critical cutting parameters.

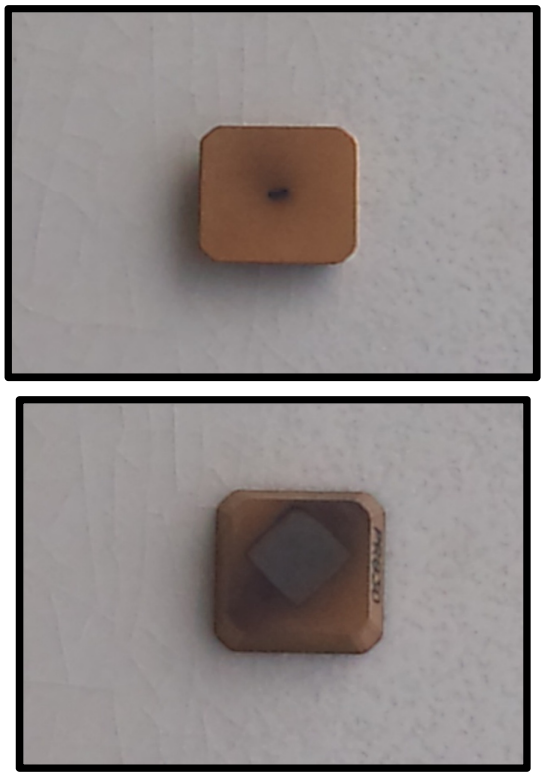

Fig B7: Coated carbide Tool insert used in experiments

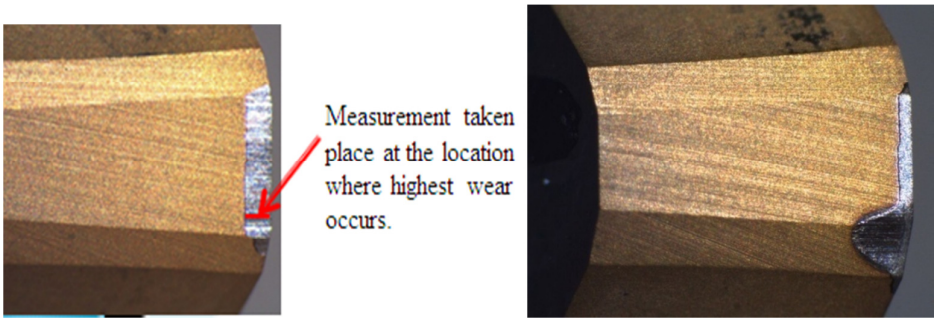

Fig B8: Coated carbide tool inserts wear and tool damage to be viewed under a microscope

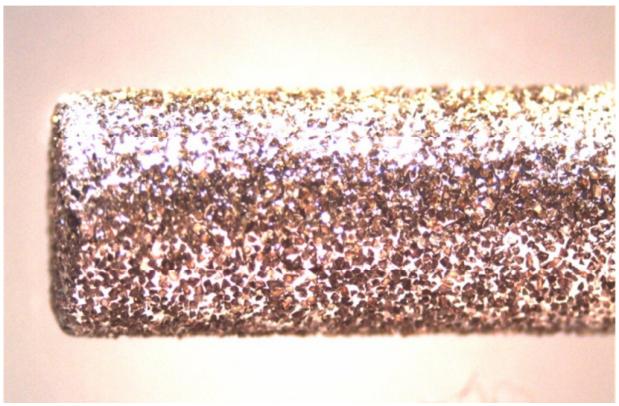

Fig B9: Wear of CBN coated internal grinding tool grit